UCLA
COMPUTATIONAL AND APPLIED MATHEMATICS

Vortex Sheets, Singular Integrals and Steady Flows (UCLA Ph.D. Thesis)

Shin-Shin Kao

June 1995

CAM Report 95-32

Department of Mathematics
University of California, Los Angeles
Los Angeles, CA. 90024-1555

UNIVERSITY OF CALIFORNIA

Los Angeles

Vortex Sheets, Singular Integrals and Steady Flows

A dissertation submitted in partial satisfaction of the

requirements for the degree Doctor of Philosophy

in Mathematics

by

Shin-Shin Kao [1]

1995

[1]This work was partially supported through a graduate research assistantship under grant NSF DMS-9306488.

TABLE OF CONTENTS

PART I

VITA

1968	Born, Taipei, Taiwan, R.O.C.
1990	Bachelor of Applied Mathematics National Tsing Hua University Hsin-chu, Taiwan
1992	Master of Arts in Mathematics University of California Los Angeles, California
1993	Ph.D. candidate in Mathematics University of California Los Angeles, California
1991–1994	Teaching Assistant, Department of Mathematics University of California Los Angeles, California
1991–1995	Research Assistant, Department of Mathematics University of California Los Angeles, California

ABSTRACT OF THE DISSERTATION

Vortex Sheets, Singular Integrals and Steady Flows

by

Shin-Shin Kao

Doctor of Philosophy in Mathematics

University of California, Los Angeles, 1995

Professor Russel Caflisch, Chair

The first part of this thesis is devoted to the study of the "shortest-distance singularity", which appears as two vortex sheets approach each other. Desingularization methods for the singular integrals in the two-sheet Birkoff-Rott equation and in the PDE system by the potential and dipole distribution formulation are developed. It is concluded that the velocity field and the related functions have a discontinuity at the collision point, but the implication of this result is not understood yet. Numerical experiments showing that desingularization can reduce the errors due to this singularity, and ensure (at least) linear convergence independent of the separation distances are performed.

The second part is a numerical study of the stationary "flying droplet" with inner vorticity and outside circulation in a uniform flow. Symmetric solutions are obtained by the collocation method for different Atwood numbers and vorticity strength. The most limiting solution reached by our method is consistent with the presence of one or more stagnation points on the boundary and has

a circular-cap shape.

The introduction of the first problem is given in chapter 1, while that of the second problem is given in the beginning of chapter 5.

CHAPTER 1

Introduction

There has been much work devoted to the study of the dynamics of a single vortex sheet. Theoretically, Moore[24] showed that a small sinusoidal perturbation of the vortex sheet leads to a curvature singularity on the sheet at a finite time, due to the well-known Kelvin-Helmholtz instability. Numerical evidence consistent with Moore's results was first provided by Baker, Meiron and Orzag (1982)[2], then by Krasny (1986)[20], who controlled the machine roundoff error by Fourier filter method, and hence confirmed that the singularity is associated with the self-rollup on the sheet.

Our work is concerned with the singularity which comes up as two vortex sheets approach each other, about which there are relatively fewer studies. This "shortest-distance singularity" can be observed in many situations (fig.1.1); the most obvious example is the collision of two droplets. Another example is the evolution of the water waves subject to a small perturbation. The interface first becomes vertical, then turns over and breaks at a finite time. In the region close to the breaking point, we can find that the distance between two sets of particles, which are initially away from each other, decreases to zero as time evolves. The other example is given by an underwater bubble subject to gravity acceleration. In the experiment described by Walters and Davidson [15], where an approximately two-dimensional air bubble was produced in a thin vertical slab of water, it is found that the

initially circular bubble with radius 1 inch rose and formed a jet at the bottom. The jet was observed to approach the top of the bubble, but never touch it. The jet instead slows and extends so that the bubble becomes a horseshoe shape and eventually detaches into three parts. In this case, we see the tips of the horseshoe and the upper interface are closer and closer as time evolves.

The above phenomena has been numerically studied by many researchers using the boundary integral methods, such as Anderson[1], Baker, Meiron and Orzag [3], Baker and Shelley [5], Beale, Hou and Lowengrub [8], Krasny [19][20], Longuet-Higgin and Cokelet [13], Moore[25] and Shelley[28] for the interfacial water wave problem, and Baker and Moore [4], Blake, Doherty and Taib [10][11], Lungren and Mansour [22] for the rising bubble problem. The key advantage of using the boundary integral methods is that only quantities on the boundary need to be computed, due to irrotationality. However, as far as we know, there is no results by the boundary integral methods that can simulate the evolution up to the breaking time. The most visible practical limitation is the numerical instability. In order to obtain acceptable accuracy, the grid-spacing must be reasonably small, at least compared to the local scale of the flow, the radius of curvature of the surface or the distance between the two interfaces described in the previous paragraph. But as the mesh size is reduced, not only the total number of mesh points is increased like N^2 (for 3-D problems, or like N for 2-D problems), but also the time step must be decreased for the numerical stability. Beale, Hou and Lowengrub have derived theoretical results for the nonlinear stability and convergence of certain boundary integral methods for time-dependent water waves[9]. They also present

numerical results to show that a modified filtering (or smoothing) of the Fourier symbol of the derivative operator is necessary for stability. Analytical results for those in the rising bubble problem are not reported yet. Baker and Moore [4] calculated the shape and position of the two-dimensional rising bubble, but the codes failed when the jet and the lateral wall were close.

Since we have not been able to analyze the full time-dependent problem of a reconnecting interface, we restrict our attention to the singular integral that appears in the vortex sheet problem. First of all, we model the situation as interaction between two interfaces. Secondly, we assume that the profile of the two surfaces remain fairly smooth or unchanged as they approach each other. Thus the problem is reduced to a stationary problem, in which we take the distance between the two surfaces as a parameter and inspect how the equations change as the distance is decreased.

We use desingularization to analyze both the Birkoff-Rott equations and the PDE system derived by the potential and dipole description for the two vortex sheets. We find that the velocity filed *jumps* as the two interfaces meet, but the implication of this result is not well understood yet. Numerically we use the boundary integral method to compute the associated function values at various distances. We find that as the distance shrinks, the numerical scheme fails to converge due to the high variation in the integrands (we call it the shortest-distance singularity), as was reported by Baker and Shelley's [6] for the same test problem. But after doing desingularization, the ill behavior in the integrands is removed and hence (at least) linear convergence is guaranteed independent of the separation distance.

Chapter 2 derives the two-sheet Birkoff-Rott equations and introduces our desingularization method. Chapter 3 gives the PDE system derived from the dipole distribution and potential description, and the corresponding desingularized equations. Chapter 4 describes the test problem, which Baker and Shelley [6] worked on, the numerical algorithms with and without desingularization, the experimental results, and the conclusion of the whole work.

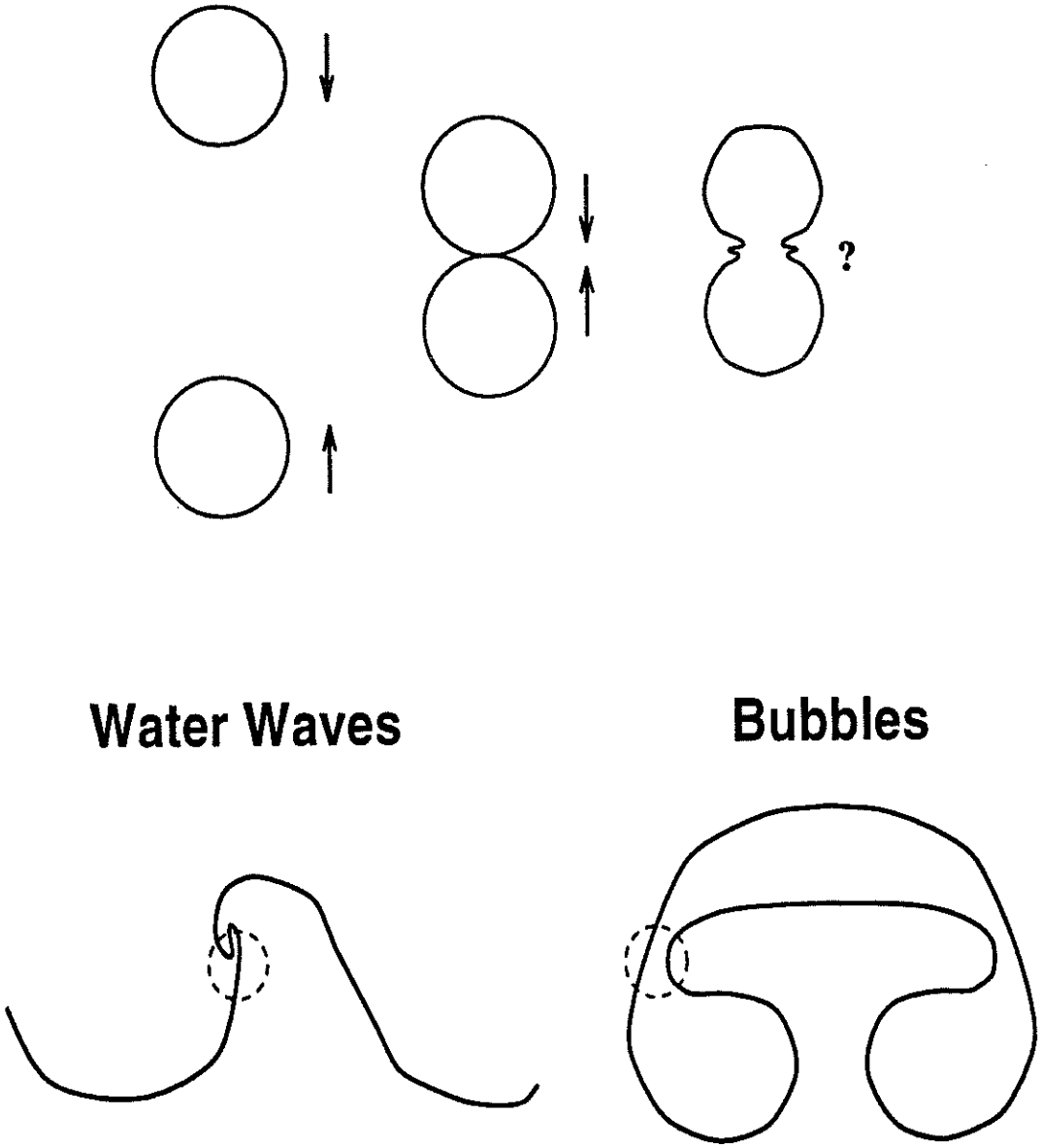

Figure 1.1: Examples of shortest-distance singularities.

CHAPTER 2

The Two-Sheet Birkoff-Rott Equation

We wish to describe the flow in which one fluid is separated into two parts by the other fluid, and the distance between the two separated parts is decreased. Both fluids are assumed to be homogeneous, inviscid, incompressible and irrotational for simplicity. Let ρ_i, U_i be density and velocity of the ith fluid, $i = 1, 2$. Then the situation is pictured below, where ρ is constant, $\nabla \cdot U_i = 0$ and $\nabla \times U_i = 0$.

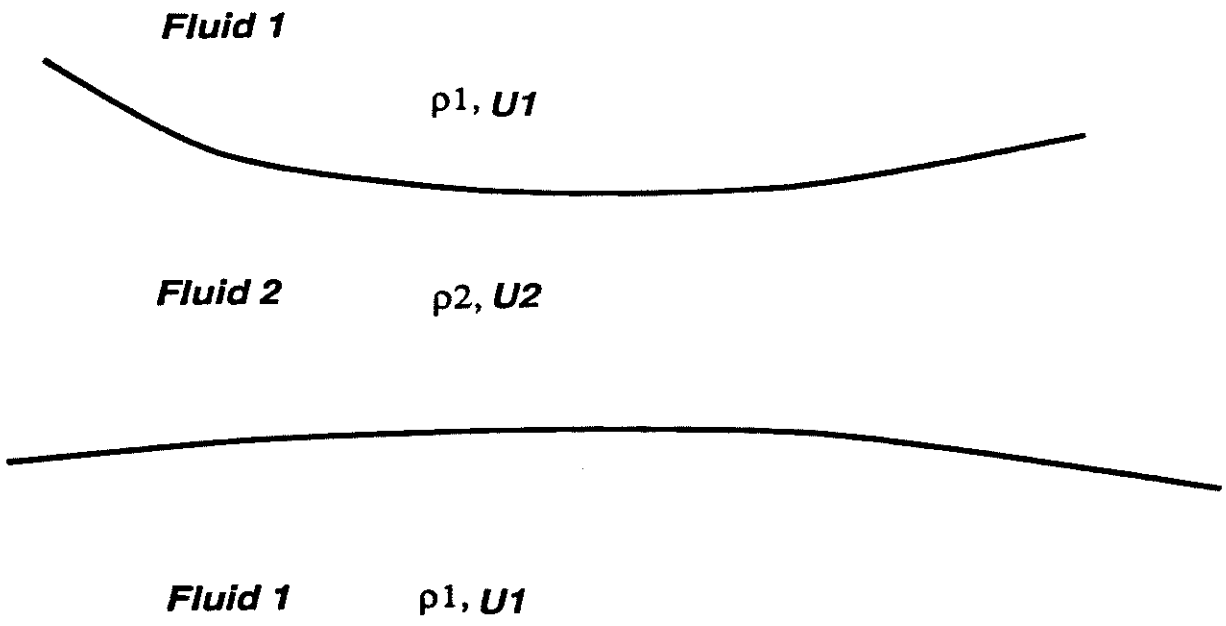

2.1 Derivation of the two-sheet Birkoff-Rott equation

Recall the derivation of 2-D single-sheet Birkoff-Rott equation. Consider an interface between two ideal fluids. In 2-D, it is a curve C represented by $Z = X + iY$. The normal velocity across C is continuous while the tangential velocity is discontinuous. Thus it is a vortex sheet.

Let $\vec{U}_+$ and $\vec{U}_-$ be the limiting velocities from above and below on the vortex sheet, and $\vec{U}$ be the velocity of the whole fluid, so $\vec{U}$ is discontinuous across C. Therefore,

$$\begin{aligned} \vec{\omega} &= \nabla \times \vec{U} \\ &= (-\partial_N(\vec{U} \cdot \vec{T}) + \partial_T(\vec{U} \cdot \vec{N})) \cdot \hat{k} \\ &= (-\vec{T} \cdot (\vec{U}_+ - \vec{U}_-)\delta_C) \cdot \hat{k} \\ &\equiv (\vec{T} \cdot \vec{\sigma}\delta_C) \cdot \hat{k}. \end{aligned} \tag{2.1}$$

Here $\hat{k}$ is the unit vector $(0, 0, 1)$, $\vec{T}$ and $\vec{N}$ are the tangential and normal vectors on C accordingly, and we define $\vec{\sigma} = -(\vec{U}_+ - \vec{U}_-)$.

On the other hand, we can express $\vec{U}$ in terms of $\vec{\omega}$:

$$\begin{aligned} \nabla \times \vec{\omega} &= \nabla \times \nabla \times \vec{U} \\ &= \nabla(\nabla \cdot \vec{U}) - \nabla \cdot (\nabla \vec{U}) \\ &= -\nabla^2 \vec{U}. \end{aligned}$$

We have used the assumption that $\nabla \cdot \vec{U} = 0$ above. This implies that

$$\begin{aligned} \vec{U}(\vec{x}) &= -\int_{R^2} G(\vec{x}-\vec{x'}) \nabla_{\vec{x'}} \times \vec{\omega}(\vec{x'}) d\vec{x'} \\ &= \int_{R^2} \nabla_{\vec{x'}} G(\vec{x}-\vec{x'}) \times \vec{\omega}(\vec{x'}) d\vec{x'}, \end{aligned} \tag{2.2}$$

where

$$G(\vec{x'}) = \frac{1}{2\pi} Log|\vec{x'}|.$$

Here G is the Green's function for R^2 and (2.2) is the Biot-Savart law.

Now we write $\vec{U}$ as $\vec{U} = (u, v, 0)$, then $\vec{\omega} = (0, 0, \omega)$, where $\omega = \omega(\vec{x}) = \partial_x v - \partial_y u$. Also $\vec{x} = (x, y)$ and $\vec{x'} = (x', y')$. Then (2.2) becomes

$$(u,v)(\vec{x}) = \frac{1}{2\pi} \int_{R^2} \frac{(-(y-y'),(x-x'))}{|\vec{x}-\vec{x'}|^2} \omega(\vec{x'}) d\vec{x'}. \tag{2.3}$$

From (2.1), $\omega = 0$ away from C, so (2.3) is rewritten as

$$(u,v)(\vec{x}) = \frac{1}{2\pi} \int_{C} \frac{(-(y-y'),(x-x'))}{|\vec{x}-\vec{x'}|^2} \vec{\sigma}(\vec{x'}) dC(\vec{x'}). \tag{2.4}$$

This gives the velocity for $\vec{x}$ away from C. Using complex variables such that $\vec{x}$ corresponds to $z = x + iy$, $\vec{x'}$ corresponds to $Z = X + iY$, and (u, v) corresponds to $u - iv$, (2.4) is:

$$(u - iv)(x,y) = \frac{1}{2\pi i} \int_{C} \frac{\vec{\sigma}(s)\, dC(s)}{z - Z(s)} \qquad for \quad (x,y) \in R^2 \setminus C. \tag{2.5}$$

In the two-sheet problem, the vorticity ω is confined to C, where $C = C_1 \cup C_2$ and they are parameterized by $C_1 = \{Z_1(s) = x_1(s) + iy_1(s) | s \in R\}$ and $C_2 = \{Z_2(s) = x_2(s) + iy_2(s) | s \in R\}$. By the same derivation, we have

$$(u - iv)(x,y) = \frac{1}{2\pi i}\left(\int_{C_1} \frac{\vec{\sigma}_1(s)\, dC_1(s)}{x + iy - Z_1(s)} + \int_{C_2} \frac{\vec{\sigma}_2(s')\, dC_2(s')}{x + iy - Z_2(s')}\right). \tag{2.6}$$

Writing (2.6) in terms of Lagrangian variables α, β, we get

$$\begin{aligned} (u - iv)(x,y) &= \frac{1}{2\pi i}\left(\int_{-\infty}^{\infty} \frac{\vec{\sigma}_1(\alpha) \cdot \vec{T}_1(\alpha)\, d\alpha}{x + iy - Z_1(\alpha)} + \int_{-\infty}^{\infty} \frac{\vec{\sigma}_2(\beta) \cdot \vec{T}_2(\beta)\, d\beta}{x + iy - Z_2(\beta)}\right) \\ &= \frac{1}{2\pi i}\left(\int_{-\infty}^{\infty} \frac{\gamma_1(\alpha)\, d\alpha}{x + iy - Z_1(\alpha)} + \int_{-\infty}^{\infty} \frac{\gamma_2(\beta)\, d\beta}{x + iy - Z_2(\beta)}\right), \end{aligned} \tag{2.7}$$

where

$$\gamma_1(\alpha) = \vec{\sigma}_1(\alpha) \cdot \vec{T}_1(\alpha) \quad , \quad \gamma_2(\beta) = \vec{\sigma}_2(\beta) \cdot \vec{T}_2(\beta).$$

The functions γ_1 , γ_2 are the "vortex sheet strengths" for sheet Z_1 , Z_2 respectively. This gives the velocity for (x,y) away from the two sheets.

To obtain the velocity for a point on the sheets, where $u - iv$ is discontinuous, we shall define the velocity at $(x_1(\alpha), y_1(\alpha)) \in C_1$ as the average of the velocities across the interface:

$$(u - iv)(x_1(\alpha), y_1(\alpha)) = \frac{(u_+ - iv_+) + (u_- - iv_-)}{2}, \tag{2.8}$$

where

$$\begin{aligned} u_+ - iv_+ &\equiv \lim_{\substack{(x,y) \to (x_1(\alpha), y_1(\alpha)) \text{ from} \\ \text{fluid above } C_1}} (u - iv)(x,y) \\ u_- - iv_- &\equiv \lim_{\substack{(x,y) \to (x_1(\alpha), y_1(\alpha)) \text{ from} \\ \text{fluid below } C_1}} (u - iv)(x,y). \end{aligned}$$

Using the *Plemelj* formula [23], we obtain

$$(u-iv)(x_1(\alpha),y_1(\alpha)) = \lim_{\epsilon\to 0}\frac{1}{2\pi i}\Big(\int_{-1/\epsilon}^{\alpha-\epsilon}+\int_{\alpha+\epsilon}^{1/\epsilon}\Big)\frac{\gamma_1(\alpha')\,d\alpha'}{x+iy-Z_1(\alpha')}+\frac{1}{2\pi i}\int_{-\infty}^{\infty}\frac{\gamma_2(\beta)\,d\beta}{x+iy-Z_2(\beta)}\Big)$$

$$= \frac{1}{2\pi i}\Big(PV\int_{-\infty}^{\infty}\frac{\gamma_1(\alpha')\,d\alpha'}{x+iy-Z_1(\alpha')}+\int_{-\infty}^{\infty}\frac{\gamma_2(\alpha')\,d\alpha'}{x+iy-Z_2(\alpha')}\Big). \tag{2.9}$$

From (2.8),(2.9),

$$\partial_t\overline{Z_1}(\alpha,t) = \frac{1}{2\pi i}PV\int_{-\infty}^{\infty}\frac{\gamma_1(\alpha',t)\,d\alpha'}{Z_1(\alpha,t)-Z_1(\alpha',t)}+\frac{1}{2\pi i}\int_{-\infty}^{\infty}\frac{\gamma_2(\alpha',t)\,d\alpha'}{Z_1(\alpha,t)-Z_2(\alpha',t)}. \tag{2.10}$$

By the same argument,

$$\partial_t\overline{Z_2}(\alpha,t) = \frac{1}{2\pi i}\int_{-\infty}^{\infty}\frac{\gamma_1(\alpha',t)\,d\alpha'}{Z_2(\alpha,t)-Z_1(\alpha',t)}+\frac{1}{2\pi i}PV\int_{-\infty}^{\infty}\frac{\gamma_2(\alpha',t)\,d\alpha'}{Z_2(\alpha,t)-Z_2(\alpha',t)}. \tag{2.11}$$

Here $PV\int$ denotes the Cauchy principal integral centered at α.

2.2 Desingularization

To simplify the notation, we denote the coupled system (2.10) and (2.11) by

$$\partial_t\overline{Z_m(\alpha,t)} = \frac{1}{2\pi i}PV\int_{-\infty}^{\infty}\frac{\gamma_m(\alpha',t)\,d\alpha'}{Z_m(\alpha,t)-Z_m(\alpha',t)}+\frac{1}{2\pi i}\int_{-\infty}^{\infty}\frac{\gamma_n(\alpha',t)\,d\alpha'}{Z_m(\alpha,t)-Z_n(\alpha',t)}$$

$$\equiv \frac{1}{2\pi i}I_{mm}(\alpha,t)+\frac{1}{2\pi i}I_{mn}(\alpha,t), \qquad \{_{m\neq n}^{m,n=1,2}. \tag{2.12}$$

The integral I_{mm} describes the influence on the velocity field $\partial_t Z_m(\alpha,t)$ of particles on the same sheet. It is the same integral as in the single-sheet Birkoff-Rott equation, where the integrand has a singularity at $\alpha'=\alpha$ at any t. The desingularization method was introduced by *Van de Vooran* in 1979[29], who replaces the singular integrand by a regular one and adds

an extra term which represents the contribution of the immediate neighborhood of the point considered. Here we study the singularity in the integrand of I_{mn}.

Let β be the singularity of I_{mn}, i.e., $Z_1(\alpha,t) - Z_2(\beta,t) = 0$. This implies that $\beta = \beta(\alpha,t)$. Since there is no real singularity unless the two sheets meet at a specific point at a certain t^*, $Im[\beta(\alpha,t)] \neq 0 \ \forall \alpha \in R$, except at the collision point at the critical time t^*. This is different from the real singularity $\alpha' = \alpha$ in the integrand of I_{mm}, which appears uniformly in time. We remove this complex singularity by the following theorems:

Theorem 2.1 *Suppose* $|Z_1(\alpha,t) - Z_2(\alpha,t)| \neq 0$ *for* $(\alpha,t) \in R \times [t_0,t^*]$ *except at* $\alpha = 0$, $t = t^*$. *Let*

$$f(\alpha,\alpha',t) = \frac{\gamma_2(\alpha',t)}{Z_1(\alpha,t) - Z_2(\alpha',t)} - \frac{\gamma_2(\alpha,t)}{Z_1(\alpha,t) - Z_2(\alpha,t) + \partial_\alpha Z_2(\alpha,t)(\alpha - \alpha')}.$$

Assume that:

(A1) For any $t_0 \leq t \leq t^*$, Z_j, γ_j *are analytic (uniformly in t) in the strip*

$$\{\alpha \in C, |Im(\alpha)| < \lambda\}, \ \lambda > 0.$$

(A2) $Z_j(\alpha + 2\pi, t) = Z_j(\alpha,t) + 2\pi$, $\gamma_j(\alpha + 2\pi, t) = \gamma_j(\alpha,t)$.

(A3) $Z_2(\alpha,t) = \overline{Z_1(\alpha,t)}$, $\forall \alpha \in R$, $t \in [t_0,t^*]$

(A4) $Re[\partial_\alpha Z_j(\alpha,t)] \geq \mu > 0 \quad \forall \alpha$, $t \in [t_0,t^*]$,

Then $f(\alpha,\alpha',t)$ *is uniformly bounded for* $(\alpha,\alpha',t) \in R \times R \times [t_0,t^*]$.

We have assumed in $(A1)$ that the two sheets are fairly smooth for $t_0 \leq t \leq t^*$, so we can consider t as a parameter controlling the distance between the two sheets in a stationary problem. To focus on the shortest-distance singularity of the two sheets, we suppose

they are so close to each other that no self-rollup is present before they meet. That is, $Re[\partial\alpha Z_j(\alpha,t)] \geq \mu > 0$ in $(A4)$ or $Z_j(\alpha,t) = \alpha + i \cdot Y(\alpha,t)$, where $Y(\alpha,t)$ is real for all $(\alpha,t) \in R \times [t_0,t^*]$. Furthermore, let these two sheets be symmetric to each other for simplicity , as in $(A3)$. The proof is in appendix; we locate the complex singularities of both terms in $f(\alpha,\alpha',t)$ and find them very close to each other. Thus the function value of each term get canceled on the real axis.

Proposition 2.1 *Under the same condition and assumptions in Theorem 2.1,*

$$\lim_{\alpha'\to\alpha} \frac{\gamma_2(\alpha',t)}{Z_1(\alpha,t) - Z_2(\alpha',t)} - \frac{\gamma_2(\alpha,t)}{Z_1(\alpha,t) - Z_2(\alpha,t) + \partial_\alpha Z_2(\alpha-\alpha')}$$

exists and is a finite number at the collision point $\alpha = 0$ at $t = t^*$.

proof: At $t = t^*$, $\alpha = 0$, $Z_1(0,t^*) = Z_2(0,t^*)$ by assumption. "t^*" is dropped to save space.

$$\begin{aligned} & \lim_{\alpha'\to\alpha} \frac{\gamma_2(\alpha')}{Z_1(0) - Z_1(\alpha')} - \frac{\gamma_2(0)}{Z_1(0) - Z_2(0) + \partial\alpha Z_2(0)(0-\alpha')} \\ = & \lim_{\alpha'\to\alpha} \frac{\gamma_2(\alpha')}{Z_2(0) - Z_2(\alpha')} - \frac{\gamma_2(0)}{\partial\alpha Z_2(0)(0-\alpha')} \\ = & \left(\frac{\gamma_2\partial^2_{\alpha\alpha} Z_2 - 2\partial_\alpha\gamma_2\partial_\alpha Z_2}{2(\partial_\alpha Z_2)^2}\right)(0), \end{aligned}$$

which is a finite number by assumption.

Theorem 2.2 *When the condition in Theorem 2.1 and the assumptions (A1)-(A4) hold,*

$$I \equiv \int_{-\infty}^{\infty} \frac{\gamma_2(\alpha,t)\, d\alpha'}{Z_1(\alpha,t) - Z_2(\alpha,t) + \partial_\alpha Z_2(\alpha,t)(\alpha-\alpha')} \tag{2.13}$$

is continuous everywhere for $(\alpha,t) \in R \times [t_0,t^*]$ except at $\alpha = 0$, $t = t^*$.

proof: The integral in (2.13) is a regular integral because

$$\text{when } t < t^*, \quad \begin{cases} \alpha' \neq \alpha & Re[\partial_\alpha Z_2(\alpha,t)](\alpha-\alpha') \neq 0 \\ \alpha' = \alpha & Z_1(\alpha,t) - Z_2(\alpha,t) \neq 0 \end{cases}$$

$$\text{when } t = t^*,\ \alpha \neq 0 \quad \begin{cases} \alpha' \neq \alpha & Re[\partial_\alpha Z_2(\alpha,t^*)](\alpha-\alpha') \neq 0 \\ \alpha' = \alpha & Z_1(\alpha,t) - Z_2(\alpha,t) \neq 0. \end{cases}$$

Only at $t = t^*$, $\alpha' = \alpha = 0$, the denominator vanishes, but it is shown to be nonsingular in Proposition 2.1. So

$$\begin{aligned} & \int_{-\infty}^{\infty} \frac{\gamma_2(\alpha,t)\,d\alpha'}{Z_1(\alpha,t) - Z_2(\alpha,t) + \partial_\alpha Z_2(\alpha,t)(\alpha-\alpha')} \\ = \ & \frac{\gamma_2(\alpha,t)}{\partial_\alpha Z_2(\alpha,t)} \int_{-\infty}^{\infty} \frac{d\alpha'}{\frac{Z_1-Z_2}{\partial_\alpha Z_2}(\alpha,t) + \alpha - \alpha'} \\ = \ & \frac{\gamma_2(\alpha,t)}{\partial_\alpha Z_2(\alpha,t)} PV \int_{-\infty}^{\infty} \frac{d\beta'}{i \cdot Im[\frac{Z_1-Z_2}{\partial_\alpha Z_2}(\alpha,t)] - \beta'} \end{aligned} \tag{2.14}$$

Here we do change of variables by $\beta' = \alpha' - Re[\frac{Z_1-Z_2}{\partial_\alpha Z_2}(\alpha,t)] - \alpha$ and the Cauchy principal integral is centered at 0 in particular. Therefore, the integral in (2.13) is approximately

$$I \simeq PV \int_{-\infty}^{\infty} \frac{d\alpha'}{\alpha' - ia} = \begin{cases} \pi i & if \quad a > 0, a \neq 0 \\ 0 & if \quad a = 0 \end{cases}$$

Since $a = Im[\frac{(Z_1-Z_2)(\alpha,t)}{\partial\alpha Z_2(\alpha,t)}] \neq 0$ except at $\alpha = 0$, $t = t^*$, this implies the velocity field jumps at the collision point. The implications of this conclusion are not understood yet.

CHAPTER 3

The Potential Description of the Two-Sheet Problem

In this chapter, we want to study the interacting vortex sheets from a different formulation. That is, the dipole distribution and potential description. The conclusion that associated functions have discontinuity at the collision point is obtained again.

3.1 Derivation of Formulation

First recall the 2-D exterior problem [6], i.e. the single-sheet formulation. Consider a bubble staying in ideal fluid. Let the boundary of the bubble be denoted by ∂D, where D is assumed simple connected and let ϕ be the potential function of the surrounding fluid. Then we have

$$\nabla^2\phi = 0 \qquad \forall (x,y) \in D^c. \tag{3.1}$$

Assuming that the bubble volume is conserved, the solution of ϕ is given by the following formula [21]:

$$\phi(p) = PV \int_{\partial D} \mu(q) \frac{\partial}{\partial N} G(p,q) dq - \frac{\mu(p)}{2} \quad on\ \partial D, \tag{3.2}$$

where G is the Green's function satisfying $\nabla_q^2 G = \delta_p(q)$ and μ is the dipole distribution function. N is the normal vector pointing into D. The principal value integral is acquired by using Plemelj formula [23].

The integral formulation for ϕ when D is multi-connected, $D = D_1 \cup D_2$, is obtained by the same derivation as for D that is simple connected (*fig 3.1*).

$$(3.3)\ \phi_1(p_1) = PV \int_{\partial D_1} \mu_1(q) \frac{\partial G}{\partial N_1}(p_1, q) dq + \int_{\partial D_2} \mu_2(q) \frac{\partial G}{\partial N_2}(p_1, q) dq + \frac{\mu_1(p_1)}{2} \quad p_1 \in \partial D_1,$$

$$(3.4)\ \phi_2(p_2) = PV \int_{\partial D_2} \mu_2(q) \frac{\partial G}{\partial N_2}(p_2, q) dq + \int_{\partial D_1} \mu_1(q) \frac{\partial G}{\partial N_1}(p_2, q) dq + \frac{\mu_2(p_2)}{2} \quad p_2 \in \partial D_2.$$

Here μ_m is the dipole distribution defined on the m-th boundary, and N_m denotes the normal pointing to D^c on the ∂D_m, ∂D_1 and ∂D_2 are parameterized counter-clockwise by $(X_1(q), Y_1(q))$ and $(X_2(q), Y_2(q))$.

The 2-D Green's function G is given by $\frac{1}{4 \cdot \pi} \log[(X - X_m)^2 + (Y - Y_m)^2]$, where (X_m, Y_m) lies on the m-th boundary ∂D_m. Denote $\frac{\partial G}{\partial N_m}(p, q)$, $p \in \partial D_n$, $q \in \partial D_m$, by K_{nm}. We have

$$(3.5)\ K_{nm}(p, q) = \frac{1}{2\pi} \frac{X'_m(q)[Y_n(p) - Y_m(q)] - Y'_m(q)[X_n(p) - X_m(q)]}{[X_n(p) - X_m(q)]^2 + [Y_n(p) - Y_m(q)]^2} \quad n, m = 1, 2.$$

Here $X'_m = \frac{\partial X_m}{\partial q}$, and $Y'_m = \frac{\partial Y_m}{\partial q}$.

To simplify the symbols, rewrite the system (3.3), (3.4) as

$$\begin{aligned} \phi_m(p) &= PV \int_{\partial D_m} \mu_m(q) K_{mm}(p, q) dq + \int_{\partial D_n} \mu_n(q) K_{mn}(p, q) dq + \frac{\mu_n(p)}{2} \\ (3.6) \qquad &= I_{mm}(p) + I_{mn}(p) + \frac{\mu_n(p)}{2} \qquad \begin{cases} m,n=1,2 \\ m \neq n \end{cases}. \end{aligned}$$

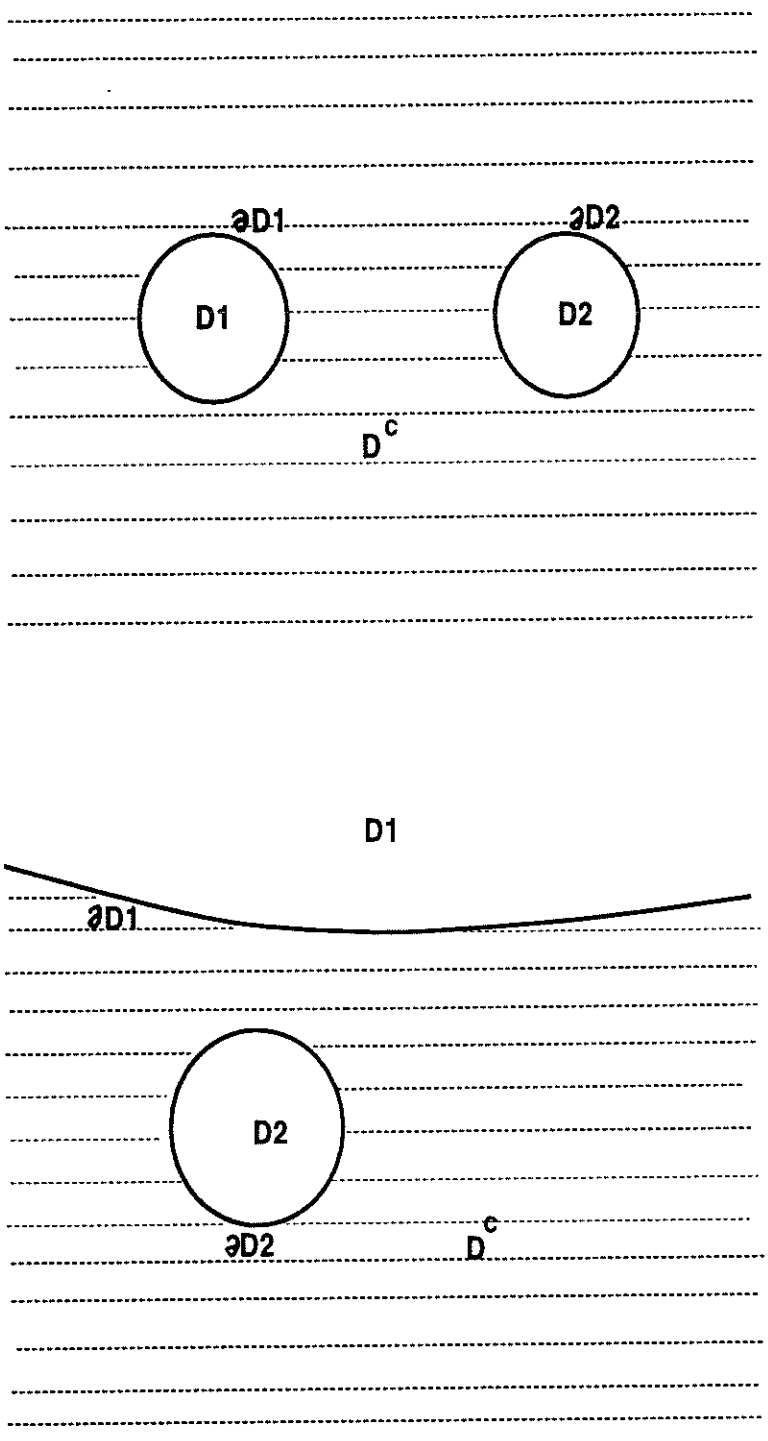

Figure 3.1: Examples of multi-domain situation.

3.2 Desingularization

To study the singularities in $I_{mm}(p)$ and $I_{mn}(p)$ in (3.6), we investigate the behavior of the kernels, $K_{mm}(p,q)$ and $K_{mn}(p,q)$.

Proposition 3.1

$$\begin{aligned}\lim_{q\to p} K_{mm}(p,q) &= \frac{1}{4\pi}\cdot\frac{(X'_m Y''_m - Y'_m X''_m)}{(Y'_m)^2+(X'_m)^2}(p)\\ &= \frac{1}{4\pi}\cdot Curvature(p)\cdot((Y'_m)^2+(X'_m)^2)^{1/2}(p).\end{aligned}$$

We conclude that $I_{mm}(p)$ has a regular integrand as long as μ_m, m=1, 2, are well-behaved, and the boundaries are smooth and have finite curvature.

The singularity in $I_{mn}(p)$ is similar to that in the two-sheet Birkoff-Rott equation. It is not present until the two interfaces meet, since $K_{mn}(p)$ is not singular until there is a specific p where $(X_m(p), Y_m(p)) = (X_n(p), Y_n(p))$. We first remove this "shortest-distance" singularity for the case where ∂D_1 and ∂D_2 form two concentric circles, then extend the desingularization method to more general problems(*fig 3.2*).

Proposition 3.2 *Let* $\partial D_1 = \{(X_1,Y_1)|X_1 = \cos(p), Y_1 = \sin(p), 0 \le p \le 2\pi\}$ *and* $\partial D_2 = \{(X_2,Y_2)|X_2 = \rho\cos(q), Y_2 = \rho\sin(q), 0 \le q \le 2\pi\}$, *then*

$$\begin{aligned}&(a)\quad \textstyle\int_0^{2\pi} K_{21}(p,q)dq = 0 && \rho > 1\\ &(b)\quad \textstyle\int_0^{2\pi} K_{21}(p,q)dq = \frac{1}{2} && \rho = 1\\ &(c)\quad \textstyle\int_0^{2\pi} K_{21}(p,q)dq = 1 && \rho < 1.\end{aligned}$$

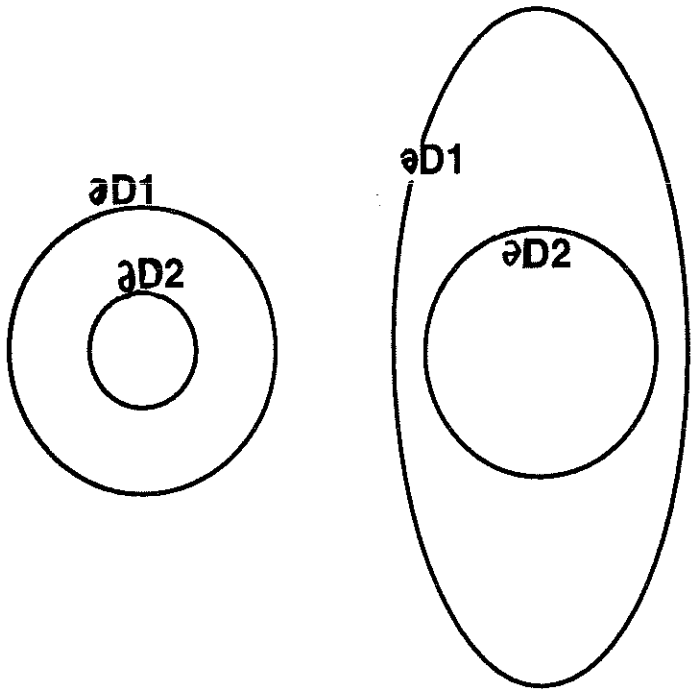

Figure 3.2: ∂D_1, ∂D_2 in Theorems.

proof: $K_{21}(p,q)$ is given by (2.7):

$$K_{21}(p,q) = \frac{1}{2\pi}\frac{X_1'(q)(Y_2(p)-Y_1(q)) - Y_1'(q)(X_2(p)-X_1(q))}{(X_1(q)-X_2(p))^2+(Y_1(q)-Y_2(p))^2},$$

or

$$K_\rho(\theta) = \frac{1}{2\pi}\cdot\frac{1-\rho\cos\theta}{1+\rho^2-2\rho\cos\theta}, \qquad \theta = p-q. \tag{3.7}$$

This is the Poisson kernel for the unit circle. Proof of property (c) can be found in many references (e.g. [14]). Proof of properties (a) and (b) is an application of the Cauchy integral theorem. The Poisson kernel for more general boundaries which are homotopic to the unit circle has these features as well. That is,

Proposition 3.3 *Let $\partial D = \{(X,Y)(q) | 0 \le q \le 2\pi\}$, which is homotopic to the unit circle. Let $\vec{z_0}$ refer to some point in the plane, and let d be the distance between $\vec{z_0}$ and ∂D. We say $d > 0$ if $\vec{z_0}$ is outside ∂D and $d < 0$ if $\vec{z_0}$ is inside ∂D. Let K denote the Poisson kernel for D. Then*

$$\begin{aligned} (a) \quad & \int_0^{2\pi} K(\vec{z_0}, q)dq = 0 && d > 0 \\ (b) \quad & \int_0^{2\pi} K(\vec{z_0}, q)dq = \frac{1}{2} && d = 0 \\ (c) \quad & \int_0^{2\pi} K(\vec{z_0}, q)dq = 1 && d < 1. \end{aligned}$$

Theorem 3.1 *Define ∂D_1 and ∂D_2 as in Proposition 3.2. $\rho \le 1$.*

(a) Let $\max_q |K_{21}(p,q)| = |K_{21}(p,p^*)|$, then $p^* = p$, and

$$\begin{aligned} (3.8) \qquad & \int_0^{2\pi} \mu_1(q) K_{21}(p,q) dq \\ = & \int_0^{2\pi} [\mu_1(q) - \mu_1(p^*) - \mu_1'(p^*)\sin(q-p^*)] K_{21}(p,q) dq + C_\rho \cdot \mu_1(p^*), \end{aligned}$$

where $C_\rho = 1$ for $\rho < 1$ and $C_1 = \frac{1}{2}$.

(b) If $L \ge 2$, then for any given $p \in [0, 2\pi]$, there exists M, independent of p, q, and ρ, such that

$$\frac{d}{dq}((q-p)^L \cdot K_{21}(p,q)) \le M.$$

proof:

(a) $\frac{\partial K_{21}(p,q)}{\partial q} = 0$ implies $q = p$. (3.8) is true by Proposition 3.2 (b),(c). That is,

let $\theta = q - p$, then

$$\begin{aligned}
\max_{\theta} |K_\rho(\theta)| &= |K_\rho(0)|, \\
\int_{\partial D_1} \mu_1(\theta) K_\rho(\theta) d\theta &= \int_{\partial D_1} [\mu_1(\theta) - \mu_1(0) - \mu_1'(0)\sin(\theta)] K_\rho(\theta) d\theta + C_\rho \cdot \mu_1(0).
\end{aligned}$$

It is observed that $K_\rho(0) = \frac{1}{2\pi}\frac{1}{1-\rho} \to +\infty$ as $\rho \to 1$. Furthermore,

$$\begin{aligned}
\theta \cdot K_\rho(\theta) &= \frac{1}{2\pi}\theta \cdot \frac{1-\rho\cos\theta}{1+\rho^2-2\rho\cos\theta} \\
\frac{\partial}{\partial\theta}(\theta \cdot K_\rho(\theta)) &= \frac{1}{2\pi}\frac{\rho\sin\theta(\rho^2-1)\theta}{(1+\rho^2-2\rho\cos\theta)^2} + \frac{1}{2\pi}\frac{1-\rho\cos\theta}{1+\rho^2-2\rho\cos\theta}
\end{aligned}$$

At $\theta = 0$, $\frac{\partial}{\partial\theta}(\theta \cdot K_\rho(\theta))|_{\theta=0} = \frac{1}{2\pi}\frac{1}{1-\rho}$ tends to $+\infty$ as ρ goes to 1.

(b) It suffices to show that $\frac{\partial}{\partial\theta}(\theta^2 \cdot K_\rho(\theta))$ is uniformly bounded.

$$\begin{aligned}
\theta^2 \cdot K_\rho(\theta) &= \frac{1}{2\pi}\theta^2 \cdot \frac{1-\rho\cos\theta}{1+\rho^2-2\rho\cos\theta} \\
\frac{\partial}{\partial\theta}(\theta^2 \cdot K_\rho(\theta)) &= \frac{1}{2\pi}\frac{\rho\sin\theta(\rho^2-1)\theta^2}{(1+\rho^2-2\rho\cos\theta)^2} + \frac{1}{2\pi}\frac{1-\rho\cos\theta}{1+\rho^2-2\rho\cos\theta}\cdot 2\theta \\
&= \frac{1}{2\pi}(A+B) \qquad (3.9)
\end{aligned}$$

Given $\epsilon > 0$, $\exists\, \delta > 0$, s.t. $\forall\, |\theta| < \delta$, we have

$$|\frac{\sin\theta}{\theta} - 1| < \epsilon \quad , \quad |\frac{\cos\theta - 1}{\theta^2} + \frac{1}{2}| < \epsilon. \qquad (3.10)$$

Since we are interested in the case where two boundaries are very close, we may assume $|1-\rho| < \delta < \frac{1}{2}$ and $|\theta| < \delta$. We prove that both A and B in (3.9) are uniformly bounded for $1-\rho \geq |\theta|$ and for $1-\rho < |\theta|$.

(Case-1) $1-\rho \geq |\theta|$:

$$\begin{aligned}
1+\rho^2-2\rho\cos\theta &= (1-\rho)^2 + 2\rho(1-\cos\theta) \\
&\geq (1-\rho)^2
\end{aligned}$$

Therefore,

$$\begin{aligned} |A| &\leq |\frac{\rho(\rho^2-1)\theta^2 \cdot \sin\theta}{(1-\rho)^4}| \\ &= |\frac{\rho(\rho+1)\theta^3 \cdot \frac{\sin\theta}{\theta}}{(1-\rho)^3}| \\ &\leq |\rho(\rho+1) \cdot \frac{\sin\theta}{\theta}|. \end{aligned}$$

$|\theta| \leq 1-\rho < \delta$ implies that $|\frac{\sin\theta}{\theta}| < 1+\epsilon$ by (3.10), so $|A| \leq 2 \cdot (1+\epsilon)$. For B,

$$\begin{aligned} |B| &\leq |\frac{1-\rho\cos\theta}{(1-\rho)^2} \cdot 2\theta| \\ &= |\frac{1-\rho+\rho\theta^2(\frac{1-\cos\theta}{\theta^2})}{(1-\rho)^2} \cdot 2\theta| \\ &\leq |\frac{2\theta}{1-\rho}| + |\frac{2\rho\,\theta^3(\frac{1-\cos\theta}{\theta^2})}{(1-\rho)^2}| \\ &\leq 2 + 2\rho\,|\theta \cdot (\frac{1-\cos\theta}{\theta^2})|. \end{aligned}$$

$|\theta| \leq 1-\rho < \delta$ implies that $|\frac{1-\cos\theta}{\theta^2}| < \frac{1}{2}+\epsilon$ by (3.10), so

$$\begin{aligned} |B| &\leq 2 + 2\rho \cdot \delta \cdot (\frac{1}{2}+\epsilon) \\ &\leq 2 + 1 \cdot (1+2\epsilon) \\ &= 3 + 2\epsilon. \end{aligned}$$

Thus $|A+B| \leq 5+4\epsilon$.

(Case-2) $1-\rho < |\theta|$:

$$\begin{aligned} 1+\rho^2-2\rho\cos\theta &= (1-\rho)^2 + 2\rho \cdot (1-\cos\theta) \\ &\geq 2\rho \cdot (1-\cos\theta) \end{aligned} \tag{3.11}$$

Therefore,

$$\begin{aligned}
|A| &\leq |\frac{\rho \sin\theta \cdot (\rho^2-1)\theta^2}{(2\rho(1-\cos\theta))^2}| \\
&= |\frac{\rho(1-\rho^2)\cdot \frac{\sin\theta}{\theta}\theta^3}{4\rho^2\theta^4(\frac{(1-cos\theta)}{\theta^2})^2}| \\
&= |\frac{(1-\rho^2)\cdot \frac{\sin\theta}{\theta}}{4\rho\theta(\frac{(1-cos\theta)}{\theta^2})^2}| \\
&\leq \frac{1+\rho}{4\rho}\cdot|\frac{\frac{\sin\theta}{\theta}}{(\frac{(1-cos\theta)}{\theta^2})^2}|.
\end{aligned}$$

$|\theta| < \delta$ implies that $|\frac{\sin\theta}{\theta}| < 1+\epsilon$ and $|\frac{1-\cos\theta}{\theta^2}| \geq \frac{1}{2}-\epsilon$, so

$$\begin{aligned}
|A| &\leq \frac{1+\rho}{4\rho}\cdot\frac{1+\epsilon}{(\frac{1}{2}-\epsilon)^2} \\
&\leq \frac{1}{2(1-\delta)}\cdot\frac{1+\epsilon}{(\frac{1}{2}-\epsilon)^2} \qquad (3.12) \\
&< \frac{1+\epsilon}{(\frac{1}{2}-\epsilon)^2}. \qquad (3.13)
\end{aligned}$$

Inequality (3.12) holds since $1+\rho < 2$ and $1-\rho < \delta$. Inequality (3.13) holds by the assumption that $\delta < \frac{1}{2}$. Also by (3.11),

$$\begin{aligned}
|B| &\leq |\frac{1-\rho\cos\theta}{2\rho(1-\cos\theta)}\cdot 2\theta| \\
&= |\frac{1-\rho+\rho(1-\cos\theta)}{2\rho(1-\cos\theta)}\cdot 2\theta| \\
&\leq \frac{1-\rho}{\rho}\cdot|\frac{\frac{1}{\theta}}{\frac{1-\cos\theta}{\theta^2}}| + |\theta| \\
&\leq \frac{1}{\rho}\cdot\frac{1}{\frac{1}{2}-\epsilon}+\delta \qquad (3.14) \\
&\leq \frac{1}{1-\delta}\cdot\frac{1}{\frac{1}{2}-\epsilon}+\delta \\
&< \frac{1}{1-2\epsilon}+\frac{1}{2}.
\end{aligned}$$

Inequality (3.14) is true because $\frac{1-\cos\theta}{\theta^2} \geq \frac{1}{2} - \epsilon$ and $\frac{1-\rho}{|\theta|} < 1$. Hence we get $|A+B| \leq \frac{1+\epsilon}{(\frac{1}{2}-\epsilon)^2} + \frac{1}{1-2\epsilon} + \frac{1}{2}$. Now we have bounds independent of ρ in both case. This proves the uniform boundedness. (b) also implies that the first derivative of the integrand on the r.h.s of (3.8) is bounded independent of ρ.

From (a) and (b), the nature of I_{mn} changes discontinuously at the contact point since C_ρ jumps from 1 as $\rho < 1$ to $\frac{1}{2}$ as $\rho = 1$. This agrees with the results by studying the two-sheet Birkoff-Rott equation.

The following proposition and theorem for K_{12} are established by the same argument.

Proposition 3.4 *Define ∂D_1 and ∂D_2 as in Proposition 3.2.*

$$\begin{aligned} (a)\quad & \int_0^{2\pi} K_{12}(p,q)dq = 1 && \rho > 1 \\ (b)\quad & \int_0^{2\pi} K_{12}(p,q)dq = \frac{1}{2} && \rho = 1 \\ (c)\quad & \int_0^{2\pi} K_{12}(p,q)dq = 0 && \rho < 1. \end{aligned}$$

Theorem 3.2 *Define ∂D_1 and ∂D_2 as in Proposition 3.2. $\rho \leq 1$.*

(a) Let $\max_q |K_{12}(p,q)| = |K_{12}(p,p^*)|$, then $p^* = p$, and

$$\begin{aligned} (3.15)\qquad & \int_0^{2\pi} \mu_2(q) K_{12}(p,q)dq \\ = & \int_0^{2\pi} [\mu_2(q) - \mu_2(p^*) - \mu_2'(p^*)\sin(q-p^*)] K_{12}(p,q)dq + C_\rho \cdot \mu_2(p^*), \end{aligned}$$

where $C_\rho = 0$ for $\rho < 1$ and $C_1 = \frac{1}{2}$.

(b) If $L \geq 2$, then for any given $p \in [0, 2\pi]$, there exists M independent of p, q, and ρ such that

$$\frac{d}{dq}((q-p)^L \cdot K_{12}(p,q)) \leq M.$$

We are able to establish the following proposition and theorem for the more arbitrary domain case (fig.3.2 right):

Corollary 3.1 *Let* $\partial D_1 = \{(X_1, Y_1) | X_1 = a\cos(p), Y_1 = b\sin(p), 0 \le p \le 2\pi\}$, *here* $a > 1$, $b > 1$; *and* $\partial D_2 = \{(X_2, Y_2) | X_2 = \cos(q), Y_2 = \sin(q), 0 \le q \le 2\pi\}$.

Then at $p = 0$ *or* $p = \pi$,

$$\begin{aligned} \int_0^{2\pi} K_{21}(p,q)dq &= 0 \qquad a > 1 \\ \int_0^{2\pi} K_{21}(p,q)dq &= \frac{1}{2} \qquad a = 1 \\ \int_0^{2\pi} K_{21}(p,q)dq &= 1 \qquad a < 1. \end{aligned}$$

For all $p \neq 0, \pi$,

$$\int_0^{2\pi} K_{21}(p,q)dq = 0 \qquad \forall a.$$

Corollary 3.2 *Define* ∂D_1 *and* ∂D_2 *as in Corollary 3.1. Let* $b > 1$ *be fixed and* $a > 1$, $a \to 1$, *but* $a \neq 1$.

(a) $\max_q |K_{21}(p,q)| = |K_{21}(p,p^*)|$. *Then at* $p = 0$ *and* $p = \pi$, $p^* = p$.

(b) For all $0 \le p \le 2\pi$,

$$\int_0^{2\pi} \mu_1(q) K_{21}(p,q)dq = \int_0^{2\pi} [\mu_1(q) - \mu_1(p^*) - \mu_1'(p^*)\sin(q-p^*)\alpha_p(q)] K_{21}(p,q)dq,$$

where α *satisfies*

$$\alpha_p(p^*) = 1 \tag{3.16}$$

$$\int_0^{2\pi} \alpha_p(q) K_{21}(p,q) \cdot \sin(q-p^*)dq = 0. \tag{3.17}$$

(c) If $L \geq 2$, then for any given $p \in [0, 2\pi]$, there exists M independent of p, q, and a such that

$$\frac{d}{dq}((q-p)^L \cdot K_{21}(p,q)) \leq M.$$

CHAPTER 4

Desingularization in Boundary Integral Method

We implement the idea of desingularization in the Boundary Integral Method for problems in multi-connected domain. The numerical experiments are performed on a test problem, in which the function values are computed on an annulus with thickness tending to zero to explore the appearance of the shortest-distance singularity. It is shown that desingularization helps to reduce the numerical errors greatly.

4.1 Boundary Integral Method in Stationary Problem

For a simple-connected domain, we use the following equation in the Boundary Integral Method:

$$\phi(p) = PV \int_{\partial D} \mu(q) \frac{\partial}{\partial \vec{N}} G(p,q) dq - \frac{\mu(p)}{2} \quad on\ \partial D. \tag{4.1}$$

We observe that this is a Fredholm integral form of the second kind of μ whenever ϕ is given. Kellogg(1929) proved that all eigenvalues of the associated homogeneous equation are real and distinct with absolute value ≥ 1, as required by the Fredholm theory. Thus one can construct μ by doing direct iteration on (4.1). Since the solution is unique up to a constant addition, one can fix $\mu(p_0) = 0$ at a certain p_0 for convergence.

The Boundary Integral Method for multi-connected domains is given in "Boundary In-

tegral Techniques for Multi-connected Domains" by G.R. Baker and M.J. Shelley [6]. The main difference from that for simple domains is that the iteration is done on a coupled system (3.3), (3.4) to compute μ_1 and μ_2 on both boundaries.

More specifically, define two operators T_1, T_2 as follows:

$$\begin{aligned} T_1(\mu_1,\mu_2)(p) &= -2PV\int_{\partial D_1}\mu_1(q)K_{11}(p,q)dq - 2\int_{\partial D_2}\mu_2(q)K_{12}(p,q)dq \\ &+ 2\cdot\phi_1(p) \\ T_2(\mu_1,\mu_2)(p) &= 2\int_{\partial D_1}\mu_1(q)K_{21}(p,q)dq + 2PV\int_{\partial D_2}\mu_2(q)K_{22}(p,q)dq \\ &- 2\cdot\phi_2(p). \end{aligned}$$

Then the iteration scheme becomes

$$\mu_1^{(n+1)}(p) = T_1(\mu_1^{(n)},\mu_2^{(n)})(p) - T_1(\mu_1^{(n)},\mu_2^{(n)})(p_0), \tag{4.2}$$

$$\mu_2^{(n+1)}(p) = T_2(\mu_1^{(n)},\mu_2^{(n)})(p) - T_2(\mu_1^{(n)},\mu_2^{(n)})(p_0), \tag{4.3}$$

where K_{mn} are given in (3.5).

4.2 Test Problem– Two Concentric Circles

To understand how this shortest-distance singularity influences the Boundary Integral Method, we work on a test problem of two concentric circles (fig.3.2 left):

$$\begin{aligned} \partial D_1 &= \{(X_1,Y_1)|X_1 = R_1\cos(q), Y_1 = R_1\sin(q)\} \\ \partial D_2 &= \{(X_2,Y_2)|X_2 = R_2\cos(q), Y_2 = R_2\sin(q)\}, \end{aligned}$$

where R_1 and R_2 are constants. In polar coordinates, a solution to

$$\nabla^2\phi(r,\theta) = 0 \quad R_2 \le r \le R_1$$

is given by

$$\phi(r,\theta) \;=\; ((\frac{r}{R_1})^m - (\frac{R_2}{r})^m) \cdot \cos(m\theta).$$

Restricted to the boundaries, we have

$$\phi_1(p) = (1 - (\frac{R_2}{R_1})^m) \cdot cos(m \cdot p)$$
$$\phi_2(p) = ((\frac{R_2}{R_1})^m - 1) \cdot cos(m \cdot p)$$

and the exact solutions for the dipole distribution μ_1, μ_2 satisfying $\mu_1(0) = 0$, $\mu_2(0) = 0$ are

$$\mu_1(p) = \mu_2(p) = 2 \cdot [\cos(m \cdot p) - 1].$$

Assuming that ϕ_1, ϕ_2 are given functions, one then constructs μ_1, μ_2 by (4.2) and (4.3).

4.3 Desingularization

Our previous investigation about the behavior of the kernel K_{mn} shows that K_{mm}, m = 1, 2, is regular as long as the boundary is smooth and well separated. However, K_{mn}, $m \neq n$, becomes singular as the distance between the two interfaces decreases to zero. The strong variation in the integrands will lead to large errors as we approximate the integrals by numerical integration methods such as trapezoidal rule. The discrepancy errors accumulate to prevent our iteration scheme from converging. In the test problem, this occurs as R_1 tends

to R_2. So we improve the iteration scheme by defining new operators S_1 and S_2 as follows:

$$\begin{aligned} S_1(\mu_1,\mu_2)(p) &= -2PV\int_{\partial D_1}\mu_1(q)K_{11}(p,q)dq \\ &- 2\int_{\partial D_2}(\mu_2(q)-\mu_2(p)-\mu_2'(p)\sin(q-p))K_{12}(p,q)dq + 2\cdot\phi_1(p) \\ S_2(\mu_1,\mu_2)(p) &= 2\int_{\partial D_1}\mu_1(q)-\mu_1(p)-\mu_1'(p)\sin(q-p))K_{21}(p,q)dq \\ &+ 2PV\int_{\partial D_2}\mu_2(q)K_{22}(p,q)dq + 2\cdot\mu_1(p) - 2\cdot\phi_2(p). \end{aligned}$$

Then the iteration scheme becomes

$$\mu_1^{(n+1)}(p) = S_1(\mu_1^{(n)},\mu_2^{(n)})(p) - S_1(\mu_1^{(n)},\mu_2^{(n)})(p_0), \tag{4.4}$$

$$\mu_2^{(n+1)}(p) = S_2(\mu_1^{(n)},\mu_2^{(n)})(p) - S_2(\mu_1^{(n)},\mu_2^{(n)})(p_0). \tag{4.5}$$

Here we apply Theorem (3.1) to ensure that the first derivative of the integrands in S_1 and in S_2 are uniformly bounded, i.e. independent of the distance between ∂D_1 and ∂D_2. In the following experiments, the central difference scheme is used to approximate the values of $u_1'(p)$ and $u_2'(p)$.

4.4 Numerical Experimental Results

We compute μ_1, μ_2 with the non-regularized operators T_1, T_2 and with the new regularized operators S_1, S_2 for $m = 1$. The results are compared with the exact solution to give the errors. There are two ways of setting the mesh points: aligned mesh and offset mesh (fig.4.1). "Aligned mesh points" means the points on the two boundaries are set as

$$\begin{aligned} \theta_1(j) &= j\cdot\frac{2\pi}{N} \\ \theta_2(j) &= j\cdot\frac{2\pi}{N} \end{aligned}$$

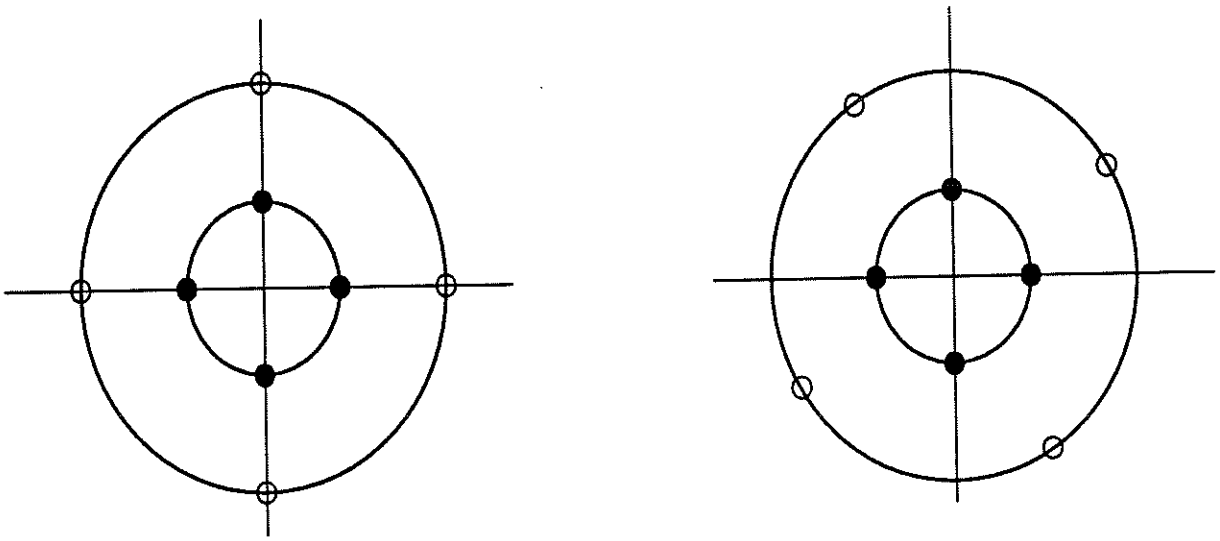

Figure 4.1: Setting the mesh points.

While "offset mesh points" means the points on the two boundaries are not aligned, for example,

$$\theta_1(j) = j \cdot \frac{2\pi}{N}$$
$$\theta_2(j) = (j + shift) \cdot \frac{2\pi}{N}, \quad shift \neq 0.$$

We did experiments for nine distances: $d_i = 10^{(-3)} \cdot 2^{10-i}$, i=1, 2,..., 9.

That is, $R_2 = 1, R_1 = 1 + d_i$. In offset mesh, $shift = 0.33$. Iteration stops when $Max\{Max_j|\mu_1^{(n+1)}(q_j) - \mu_1^{(n)}(q_j)|, Max_j|\mu_2^{(n+1)}(q_j) - \mu_2^{(n)}(q_j)|\} < 5 \cdot 10^{-13}$.

4.4.1 Aligned Mesh

Without regularization (using (T_1, T_2)), the iteration scheme converges for all values of N for d_1 only (Table 1, fig.4.3). Since when the distance is small, the kernel is very singular near the point closest to the other boundary, the numerical approximation of the ill-behaved integrand using aligned mesh points does take the singular value and might result in large errors after several iterations. The convergence, for d_1 only, is spectral.

However, after doing regularization (using (S_1, S_2)), the iteration scheme converges for all distances from d_1 to d_9 (Table 2, fig.4.4). For large distances, d_1 to d_4, spectral convergence is clearly observed. For small distances, d_5 to d_9, linear convergence is observed due to the uniform boundedness of the first derivative of the new integrand.

We call the new operators (S_1, S_2) second-order desingularization of the original integrands, since the regularized integrands in (S_1, S_2) are proportional to $(q-p)^2$. Although mathematically it is shown that the first derivatives of the integrands are uniformly bounded only if one does second or higher order desingularization (Theorem 3.1, 3.2), we find numerically the first-order desingularization perform as well as the higher-order desingularization.

The first-order desingularization scheme is expressed as:

$$\begin{aligned}
\tilde{S}_1(\mu_1,\mu_2)(p) &= -2PV\int_{\partial D_1}\mu_1(q)K_{11}(p,q)dq \\
&- 2\int_{\partial D_2}(\mu_2(q)-\mu_2(p))K_{12}(p,q)dq + 2\cdot\phi_1(p) \\
\tilde{S}_2(\mu_1,\mu_2)(p) &= 2\int_{\partial D_1}\mu_1(q)-\mu_1(p))K_{21}(p,q)dq \\
&+ 2PV\int_{\partial D_2}\mu_2(q)K_{22}(p,q)dq - 2\cdot\phi_2(p).
\end{aligned}$$

$$\mu_1^{(n+1)}(p) = \tilde{S}_1(\mu_1^{(n)},\mu_2^{(n)})(p) - \tilde{S}_1(\mu_1^{(n)},\mu_2^{(n)})(p_0), \tag{4.6}$$

$$\mu_2^{(n+1)}(p) = \tilde{S}_2(\mu_1^{(n)},\mu_2^{(n)})(p) - \tilde{S}_2(\mu_1^{(n)},\mu_2^{(n)})(p_0). \tag{4.7}$$

The results generated by the first-order and the second-order regularization are nearly identical. The differences are no greater than 10^{-10}, as shown in Table 3.

4.4.2 Offset Mesh

Without regularization (using (T_1, T_2)), the iteration scheme converges for all distances from d_1 to d_9 and the convergence is spectral from d_1 to d_3(Table 4, fig.4.5). However, they converge to the exact solution only at large distances, i.e. from d_1 to d_4. At small distances, they do not converge to the correct answers. The singularity of the kernel is concentrated in a very narrow region, thus by offsetting the mesh points, one always misses the contribution from the singularity, and hence reports errors of $O(1)$.

When the integrands are regularized (using (S_1, S_2)) and when the mesh points are offset, the values of $\mu_2(p)$ in S_1 (or $\mu_1(p)$ in S_2) are obtained by interpolation, which is different from using aligned mesh points, since in this case p^* does not refer to any of the mesh points on ∂D_2 for S_1 (or ∂D_1 for S_2). We use interpolation of order zero, i.e. $\mu(p) \sim \mu(q_i)$, where $|p - q_i| = Min_j|p - q_j|$.

When the integrands are regularized (using (S_1, S_2)), the results are similar to those by aligned mesh points(Table 5, fig.4.6): spectral convergence at large distances and linear convergence at small distances. The results by the first-order regularization (using $(\tilde{S}_1, \tilde{S}_2)$) also report similar convergence, but the errors are in general slightly greater than those by the second-order regularization (Table 6, fig.4.7).

4.5 Test Problem– Circle inside Ellipse

In this section, numerical experiments are performed on a more general problem. A circle is placed inside an ellipse (fig.4.2). We increase the radius of the inner circle so that the shortest distance between them are decreasing. In this problem, singular integrands appear only as one computes $\mu_1(p)$, $\mu_2(p)$ for p lying on the top or at the bottom of the boundaries when the two boundaries are very close to each other. This is different from the two-circled problem, where $K_{12}(p,q)$ and $K_{21}(p,q)$ are singular for all p as long as the distance between the two circles is small.

The geometry in this case is set as the following:

$$\partial_1 D = \{(x,y)|x = a \cdot cos(\theta), y = b \cdot sin(\theta), 0 \leq \theta \leq 2\pi\}$$

$$\partial_2 D = \{(x,y)|x = r \cdot cos(\theta), y = r \cdot sin(\theta), 0 \leq \theta \leq 2\pi\},$$

where $a = 2 \cdot cosh(0.5)$, $b = 2 \cdot sinh(0.5)$, $r = b - 2^{10-n} \cdot 10^{-4}$ for n=1,....,10. That is, $d_n = 2^{10-n} \cdot 10^{-4}$. The iteration scheme without desingularization is the same as in the

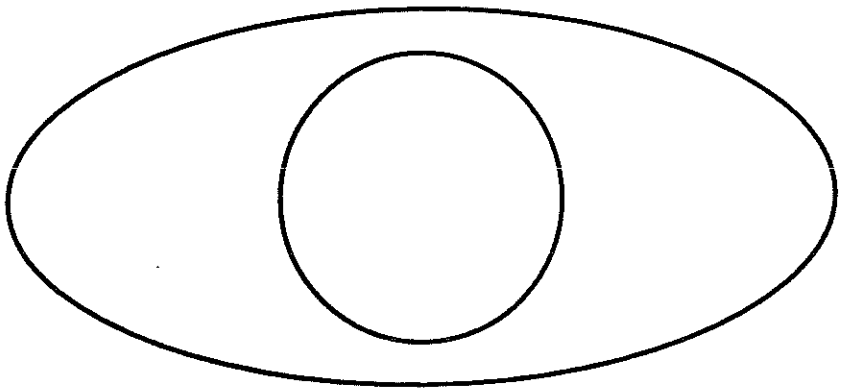

Figure 4.2: Geometry in the test problem for a more arbitrary domain.

two-circled case, while with desingularization, (S_1, S_2) are modified as follows:

$$\begin{aligned} S_1(\mu_1,\mu_2)(p) &= -2PV\int_{\partial D_1}\mu_1(q)K_{11}(p,q)dq \\ &- 2\int_{\partial D_2}(\mu_2(q)-\mu_2(p)-\mu_2'(p)\sin(q-p))\alpha_p(q)K_{12}(p,q)dq + 2\cdot\phi_1(p) \\ S_2(\mu_1,\mu_2)(p) &= 2\int_{\partial D_1}\mu_1(q)-\mu_1(p)-\mu_1'(p)\sin(q-p))\beta_p(q)K_{21}(p,q)dq \\ &+ 2PV\int_{\partial D_2}\mu_2(q)K_{22}(p,q)dq - 2\cdot\phi_2(p). \end{aligned}$$

These regularized operators are used for all $0 \le p \le 2\pi$, not for top or bottom points only, in order to make the scheme uniform. The uniform boundedness of the first derivatives of the integrands in S_1, S_2 are proved in Corollary 3.2. $\alpha_p(q)$ satisfies (3.16), (3.17) and we construct it by reflection:

$$\text{If } p^* \le \pi, \text{ then } \begin{cases} \alpha_p(q) = 1 & p^* \le q < p^* + \pi \\ \alpha_p(q) = \frac{K_{12}(p,2p^*-q)}{K_{12}(p,q)} & Otherwise \end{cases}$$

$$\text{If } p^* > \pi, \text{ then } \begin{cases} \alpha_p(q) = 1 & p^* - \pi \le q \le p^* \\ \alpha_p(q) = \frac{K_{12}(p,2p^*-q)}{K_{12}(p,q)} & Otherwise \end{cases}$$

If $K_{12}(p,q) = 0$ for some q, simply make $\alpha_p(q) \cdot K_{12}(p,q) = K_{12}(p, 2p^* - q)$. Since $\alpha_p(q) \cdot K_{12}(p,q)$ is an even function centered at p^*, (3.17) is true. One can construct $\beta_p(q)$ in the similar fashion, by changing K_{12} to K_{21} in the formula above.

There is no analytical solution for μ_1, μ_2 in this problem, so we examine the errors in the integration (without iteration) by comparing the numerical solution obtained at various number of mesh points (N=16, 32, 64, 128, 256) with the solution generated at very fine mesh points (N=1024). In offset-mesh experiments, we take

$$\begin{aligned} \theta_1(j) &= j \cdot \frac{2\pi}{N} \\ \theta_2(j) &= j \cdot \frac{2\pi}{N} + shift * \frac{\pi}{4}, \quad shift = 0.33, \end{aligned}$$

which is different from the two-circled case. Since by setting mesh points in the above manner, we can compare the errors without the exact solution.

4.5.1 Aligned Mesh

When the mesh points are aligned, without regularization (using (T_1, T_2)), we have convergence at all distances (Table 7, fig.4.8): spectral convergence for larger distances (d_1, d_2, d_3), and at least linear convergence otherwise. However, the absolute value of the first derivatives of the non-regularized integrands are so large that the errors are of very large size. In Table 7 and Table 10, the ratio of the distance and the mesh size $(\frac{d}{dx})$ of the entries with parenthesis is 0.3259. Above this diagonal, $\frac{d}{dx} > 0.3259$; below, $\frac{d}{dx} < 0.3259$.

After doing desingularization (using (S_1, S_2)), we still have linear convergence and the

errors are of reasonable size even for the very small distances (Table 8 , fig.4.9). The errors for large distances with N=128 and N=256 are greater then those without regularization because of the extra term $\alpha_p(q)\sin(q-p)\cdot K_{12}(p,q)$ and $\beta_p(q)\sin(q-p)\cdot K_{21}(p,q)$.

Experimentally, we try the first order desingularization (using $(\tilde{S}_1, \tilde{S}_2)$), where neither $\alpha_p(q)$ nor $\beta_p(q)$ needs to be constructed for each p. It is found that the errors are only slightly greater than those by the second order regularization when the distances are small (Table 9, fig.4.10), the same as in the two-circled case.

4.5.2 Offset Mesh

When the mesh points are offset, without regularization (using (T_1, T_2)), the errors are about 0.5 or greater as $\frac{d}{dx} = 0.3259$, and do not converge at small distances d_7 to d_{10} (Table 10, fig.4.11). On the other hand, the error goes to zero faster than linear convergence if we use the second order regularized operators (S_1, S_2) (Table 11, fig.4.12). Our experiments also show that the errors are only slightly greater if the first order regularized operators $(\tilde{S}_1, \tilde{S}_2)$ are used (Table 12, fig.4.13).

4.6 Conclusion

In conclusion, we have been able to remove the shortest-distance singularity that appears in two-sheet stationary problems, assuming the interfaces are sufficiently smooth, using the iterative boundary integral method. Although the kernel is very singular near the points where the two sheets are most close to each other as the separation distance is small, we

still maintain high accuracy and at least linear convergence by desingularization, and the implementation of this idea is a lot easier than the interpolated quadrature techniques that Baker and Shelly introduced in [6]. The theorems show that the second order desingularization is necessary to ensure the linear convergence, but practically the differences between the results obtained by the first and the second order desingularization are fairly small.

We also find that the values of related functions such as the velocity fields and dipole distribution functions jump as the two sheet meet, but the implication of such results is not realized yet.

Errors– Aligned Mesh W/O Regularization

D \ N	8	16	32	64	128
\ dx	0.7854	0.3927	0.1963	0.0982	0.0491
d_1=0.5120	1.290	$3.475 \cdot 10^{-2}$	$4.611 \cdot 10^{-5}$	$8.224 \cdot 10^{-11}$	$8.304 \cdot 10^{-13}$
d_2=0.2560	NaN	1.476	$2.758 \cdot 10^{-2}$	$1.861 \cdot 10^{-5}$	$7.093 \cdot 10^{-12}$
d_3=0.1280	NaN	NaN	2.497	$3.215 \cdot 10^{-2}$	$1.431 \cdot 10^{-5}$
d_4=0.0640	NaN	NaN	NaN	7.132	$4.803 \cdot 10^{-2}$
d_5=0.0320	NaN	NaN	NaN	NaN	NaN
d_6=0.0160	NaN	NaN	NaN	NaN	NaN
d_7=0.0080	NaN	NaN	NaN	NaN	NaN
d_8=0.0040	NaN	NaN	NaN	NaN	NaN
d_9=0.0020	NaN	NaN	NaN	NaN	NaN

Table 1 (Two Concentric Circles)

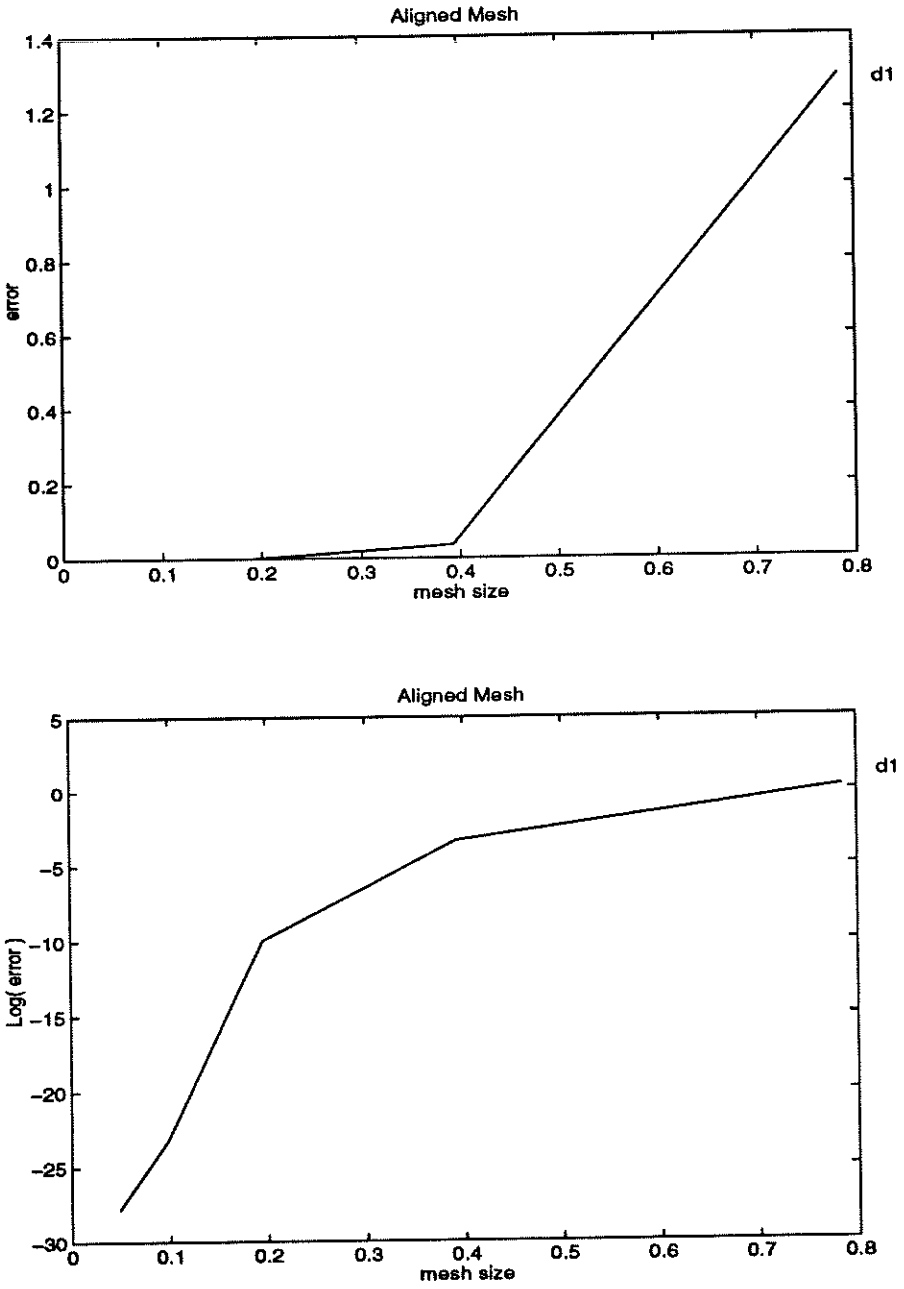

Figure 4.3: Error vs. Mesh size and Log(error) vs. Mesh size W/O regularization.

Errors– Aligned Mesh W/ 2-nd Order Regularization

D \ N	8	16	32	64	128
\ dx	0.7854	0.3927	0.1963	0.0982	0.0491
d_1=0.5120	$7.937 \cdot 10^{-2}$	$2.750 \cdot 10^{-3}$	$3.679 \cdot 10^{-6}$	$6.011 \cdot 10^{-12}$	$8.371 \cdot 10^{-13}$
d_2=0.2560	$2.074 \cdot 10^{-1}$	$2.760 \cdot 10^{-2}$	$6.966 \cdot 10^{-4}$	$4.731 \cdot 10^{-7}$	$1.648 \cdot 10^{-12}$
d_3=0.1280	$3.429 \cdot 10^{-1}$	$8.917 \cdot 10^{-2}$	$1.111 \cdot 10^{-2}$	$2.300 \cdot 10^{-4}$	$1.032 \cdot 10^{-7}$
d_4=0.0640	$4.424 \cdot 10^{-1}$	$1.567 \cdot 10^{-1}$	$4.118 \cdot 10^{-2}$	$4.929 \cdot 10^{-3}$	$9.118 \cdot 10^{-5}$
d_5=0.0320	$5.028 \cdot 10^{-1}$	$2.054 \cdot 10^{-1}$	$7.494 \cdot 10^{-2}$	$1.977 \cdot 10^{-2}$	$2.313 \cdot 10^{-3}$
d_6=0.0160	$5.360 \cdot 10^{-1}$	$2.343 \cdot 10^{-1}$	$9.909 \cdot 10^{-2}$	$3.666 \cdot 10^{-2}$	$9.680 \cdot 10^{-3}$
d_7=0.0080	$5.534 \cdot 10^{-1}$	$2.501 \cdot 10^{-1}$	$1.133 \cdot 10^{-1}$	$4.869 \cdot 10^{-2}$	$1.813 \cdot 10^{-2}$
d_8=0.0040	$5.624 \cdot 10^{-1}$	$2.582 \cdot 10^{-1}$	$1.210 \cdot 10^{-1}$	$5.573 \cdot 10^{-2}$	$2.414 \cdot 10^{-2}$
d_9=0.0020	$5.669 \cdot 10^{-1}$	$2.624 \cdot 10^{-1}$	$1.250 \cdot 10^{-1}$	$5.952 \cdot 10^{-2}$	$2.764 \cdot 10^{-2}$

Table 2 (Two Concentric Circles)

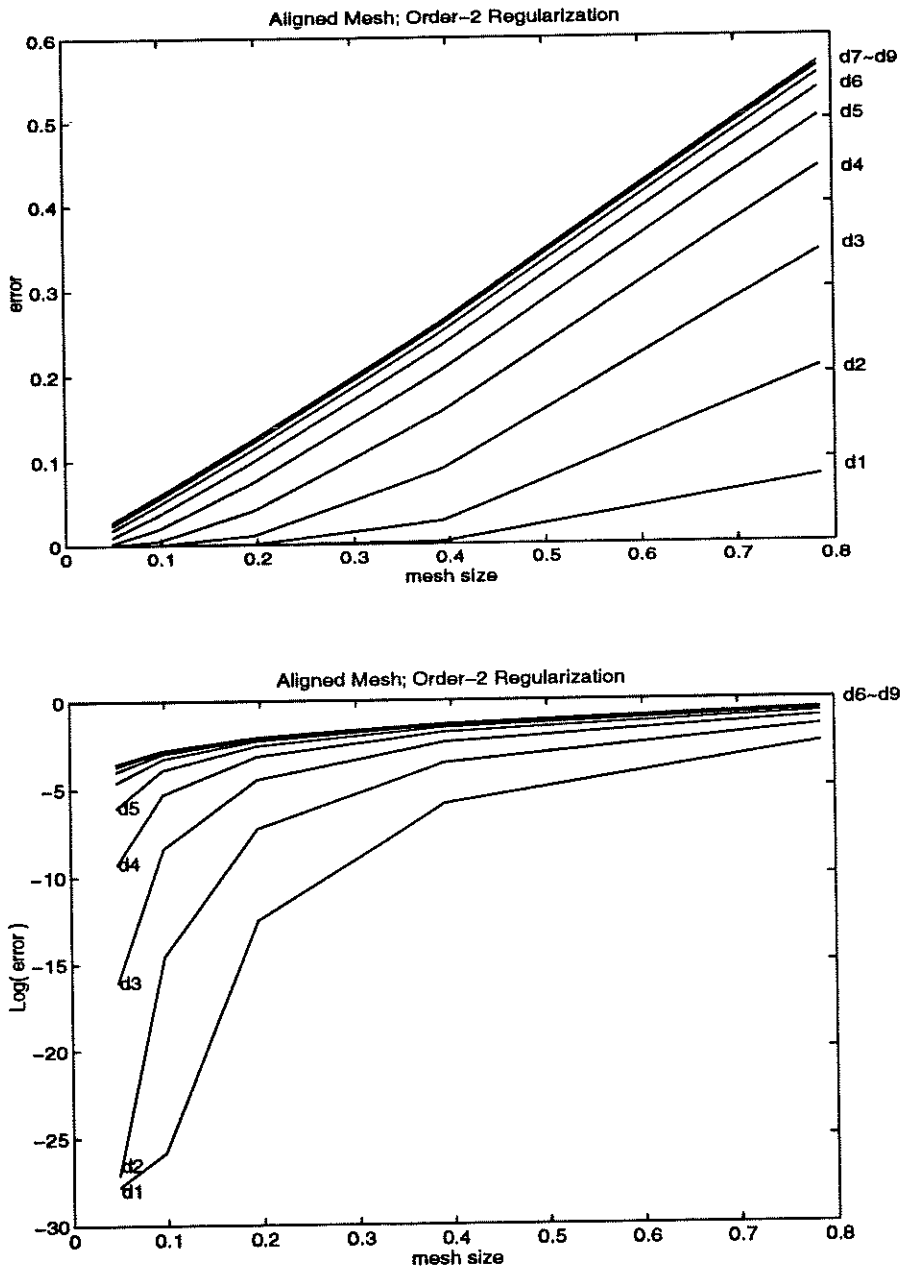

Figure 4.4: Error vs. Mesh size and Log(error) vs. Mesh size W/ 2nd-order regularization.

Aligned Mesh

Error(Order-1 Regularization)-Error(Order-2 Regularization)

D \ N	8	16	32	64	128
\ dx	0.7854	0.3927	0.1963	0.0982	0.0491
d_1=0.5120	$2.7\cdot10^{-15}$	$-1.8\cdot10^{-15}$	$9.0\cdot10^{-16}$	$0.0\cdot10^{-16}$	$5.0\cdot10^{-16}$
d_2=0.2560	$0.0\cdot10^{-16}$	$-9.0\cdot10^{-16}$	$-5.3\cdot10^{-15}$	$9.0\cdot10^{-16}$	$1.8\cdot10^{-15}$
d_3=0.1280	$-2.6\cdot10^{-15}$	$-4.4\cdot10^{-15}$	$-6.2\cdot10^{-15}$	$-4.4\cdot10^{-15}$	$0.0\cdot10^{-16}$
d_4=0.0640	$-3.6\cdot10^{-15}$	$-3.6\cdot10^{-15}$	$-5.3\cdot10^{-15}$	$-6.3\cdot10^{-15}$	$-3.6\cdot10^{-15}$
d_5=0.0320	$0.0\cdot10^{-16}$	$-3.5\cdot10^{-15}$	$-1.8\cdot10^{-15}$	$4.778\cdot10^{-13}$	$-9.0\cdot10^{-16}$
d_6=0.0160	$-4.956\cdot10^{-13}$	$4.938\cdot10^{-13}$	$-4.956\cdot10^{-13}$	$4.805\cdot10^{-13}$	$4.894\cdot10^{-13}$
d_7=0.0080	$-1.026\cdot10^{-12}$	$-1.24\cdot10^{-14}$	$9.823\cdot10^{-13}$	$5.063\cdot10^{-13}$	$9.983\cdot10^{-13}$
d_8=0.0040	$-2.038\cdot10^{-12}$	$2.577\cdot10^{-12}$	$3.470\cdot10^{-13}$	$-1.517\cdot10^{-11}$	$-9.837\cdot10^{-12}$
d_9=0.0020	$-2.587\cdot10^{-11}$	$-1.358\cdot10^{-11}$	$2.315\cdot10^{-11}$	$-2.500\cdot10^{-12}$	$-2.318\cdot10^{-11}$

Table 3 (Two Concentric Circles)

Errors– Offset Mesh W/O Regularization

D \ N	8	16	32	64	128
\ dx	0.7854	0.3927	0.1963	0.0982	0.0491
d_1=0.5120	$4.165 \cdot 10^{-1}$	$1.652 \cdot 10^{-2}$	$2.232 \cdot 10^{-5}$	$4.296 \cdot 10^{-11}$	$2.883 \cdot 10^{-12}$
d_2=0.2560	1.868	$4.591 \cdot 10^{-1}$	$1.315 \cdot 10^{-2}$	$8.964 \cdot 10^{-6}$	$1.144 \cdot 10^{-11}$
d_3=0.1280	3.175	2.328	$6.251 \cdot 10^{-1}$	$1.531 \cdot 10^{-2}$	$6.896 \cdot 10^{-6}$
d_4=0.0640	3.674	3.502	2.844	$9.440 \cdot 10^{-1}$	$2.273 \cdot 10^{-2}$
d_5=0.0320	3.856	3.824	3.723	3.827	1.439
d_6=0.0160	3.932	3.926	3.908	3.853	3.597
d_7=0.0080	3.967	3.966	3.962	3.953	3.924
d_8=0.0040	3.984	3.983	3.983	3.981	3.976
d_9=0.0020	3.992	3.992	3.992	3.991	3.990

Table 4 (Two Concentric Circles)

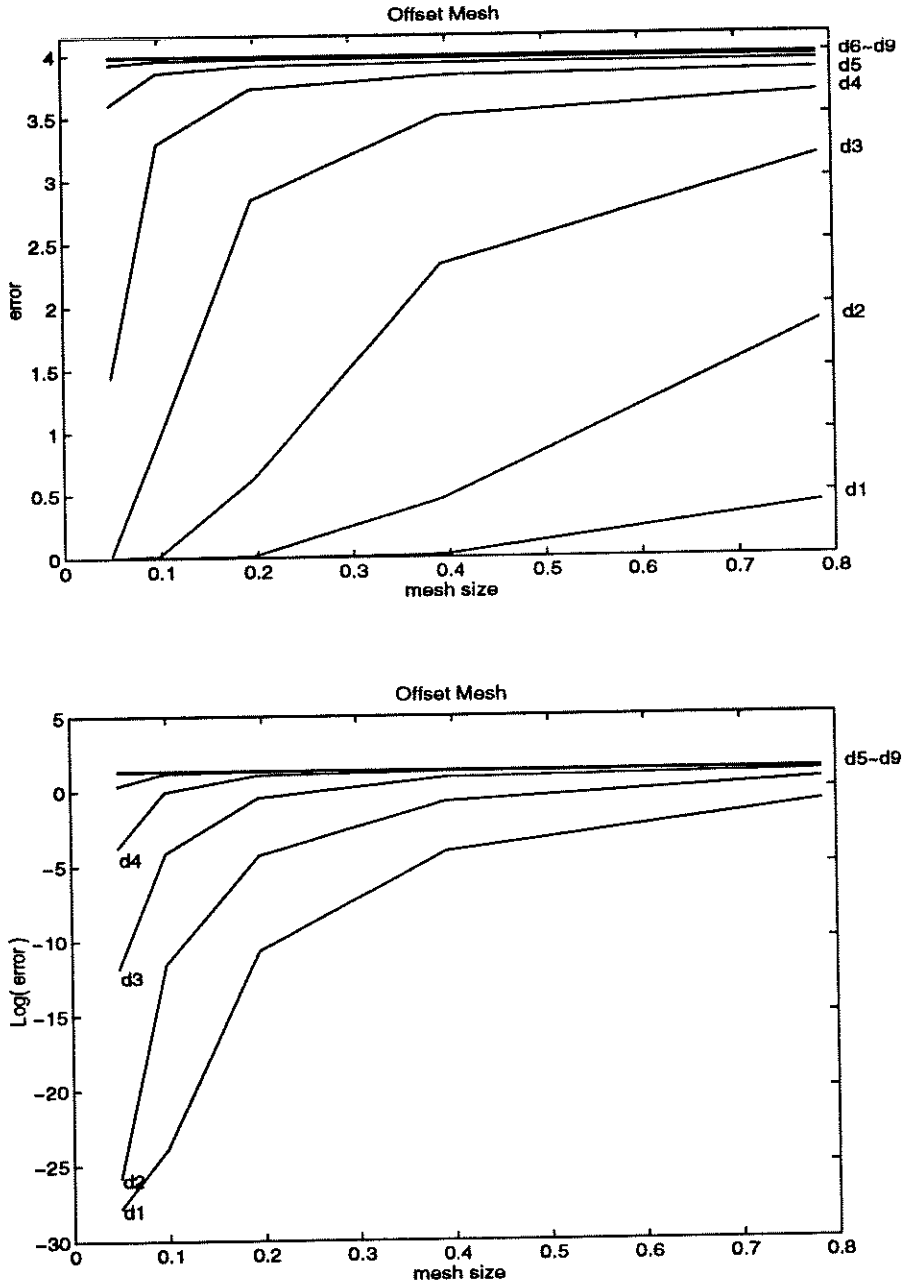

Figure 4.5: Error vs. Mesh size and Log(error) vs. Mesh size W/O regularization.

Errors– Offset Mesh W/ 2-nd Order Regularization

D \ N	8	16	32	64	128
\ dx	0.7854	0.3927	0.1963	0.0982	0.0491
d_1=0.5120	$3.283 \cdot 10^{-2}$	$2.847 \cdot 10^{-4}$	$8.241 \cdot 10^{-7}$	$5.172 \cdot 10^{-12}$	$2.883 \cdot 10^{-12}$
d_2=0.2560	$1.215 \cdot 10^{-1}$	$1.020 \cdot 10^{-2}$	$5.902 \cdot 10^{-5}$	$1.167 \cdot 10^{-7}$	$7.397 \cdot 10^{-12}$
d_3=0.1280	$1.985 \cdot 10^{-1}$	$5.279 \cdot 10^{-2}$	$3.780 \cdot 10^{-3}$	$2.123 \cdot 10^{-5}$	$2.671 \cdot 10^{-8}$
d_4=0.0640	$2.366 \cdot 10^{-1}$	$8.989 \cdot 10^{-2}$	$2.419 \cdot 10^{-2}$	$1.593 \cdot 10^{-3}$	$8.931 \cdot 10^{-6}$
d_5=0.0320	$2.656 \cdot 10^{-1}$	$1.049 \cdot 10^{-1}$	$4.210 \cdot 10^{-2}$	$1.150 \cdot 10^{-2}$	$7.257 \cdot 10^{-4}$
d_6=0.0160	$2.811 \cdot 10^{-1}$	$1.155 \cdot 10^{-1}$	$4.892 \cdot 10^{-2}$	$2.029 \cdot 10^{-2}$	$5.595 \cdot 10^{-3}$
d_7=0.0080	$2.892 \cdot 10^{-1}$	$1.320 \cdot 10^{-1}$	$5.859 \cdot 10^{-2}$	$2.348 \cdot 10^{-2}$	$9.950 \cdot 10^{-3}$
d_8=0.0040	$2.934 \cdot 10^{-1}$	$1.402 \cdot 10^{-1}$	$6.798 \cdot 10^{-2}$	$2.969 \cdot 10^{-2}$	$1.148 \cdot 10^{-2}$
d_9=0.0020	$2.955 \cdot 10^{-1}$	$1.442 \cdot 10^{-1}$	$7.273 \cdot 10^{-2}$	$3.450 \cdot 10^{-2}$	$1.493 \cdot 10^{-2}$

Table 5 (Two Concentric Circles)

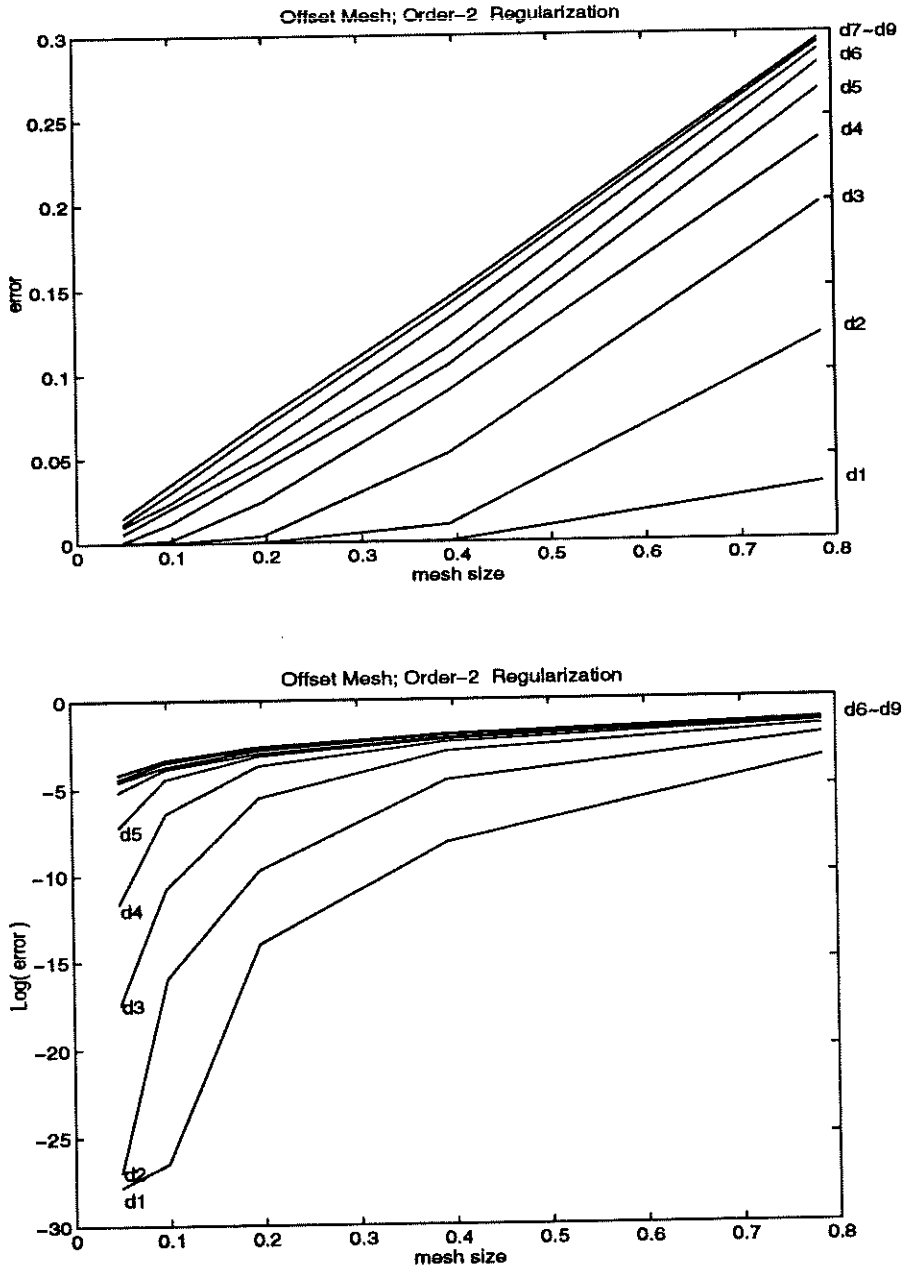

Figure 4.6: Error vs. Mesh size and Log(error) vs. Mesh size W/ 2nd-order regularization.

Errors– Offset Mesh W/ 1-st Order Regularization

D \ N	8	16	32	64	128
\ dx	0.7854	0.3927	0.1963	0.0982	0.0491
d_1=0.5120	$6.634 \cdot 10^{-2}$	$2.292 \cdot 10^{-3}$	$2.868 \cdot 10^{-6}$	$7.334 \cdot 10^{-12}$	$2.889 \cdot 10^{-12}$
d_2=0.2560	$1.567 \cdot 10^{-1}$	$2.456 \cdot 10^{-2}$	$5.751 \cdot 10^{-4}$	$3.680 \cdot 10^{-7}$	$7.426 \cdot 10^{-12}$
d_3=0.1280	$2.257 \cdot 10^{-1}$	$7.664 \cdot 10^{-2}$	$9.947 \cdot 10^{-3}$	$1.891 \cdot 10^{-4}$	$8.007 \cdot 10^{-8}$
d_4=0.0640	$2.587 \cdot 10^{-1}$	$1.183 \cdot 10^{-1}$	$3.656 \cdot 10^{-2}$	$4.426 \cdot 10^{-3}$	$7.473 \cdot 10^{-5}$
d_5=0.0320	$2.720 \cdot 10^{-1}$	$1.364 \cdot 10^{-1}$	$5.948 \cdot 10^{-2}$	$1.782 \cdot 10^{-2}$	$2.077 \cdot 10^{-3}$
d_6=0.0160	$2.777 \cdot 10^{-1}$	$1.427 \cdot 10^{-1}$	$6.992 \cdot 10^{-2}$	$2.981 \cdot 10^{-2}$	$8.791 \cdot 10^{-3}$
d_7=0.0080	$2.875 \cdot 10^{-1}$	$1.453 \cdot 10^{-1}$	$7.430 \cdot 10^{-2}$	$3.549 \cdot 10^{-2}$	$1.492 \cdot 10^{-2}$
d_8=0.0040	$2.925 \cdot 10^{-1}$	$1.468 \cdot 10^{-1}$	$7.604 \cdot 10^{-2}$	$3.772 \cdot 10^{-2}$	$1.785 \cdot 10^{-2}$
d_9=0.0020	$2.951 \cdot 10^{-1}$	$1.476 \cdot 10^{-1}$	$7.677 \cdot 10^{-2}$	$3.864 \cdot 10^{-2}$	$1.902 \cdot 10^{-2}$

Table 6 (Two Concentric Circles)

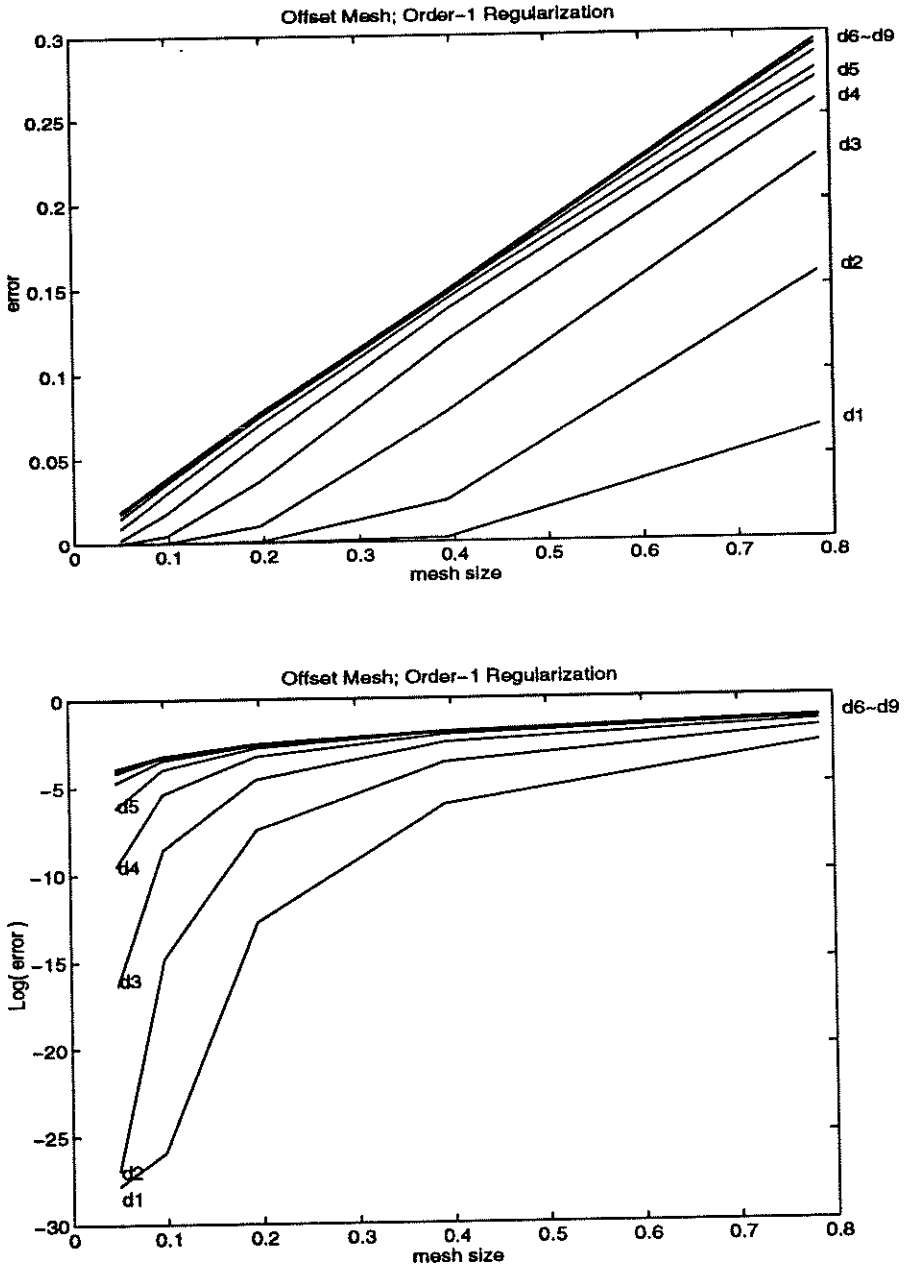

Figure 4.7: Error vs. Mesh size and Log(error) vs. Mesh size W/ 1st-order regularization.

Errors– Aligned Mesh W/O Regularization

D \ N	16	32	64	128	256
\ dx	0.3927	0.1963	0.0982	0.0491	0.0245
d_1=0.5120	$4.6735 \cdot 10^{-2}$	$1.0163 \cdot 10^{-3}$	$5.0163 \cdot 10^{-7}$	$1.3101 \cdot 10^{-13}$	$8.8818 \cdot 10^{-15}$
d_2=0.2560	$3.7031 \cdot 10^{-1}$	$4.9791 \cdot 10^{-2}$	$1.1732 \cdot 10^{-3}$	$6.8275 \cdot 10^{-7}$	$2.3848 \cdot 10^{-13}$
d_3=0.1280	(1.3277)	$3.7839 \cdot 10^{-1}$	$5.1876 \cdot 10^{-2}$	$1.2772 \cdot 10^{-3}$	$8.1321 \cdot 10^{-7}$
d_4=0.0640	3.4536	(1.3390)	$3.8318 \cdot 10^{-1}$	$5.3061 \cdot 10^{-2}$	$1.3363 \cdot 10^{-3}$
d_5=0.0320	7.8196	3.4665	(1.3451)	$3.8576 \cdot 10^{-1}$	$5.3690 \cdot 10^{-2}$
d_6=0.0160	16.610	7.8333	3.4732	(1.3484)	$3.8710 \cdot 10^{-1}$
d_7=0.0080	34.219	16.624	7.8403	3.4767	(1.3500)
d_8=0.0040	69.453	34.233	16.631	7.8438	3.4784
d_9=0.0020	139.93	69.467	34.241	16.634	7.8456
d_{10}=0.0010	280.88	139.94	69.474	34.244	16.636

Table 7 (Circle inside Ellipse)

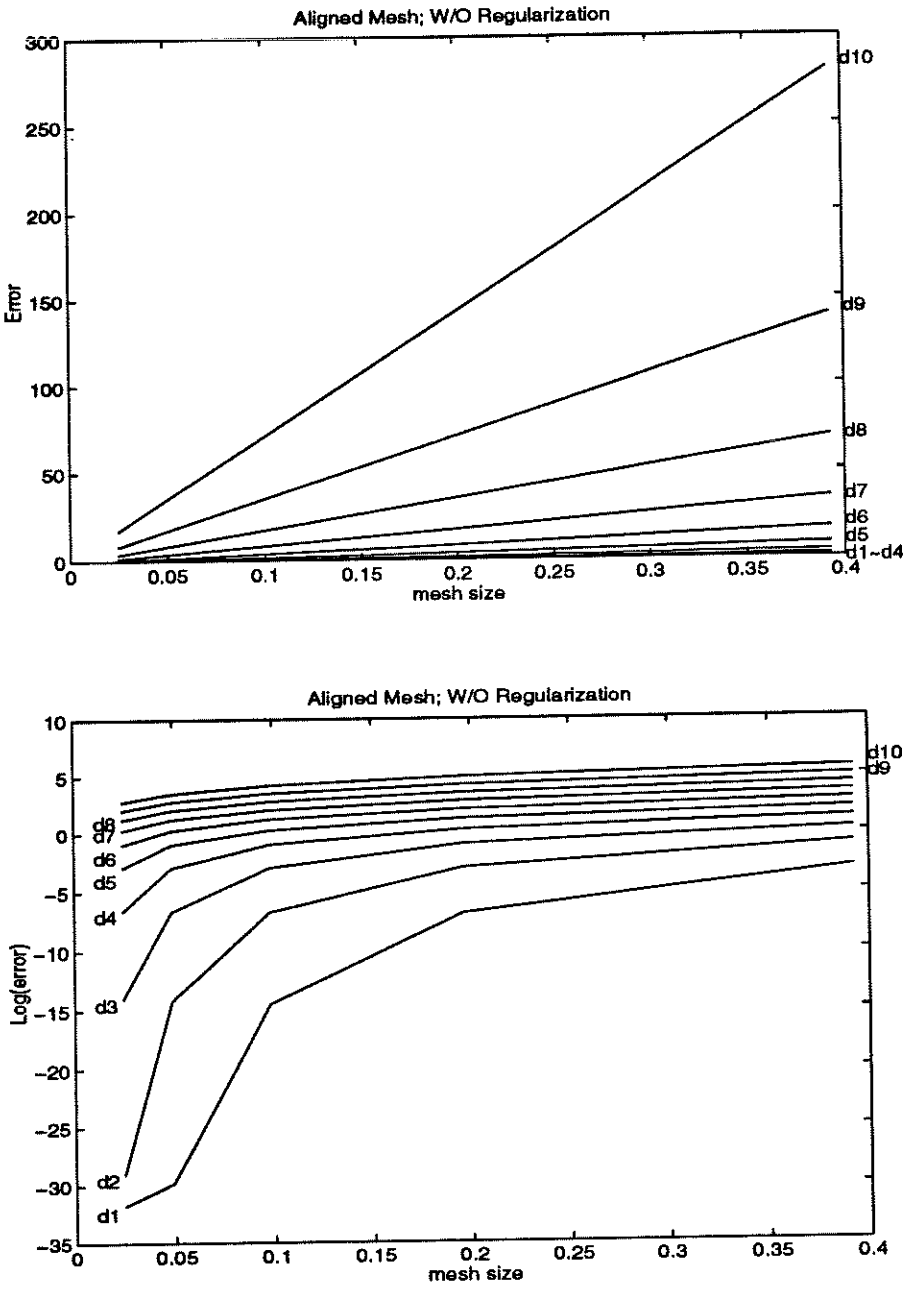

Figure 4.8: Error vs. Mesh size and Log(error) vs. Mesh size W/O regularization.

Errors– Aligned Mesh W/ 2-nd Order Regularization

D \ N	16	32	64	128	256
\ dx	0.3927	0.1963	0.0982	0.0491	0.0245
d_1=0.5120	$1.3658 \cdot 10^{-3}$	$4.9927 \cdot 10^{-5}$	$1.0351 \cdot 10^{-5}$	$1.5380 \cdot 10^{-6}$	$1.5914 \cdot 10^{-7}$
d_2=0.2560	$3.6767 \cdot 10^{-3}$	$3.7386 \cdot 10^{-4}$	$1.4082 \cdot 10^{-5}$	$1.5075 \cdot 10^{-6}$	$2.1459 \cdot 10^{-7}$
d_3=0.1280	$6.1836 \cdot 10^{-3}$	$9.3739 \cdot 10^{-4}$	$8.6896 \cdot 10^{-5}$	$2.3966 \cdot 10^{-6}$	$1.9723 \cdot 10^{-7}$
d_4=0.0640	$9.3761 \cdot 10^{-3}$	$1.9067 \cdot 10^{-3}$	$3.2850 \cdot 10^{-4}$	$2.8032 \cdot 10^{-5}$	$6.7387 \cdot 10^{-7}$
d_5=0.0320	$1.1132 \cdot 10^{-2}$	$2.7610 \cdot 10^{-3}$	$8.3279 \cdot 10^{-4}$	$1.4470 \cdot 10^{-4}$	$7.6012 \cdot 10^{-6}$
d_6=0.0160	$1.2126 \cdot 10^{-2}$	$3.2512 \cdot 10^{-3}$	$1.3889 \cdot 10^{-3}$	$3.7103 \cdot 10^{-4}$	$5.1037 \cdot 10^{-5}$
d_7=0.0080	$1.2642 \cdot 10^{-2}$	$3.5037 \cdot 10^{-3}$	$1.7606 \cdot 10^{-3}$	$5.6604 \cdot 10^{-4}$	$1.2295 \cdot 10^{-4}$
d_8=0.0040	$1.2905 \cdot 10^{-2}$	$3.6313 \cdot 10^{-3}$	$1.9715 \cdot 10^{-3}$	$6.8491 \cdot 10^{-4}$	$1.8862 \cdot 10^{-4}$
d_9=0.0020	$1.3038 \cdot 10^{-2}$	$3.6954 \cdot 10^{-3}$	$2.0832 \cdot 10^{-3}$	$7.4844 \cdot 10^{-4}$	$2.3605 \cdot 10^{-4}$
d_{10}=0.0010	$1.3105 \cdot 10^{-2}$	$3.7276 \cdot 10^{-3}$	$2.1406 \cdot 10^{-3}$	$7.8084 \cdot 10^{-4}$	$2.6481 \cdot 10^{-4}$

Table 8 (Circle inside Ellipse)

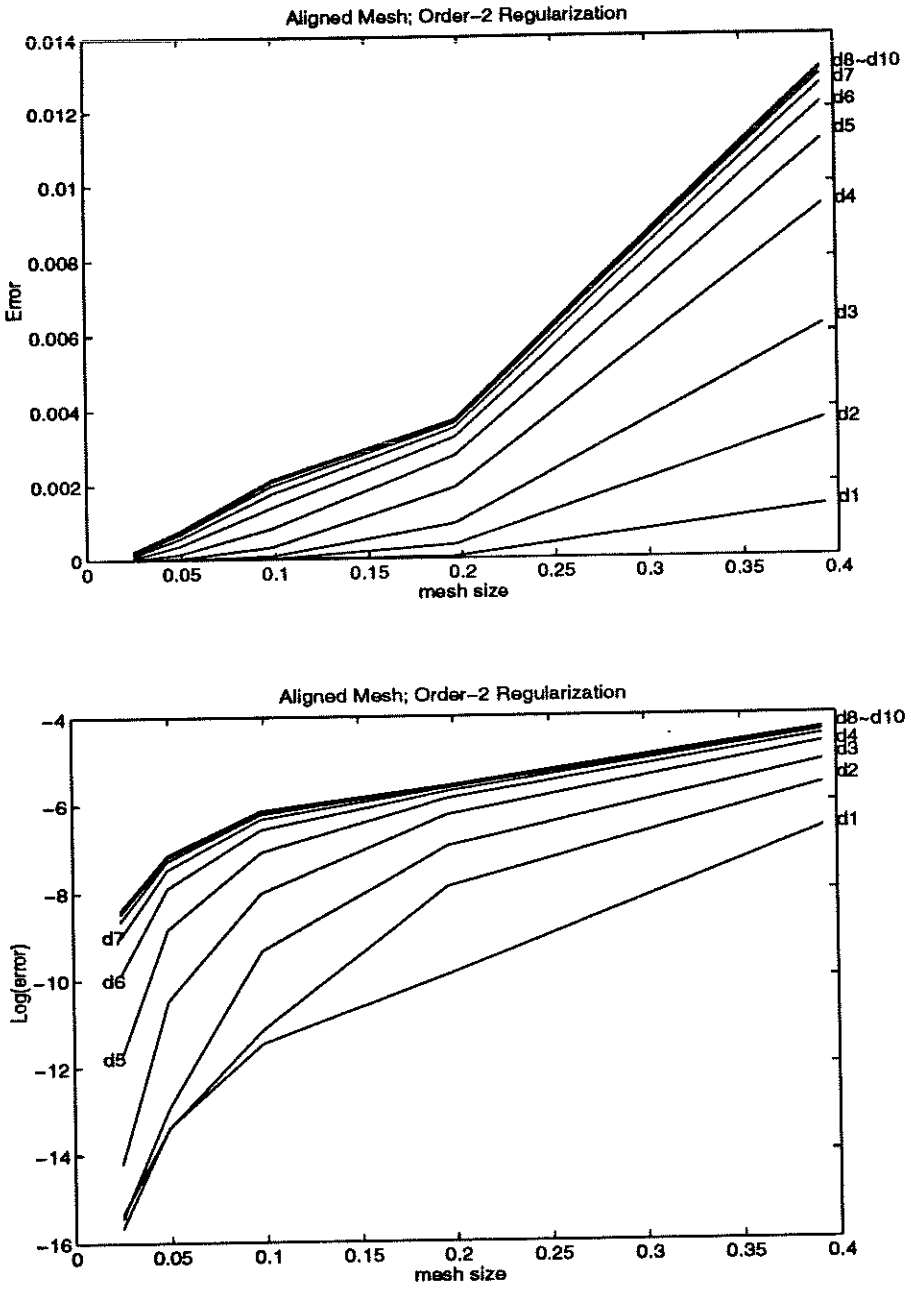

Figure 4.9: Error vs. Mesh size and Log(error) vs. Mesh size W/ 2nd-order regularization.

Errors– Aligned Mesh W/ 1-st Order Regularization

D \ N	16	32	64	128	256
\ dx	0.3927	0.1963	0.0982	0.0491	0.0245
d_1=0.5120	$1.7745 \cdot 10^{-3}$	$2.8377 \cdot 10^{-5}$	$1.3870 \cdot 10^{-8}$	$1.1102 \cdot 10^{-14}$	$1.0214 \cdot 10^{-14}$
d_2=0.2560	$6.1316 \cdot 10^{-3}$	$5.0969 \cdot 10^{-4}$	$7.9008 \cdot 10^{-6}$	$4.5980 \cdot 10^{-9}$	$9.7700 \cdot 10^{-15}$
d_3=0.1280	$6.4229 \cdot 10^{-3}$	$1.2386 \cdot 10^{-3}$	$1.7031 \cdot 10^{-4}$	$3.4366 \cdot 10^{-6}$	$1.6825 \cdot 10^{-9}$
d_4=0.0640	$9.3486 \cdot 10^{-3}$	$2.5879 \cdot 10^{-3}$	$7.2132 \cdot 10^{-4}$	$6.5036 \cdot 10^{-5}$	$1.1564 \cdot 10^{-6}$
d_5=0.0320	$1.1312 \cdot 10^{-2}$	$3.6676 \cdot 10^{-3}$	$1.4191 \cdot 10^{-3}$	$2.6863 \cdot 10^{-4}$	$2.5943 \cdot 10^{-5}$
d_6=0.0160	$1.2424 \cdot 10^{-2}$	$4.3528 \cdot 10^{-3}$	$1.9571 \cdot 10^{-3}$	$5.1053 \cdot 10^{-4}$	$9.7305 \cdot 10^{-5}$
d_7=0.0080	$1.3000 \cdot 10^{-2}$	$4.7393 \cdot 10^{-3}$	$2.2852 \cdot 10^{-3}$	$6.8149 \cdot 10^{-4}$	$1.7736 \cdot 10^{-4}$
d_8=0.0040	$1.3292 \cdot 10^{-2}$	$4.9447 \cdot 10^{-3}$	$2.4651 \cdot 10^{-3}$	$7.7875 \cdot 10^{-4}$	$2.5876 \cdot 10^{-4}$
d_9=0.0020	$1.3439 \cdot 10^{-2}$	$5.0505 \cdot 10^{-3}$	$2.5592 \cdot 10^{-3}$	$8.2941 \cdot 10^{-4}$	$3.5194 \cdot 10^{-4}$
d_{10}=0.0010	$1.3513 \cdot 10^{-2}$	$5.1043 \cdot 10^{-3}$	$2.6072 \cdot 10^{-3}$	$8.5495 \cdot 10^{-4}$	$4.0459 \cdot 10^{-4}$

Table 9 (Circle inside Ellipse)

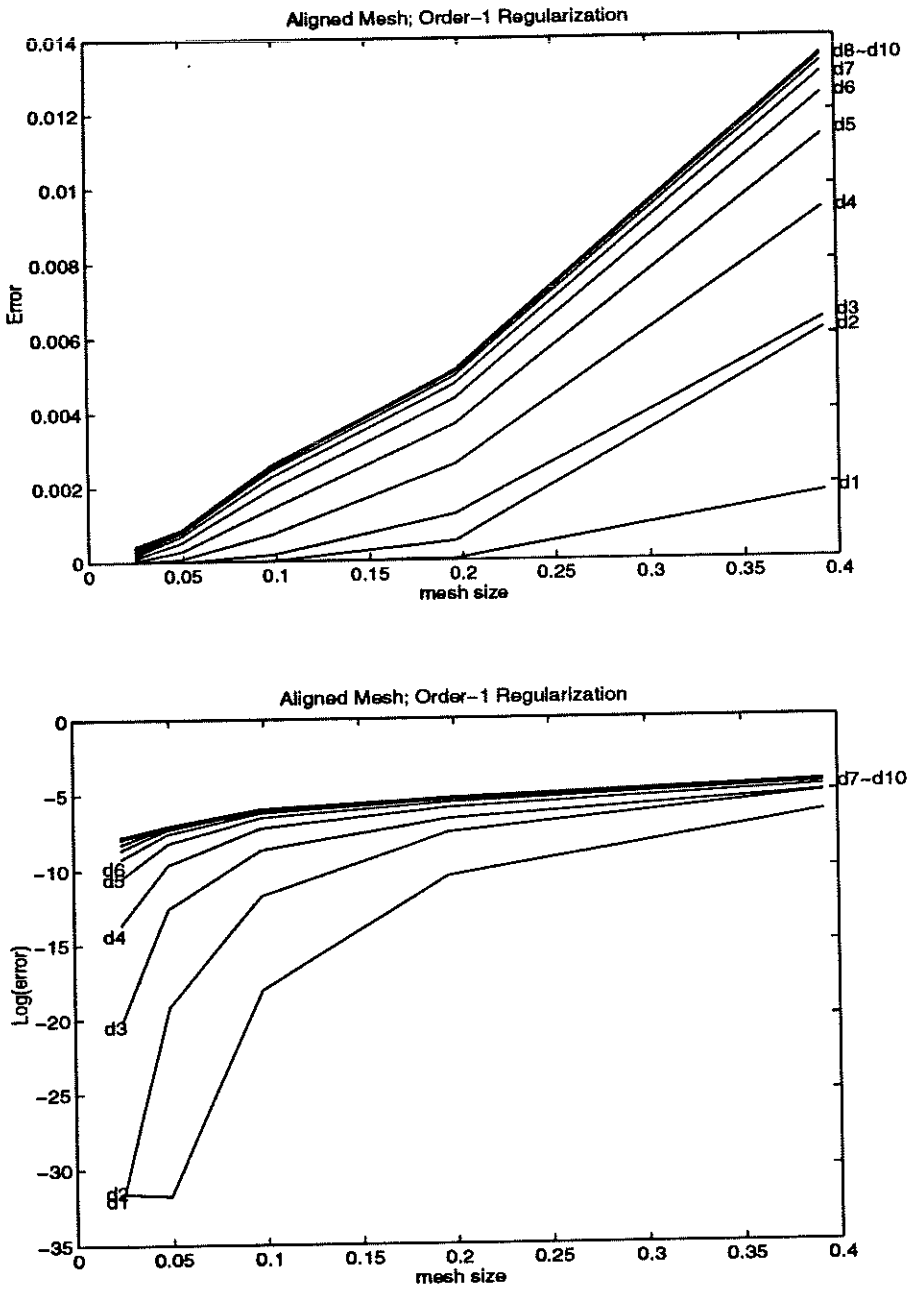

Figure 4.10: Error vs. Mesh size and Log(error) vs. Mesh size W/ 1st-order regularization.

Errors– Offset Mesh W/O Regularization

D \ N	16	32	64	128	256
\ dx	0.3927	0.1963	0.0982	0.0491	0.0245
d_1=0.5120	$2.9887 \cdot 10^{-2}$	$8.0069 \cdot 10^{-4}$	$3.6814 \cdot 10^{-7}$	$1.2523 \cdot 10^{-13}$	$1.0214 \cdot 10^{-14}$
d_2=0.2560	$2.3230 \cdot 10^{-1}$	$3.9105 \cdot 10^{-2}$	$1.0629 \cdot 10^{-3}$	$5.6004 \cdot 10^{-7}$	$2.1005 \cdot 10^{-13}$
d_3=0.1280	$(5.5738 \cdot 10^{-1})$	$2.2437 \cdot 10^{-1}$	$4.3553 \cdot 10^{-2}$	$9.7956 \cdot 10^{-4}$	$7.8262 \cdot 10^{-7}$
d_4=0.0640	$7.1334 \cdot 10^{-1}$	$(4.4146 \cdot 10^{-1})$	$2.7601 \cdot 10^{-1}$	$3.3579 \cdot 10^{-2}$	$1.3001 \cdot 10^{-3}$
d_5=0.0320	$8.5406 \cdot 10^{-1}$	$6.9220 \cdot 10^{-1}$	$(6.6341 \cdot 10^{-1})$	$1.8926 \cdot 10^{-1}$	$5.2052 \cdot 10^{-2}$
d_6=0.0160	$9.2714 \cdot 10^{-1}$	$8.4203 \cdot 10^{-1}$	$7.4477 \cdot 10^{-1}$	$(4.5823 \cdot 10^{-1})$	$3.7118 \cdot 10^{-1}$
d_7=0.0080	$9.6400 \cdot 10^{-1}$	$9.2052 \cdot 10^{-1}$	$8.6223 \cdot 10^{-1}$	$6.4941 \cdot 10^{-1}$	(1.2537)
d_8=0.0040	$9.8245 \cdot 10^{-1}$	$9.6020 \cdot 10^{-1}$	$9.3559 \cdot 10^{-1}$	$8.1119 \cdot 10^{-1}$	2.9460
d_9=0.0020	$9.9168 \cdot 10^{-1}$	$9.8010 \cdot 10^{-1}$	1.0120	$9.0469 \cdot 10^{-1}$	5.1772
d_{10}=0.0010	$9.9629 \cdot 10^{-1}$	$9.9005 \cdot 10^{-1}$	1.0528	$9.5223 \cdot 10^{-1}$	6.3345

Table 10 (Circle inside Ellipse)

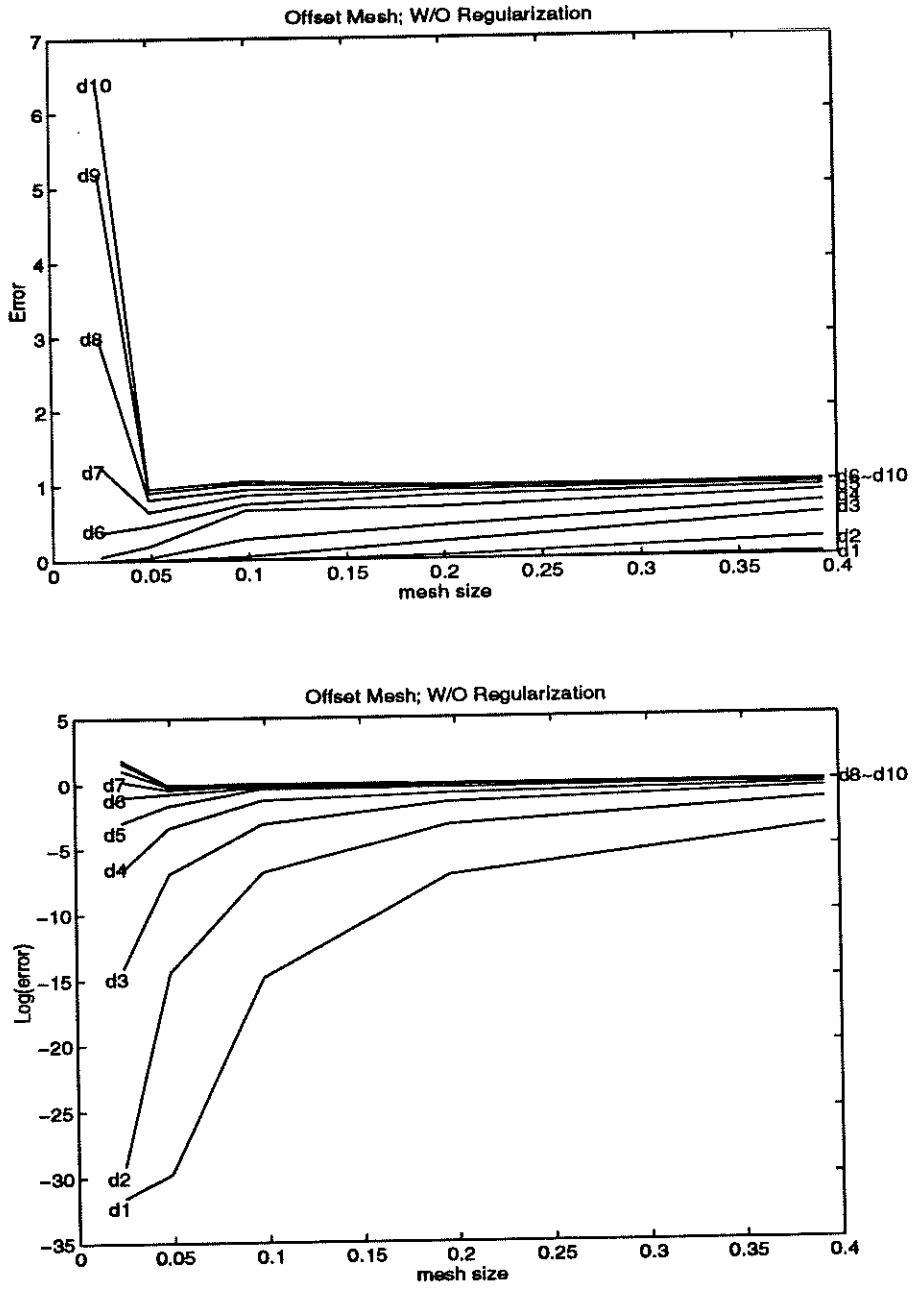

Figure 4.11: Error vs. Mesh size and Log(error) vs. Mesh size W/O egularization.

Errors– Offset Mesh W/ 2-nd Order Regularization

D \ N	16	32	64	128	256
\ dx	0.3927	0.1963	0.0982	0.0491	0.0245
d_1=0.5120	$3.5401 \cdot 10^{-3}$	$3.3064 \cdot 10^{-4}$	$6.8614 \cdot 10^{-5}$	$1.1113 \cdot 10^{-5}$	$1.0064 \cdot 10^{-6}$
d_2=0.2560	$9.5564 \cdot 10^{-3}$	$5.4759 \cdot 10^{-4}$	$1.1086 \cdot 10^{-4}$	$1.1800 \cdot 10^{-5}$	$1.6574 \cdot 10^{-6}$
d_3=0.1280	$7.3615 \cdot 10^{-3}$	$3.2612 \cdot 10^{-3}$	$9.9727 \cdot 10^{-5}$	$1.0658 \cdot 10^{-5}$	$2.0389 \cdot 10^{-6}$
d_4=0.0640	$1.9320 \cdot 10^{-2}$	$5.6029 \cdot 10^{-3}$	$1.0642 \cdot 10^{-3}$	$5.0169 \cdot 10^{-5}$	$2.2954 \cdot 10^{-6}$
d_5=0.0320	$2.0201 \cdot 10^{-2}$	$7.0080 \cdot 10^{-3}$	$2.1546 \cdot 10^{-3}$	$3.1439 \cdot 10^{-4}$	$1.0408 \cdot 10^{-5}$
d_6=0.0160	$2.0588 \cdot 10^{-2}$	$7.9174 \cdot 10^{-3}$	$2.8361 \cdot 10^{-3}$	$6.3320 \cdot 10^{-4}$	$6.3068 \cdot 10^{-5}$
d_7=0.0080	$2.0769 \cdot 10^{-2}$	$8.9192 \cdot 10^{-3}$	$3.2481 \cdot 10^{-3}$	$8.8174 \cdot 10^{-4}$	$1.5202 \cdot 10^{-4}$
d_8=0.0040	$2.0856 \cdot 10^{-2}$	$9.8447 \cdot 10^{-3}$	$3.4711 \cdot 10^{-3}$	$1.1639 \cdot 10^{-3}$	$2.3142 \cdot 10^{-4}$
d_9=0.0020	$2.0899 \cdot 10^{-2}$	$1.0329 \cdot 10^{-2}$	$3.5866 \cdot 10^{-3}$	$1.3849 \cdot 10^{-3}$	$3.0168 \cdot 10^{-4}$
d_{10}=0.0010	$2.0920 \cdot 10^{-2}$	$1.0577 \cdot 10^{-2}$	$3.6453 \cdot 10^{-3}$	$1.5100 \cdot 10^{-3}$	$3.7513 \cdot 10^{-4}$

Table 11 (Circle inside Ellipse)

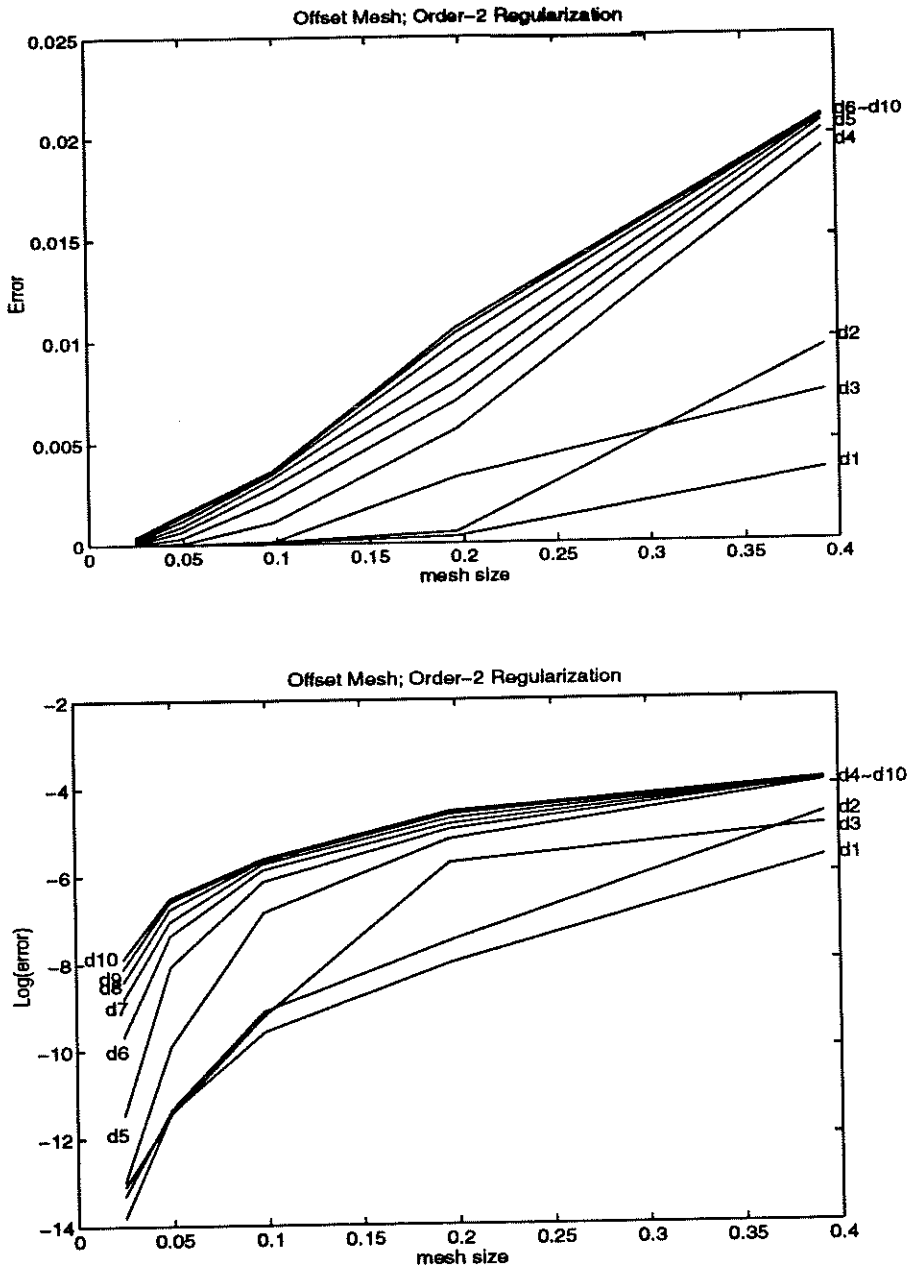

Figure 4.12: Error vs. Mesh size and Log(error) vs. Mesh size W/ 2nd-order regularization.

Errors– Offset Mesh W/ 1-st Order Regularization

D \ N	16	32	64	128	256
\ dx	0.3927	0.1963	0.0982	0.0491	0.0245
d_1=0.5120	$2.9441 \cdot 10^{-3}$	$3.3193 \cdot 10^{-5}$	$1.2093 \cdot 10^{-8}$	$1.0214 \cdot 10^{-14}$	$9.3259 \cdot 10^{-15}$
d_2=0.2560	$6.9501 \cdot 10^{-3}$	$5.4114 \cdot 10^{-4}$	$8.2862 \cdot 10^{-6}$	$4.4416 \cdot 10^{-9}$	$1.0214 \cdot 10^{-14}$
d_3=0.1280	$1.0453 \cdot 10^{-2}$	$3.0492 \cdot 10^{-3}$	$2.2558 \cdot 10^{-4}$	$3.6072 \cdot 10^{-6}$	$1.5971 \cdot 10^{-9}$
d_4=0.0640	$1.8384 \cdot 10^{-2}$	$6.3528 \cdot 10^{-3}$	$1.1441 \cdot 10^{-3}$	$8.8195 \cdot 10^{-5}$	$1.2990 \cdot 10^{-6}$
d_5=0.0320	$2.2120 \cdot 10^{-2}$	$8.4977 \cdot 10^{-3}$	$2.2625 \cdot 10^{-3}$	$3.5546 \cdot 10^{-4}$	$2.8271 \cdot 10^{-5}$
d_6=0.0160	$2.5292 \cdot 10^{-2}$	$9.6489 \cdot 10^{-3}$	$3.0083 \cdot 10^{-3}$	$7.3307 \cdot 10^{-4}$	$1.0292 \cdot 10^{-4}$
d_7=0.0080	$2.6961 \cdot 10^{-2}$	$1.0236 \cdot 10^{-2}$	$3.4160 \cdot 10^{-3}$	$1.0107 \cdot 10^{-3}$	$1.9610 \cdot 10^{-4}$
d_8=0.0040	$2.7816 \cdot 10^{-2}$	$1.0792 \cdot 10^{-2}$	$3.6260 \cdot 10^{-3}$	$1.2550 \cdot 10^{-3}$	$2.8775 \cdot 10^{-4}$
d_9=0.0020	$2.8248 \cdot 10^{-2}$	$1.1253 \cdot 10^{-2}$	$3.7322 \cdot 10^{-3}$	$1.4527 \cdot 10^{-3}$	$3.8842 \cdot 10^{-4}$
d_{10}=0.0010	$2.8465 \cdot 10^{-2}$	$1.1488 \cdot 10^{-2}$	$3.7855 \cdot 10^{-3}$	$1.5638 \cdot 10^{-3}$	$4.4065 \cdot 10^{-4}$

Table 12 (Circle inside Ellipse)

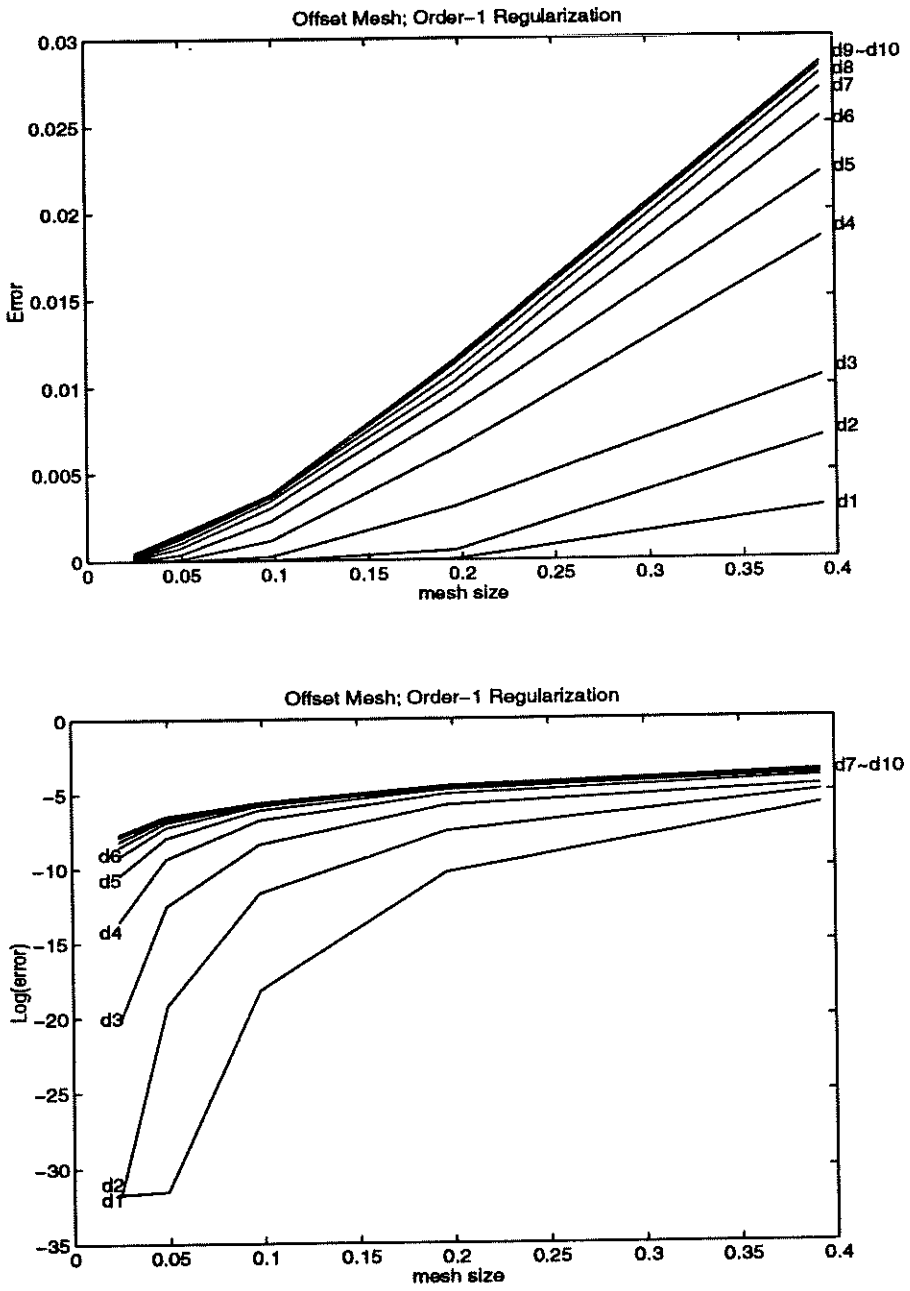

Figure 4.13: Error vs. Mesh size and Log(error) vs. Mesh size W/ 1st-order regularization.

CHAPTER 5

Stationary Droplets

There are many studies about the permanent form of vortex sheets that separate two inviscid, incompressible fluids, one of which is filled with fluid of uniform vorticity while the other is irrotational. The importance of such flows, as was pointed out by Batchelor [7], is that they may be the zero-viscosity limits of viscid flows, and such flows can describe the wake at the rear of a body. When a rigid body is placed in a stream of fluid of high Reynolds number, one can observe that the streamlines passing the front face of the body break at the sides of the body and enclose fluid at its rear. The whole region at the rear of the body is called the wake. Batchelor proposed that the flow in the wake is characterized by two adjacent regions with constant vorticity, which might be of different constants, and separated by a common streamline. The stationary profile of the vortex sheet lying between the wake and the otherwise uniform stream of fluid is of considerable interest[7].

Moore, Saffman and Tanveer [26] calculated the steady, inviscid, incompressible, two-dimensional flow with uniform vortex patches bounded by a vortex sheet, for the vortex on the plane wall (the Sadovskii vortex) and the vortex in a right-angled corner (fig.5.1). They applied a hybrid collocation method to two different formulations for the problem: one is basically a representation as the Birkoff-Rott equation of the complex velocity field, which is a boundary integral over the interface between rotational and irrotational flows; the other is

a boundary integral form of the harmonic part of the stream function. In both methods, they represented the shape of the vortex sheet in a Fourier expansion and performed Newton's iteration to solve the descretized equations. The numerical scheme was successful and results were reported to confirm the previous work by other researchers [27][12].

With the same numerical scheme, the collocation method, Pullin and Grimshaw [16] presented numerical solutions to the problem of the steady profiles of finite-amplitude solitary waves at the interface between two homogeneous fluids, of which the upper layer consists of a constant vorticity and is bounded by a rigid surface and the lower layer is irrotational with infinite depth. Their work on such problems allowed them to generate results showing the existence of the "mushroom" shape solution for the interface between two fluids of different densities and in the Boussinesq approximation [17][18], which is beyond the S-shape profile obtained in [16]. (fig.5.1)

In all studies above, only symmetric solutions are sought and no conclusion is made about the existence of the non-symmetric solutions, which cannot be reached by the present numerical methods. In addition, special techniques, such as introducing canceling functions to give accurate evaluation of the contribution near the singularities , using adaptive mesh points or a suitable choice of the interface parameterization to handle severe deformations in overhanging portions, were developed to improve the original collocation method.

Inspired by the success of the collocation method adopted in these steady flow calculations, we employ the same technique to look for the steady profile of a "flying droplet", which is a closed vortex sheet between two inviscid, incompressible, homogeneous fluids of different

densities under the influence of gravity. Inside the sheet there is a constant vorticity, around the boundary there is a circulation, and away from the sheet the flow is uniform (fig.5.2). The steady state solution to this problem will be the result of a balance between the lift force (Magnus effect) due to the flow and the buoyancy forces due to the gravity. We seek to know how the magnitude of the inner vorticity, the surrounding circulation, the far-field uniform velocity and the density ratio influence the resulting steady shape, the velocity field, and associated quantities. In our work, no particular modification is done to the collocation method.

Section 5.1 sets up the PDE system of the stationary motion of the flying droplet; section 5.2 describes the numerical method we use for the descretized equations; section 5.3 shows two tests of numerical consistency; section 5.4 gives the results and discussion; section 5.5 is the conclusion.

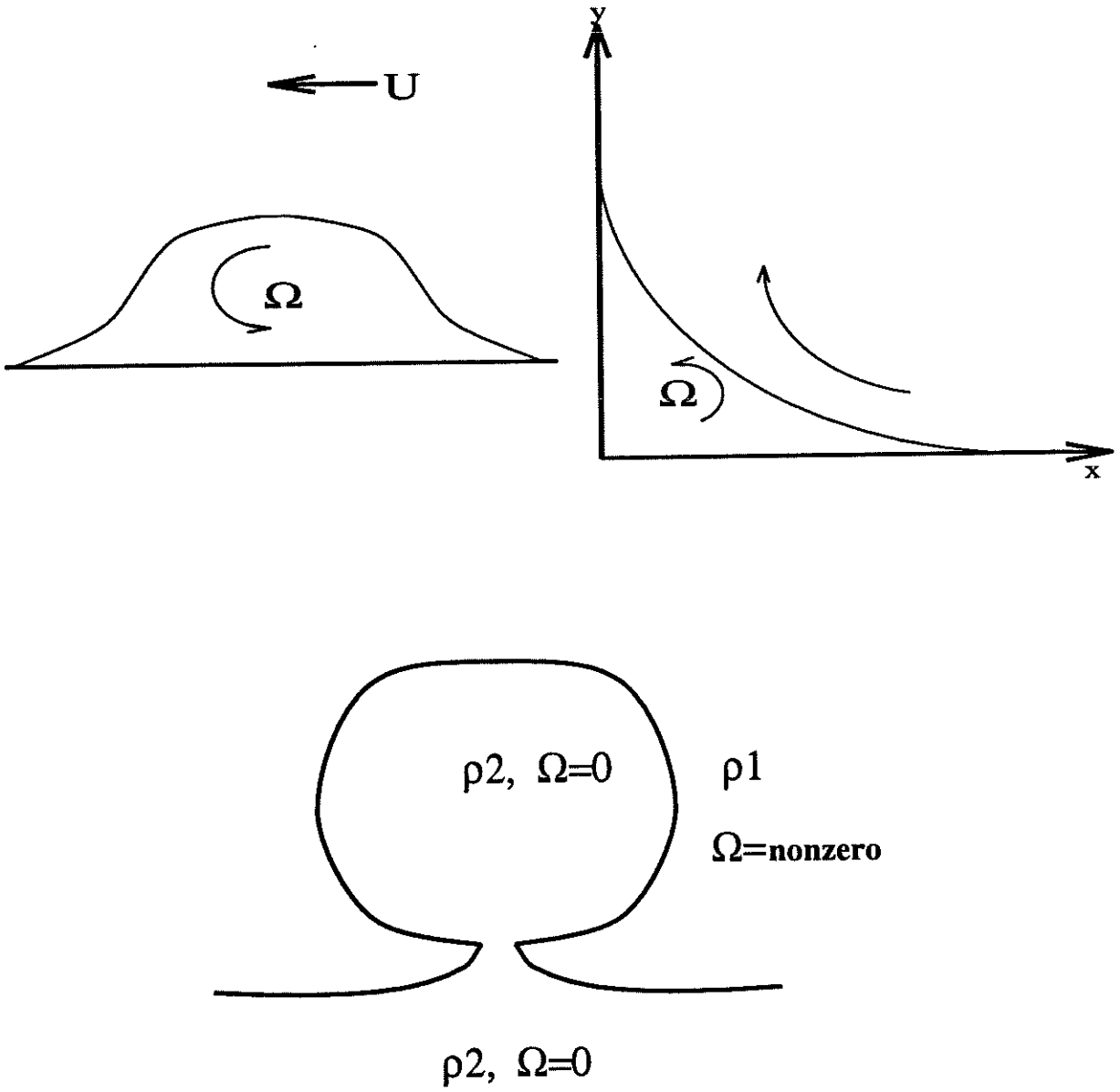

Figure 5.1: Upper: Sketches of the Sadovskii vortex (left) and the rotational corner flow (right). Lower: Steady wave profile for interfacial solitary waves.

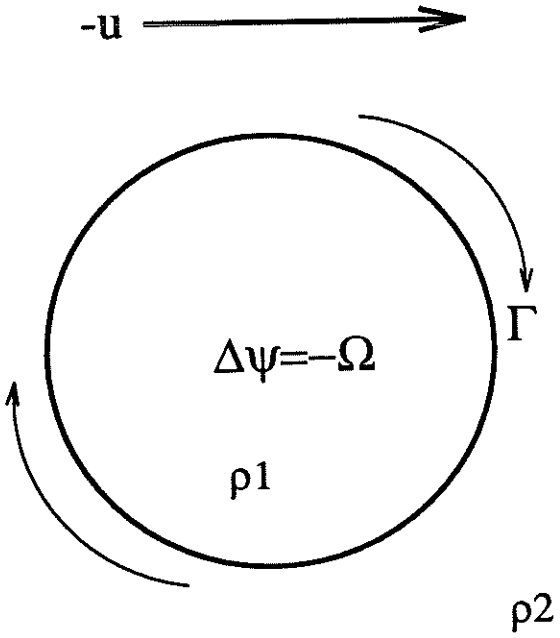

Figure 5.2:

5.1 Equations of Stationary Motion

We set up the PDE system describing the situation in fig.5.2 in a manner similar to the one that Pullin and Grimshaw derived for the interfacial waves in a two-layer shear flow [16].

5.1.1 Equation for the sheet strength– γ

First of all, we derive the Bernoulli's equation modified for rotational flows with constant vorticity. Starting from the momentum equation:

$$\frac{\partial}{\partial t}\vec{u} + \nabla(\frac{1}{2}|\vec{u}|^2 + \frac{p}{\rho} + gy) \;=\; \vec{u} \times \vec{w}.$$

We are working on 2-D flows, in which $\vec{u} = (u, v)$ is the velocity field and $\vec{w} \equiv \nabla \times \vec{u} = (0, 0, \Omega)$ is the vorticity, where Ω is a constant. Also p is the pressure, ρ is the density of the fluid, and g is the gravity acceleration in the negative y direction. $\vec{u} \times \vec{w} = (v\Omega, -u\Omega)$, and we express the above equation in the component form:

$$\begin{aligned}
\frac{\partial}{\partial t}u \;+\; \partial_x[\frac{1}{2}u^2 + \frac{1}{2}v^2 + \frac{p}{\rho} + gy] &= v\Omega = -\psi_x\Omega \\
\frac{\partial}{\partial t}v \;+\; \partial_y[\frac{1}{2}u^2 + \frac{1}{2}v^2 + \frac{p}{\rho} + gy] &= -u\Omega = -\psi_y\Omega.
\end{aligned}$$

Here ψ is the stream function and $\nabla\psi = (-v, u)$. This implies that

$$\begin{aligned}
\frac{\partial}{\partial t}u &= -\partial_x[\frac{1}{2}u^2 + \frac{1}{2}v^2 + \frac{p}{\rho} + gy + \psi\Omega] \\
\frac{\partial}{\partial t}v &= -\partial_y[\frac{1}{2}u^2 + \frac{1}{2}v^2 + \frac{p}{\rho} + gy + \psi\Omega].
\end{aligned}$$

So for stationary flow,

$$\frac{1}{2}u^2 + \frac{1}{2}v^2 + \frac{p}{\rho} + gy + \psi\Omega \;=\; constant.$$

We shall denote the boundary of the two-dimensional droplet by ∂D, which is between two inviscid, incompressible fluids. We have constant vorticity Ω inside the droplet and constant circulation Γ surrounding it (fig.5.2). The governing equations are:

$$\frac{1}{2}u_1^2 + \frac{1}{2}v_1^2 + \frac{p_1}{\rho_1} + gy + \psi_1\Omega = B_1 \qquad inside \quad \partial D \tag{5.1}$$

$$\frac{1}{2}u_2^2 + \frac{1}{2}v_2^2 + \frac{p_2}{\rho_2} + gy + 0 = B_2 \qquad outside \quad \partial D. \tag{5.2}$$

Here all quantities with index 1 or 2 refer to those inside or outside the droplet, respectively. In particular, $\vec{u_i} = (u_i, v_i)$ is the velocity field, ψ_i is the stream function, and B_i is the Bernoulli constant. The boundary conditions are:

$$p_1 \;=\; p_2 \qquad on \quad \partial D \tag{5.3}$$

$$\vec{u_1}\cdot\vec{n} \;=\; \vec{u_2}\cdot\vec{n} = 0 \qquad on \quad \partial D. \tag{5.4}$$

Equation (5.4) holds because at the steady state the normal velocity along the boundary vanishes. Represent ∂D by $\partial D = \{Z(\theta) = x(\theta) + iy(\theta) | 0 \le \theta < 2\pi\}$ in the complex plane. Define q_1 and q_2 as follows:

$$q_1 \;\equiv\; \lim_{Z\to\partial D \ from\ inside}(u_1 + iv_1)(Z)$$

$$q_2 \;\equiv\; \lim_{Z\to\partial D \ from\ outside}(u_2 + iv_2)(Z).$$

Then (5.1) and (5.2) can be written as

$$\frac{1}{2}\bar{q}_1 q_1 + \frac{p_1}{\rho_1} + gy + \psi_1\Omega = B_1 \tag{5.5}$$

$$\frac{1}{2}\bar{q}_2 q_2 + \frac{p_2}{\rho_2} + gy = B_2. \tag{5.6}$$

Consider $-1 \le \beta \le 1$ and let

$$\begin{aligned} \bar{q_1} &= \bar{q} - \frac{(1+\beta)\gamma}{2Z_\theta} \\ \bar{q_2} &= \bar{q} + \frac{(1-\beta)\gamma}{2Z_\theta}. \end{aligned}$$

Here $\gamma = (\bar{q_2} - \bar{q_1})Z_\theta$ is the sheet strength, which is equal to jump of the tangential velocities across the sheet. We denote by q the velocity defined on ∂D. By (5.3), $p_1 = p_2 = p$ on ∂D.

Subtracting (5.5) from (5.6) implies that

$$\frac{1}{2}\cdot(\bar{q}_2 q_2 - \bar{q}_1 q_1) \;+\; p\cdot(\frac{\rho_1-\rho_2}{\rho_1\rho_2}) - \psi_1\Omega = B_2 - B_1. \tag{5.7}$$

Adding (5.5) and (5.6), we get

$$\frac{1}{2}\cdot(\bar{q}_2 q_2 + \bar{q}_1 q_1) \;+\; p\cdot(\frac{\rho_1+\rho_2}{\rho_1\rho_2}) + 2\cdot gy + \psi_1\Omega = B_2 + B_1. \tag{5.8}$$

Replacing q_1 and q_2 in (5.7) and (5.8) by their definitions, then we have

$$\gamma\cdot Re[\tfrac{q}{Z_\theta}] \quad -\frac{1}{2}\frac{\beta\gamma^2}{|Z_\theta|^2} + p\cdot(\frac{\rho_1-\rho_2}{\rho_1\rho_2}) - \psi_1\Omega = B_2 - B_1 \tag{5.9}$$

$$\bar{q}q - \;\; Re[\tfrac{q}{Z_\theta}]\cdot\gamma\beta \;+\frac{(1+\beta)^2\gamma^2}{4|Z_\theta|^2} + p\cdot(\frac{\rho_1+\rho_2}{\rho_1\rho_2}) + 2\cdot gy + \psi_1\Omega = B_2 + B_1. \tag{5.10}$$

Eliminating p from (5.9), (5.10), the resulting equation is

$$\begin{aligned} &\gamma\cdot Re[\frac{q}{Z_\theta}] - \frac{1}{2}\frac{\beta\gamma^2}{|Z_\theta|^2} + A\cdot(\beta\gamma Re[\frac{q}{Z_\theta}] - \frac{(1+\beta)^2\gamma^2}{4|Z_\theta|^2} - \bar{q}q - 2\cdot gy) \\ &= B_2 - B_1 + A(B_2+B_1) + (1+A)\psi\Omega. \end{aligned} \tag{5.11}$$

Here $A \equiv \frac{\rho_1 - \rho_2}{\rho_1 + \rho_2}$ is the Atwood number. Equation (5.11) is defined on ∂D and the right hand side of (5.11) is a constant, which we denote by B, since ψ is constant along the streamline.

Note that $\beta = 1$ means the particles on the boundary follow the motion of the outside flow, while $\beta = -1$ means they follow that of the inside flow. Specific choices of β might facilitate the numerical computation for some problems. We take $\beta = 0$ in our calculation; thus (5.11) is expressed as

$$\gamma \cdot Re[\frac{q}{Z_\theta}] - A \cdot (\frac{\gamma^2}{4|Z_\theta|^2} + \bar{q}q + 2 \cdot gy) \;=\; B. \tag{5.12}$$

5.1.2 Equation for $u + iv$

The equation for the stationary velocity field $q \equiv (u + iv)(Z), Z = x + iy$, is derived by adding the velocity field due to the vorticity inside and the velocity field due to the circulation outside to the Birkoff-Rott formulation for this droplet problem, then correcting the integrand so that the resulting formula when restricted to the boundary has jumps in the tangential direction only.

The velocity field due to the constant-vorticity rotational flow centered at a complex point $Z_0 = X_0 + iY_0$ satisfies

$$\nabla^2 \psi_1 = -\Omega.$$

There exists a particular solution of ψ_1:

$$\psi_1 = -\frac{\Omega}{2}r^2 = -\frac{\Omega}{2}|(x,y) - (X_0, Y_0)|^2$$

$$\Rightarrow \quad (u,v)(Z) = (\partial_y\psi_1, -\partial_x\psi_1) = -\frac{\Omega}{2}(y - Y_0, -x + X_0)$$

$$\Rightarrow \quad \overline{q}(Z) = (u - iv)(Z) = -\frac{\Omega}{2}i\overline{(Z - Z_0)}. \tag{5.13}$$

The velocity field due to the circulation surrounding ∂D centered at the same Z_0 also has a particular solution:

$$\psi_2 = \frac{\Gamma}{2\pi} \cdot \log r$$

$$\Rightarrow \quad (u,v)(Z) = \frac{\Gamma}{2\pi r^2}(y - Y_0, -x + X_0)$$

$$\Rightarrow \quad \overline{q}(Z) = \frac{\Gamma}{2\pi}\frac{i}{\overline{Z - Z_0}}. \tag{5.14}$$

Now, we include the sheet strength due to the difference of the tangential velocities from the inner vorticity and outer circulation in the numerator of the Birkoff-Rott equation, which is derived from the Biot-Savart law. Note that the velocity field given in (5.13) is in the counterclockwise direction ($\Omega > 0$), while in (5.14), it's in the clockwise direction ($\Gamma > 0$). So the jump in their tangential components at θ' is

$$-\frac{\Omega i}{2}\overline{(Z(\theta') - Z_0)}Z_\theta(\theta') \quad + \quad \frac{i}{2\pi}\Gamma Z_\theta(\theta')/(Z(\theta') - Z_0).$$

Therefore, we have the following equations,

$$\overline{q}(Z) = \frac{1}{2\pi i}\int_0^{2\pi} \frac{\gamma' - \frac{\Omega i}{2}\overline{(Z' - Z_0)}Z'_\theta + \frac{i}{2\pi}\Gamma Z'_\theta/(Z' - Z_0)}{Z - Z'}d\theta'$$

$$\begin{cases} -\frac{\Omega i}{2}\overline{(Z - Z_0)} - u & Z \text{ inside } \partial D \\ +\frac{i}{2\pi}\frac{\Gamma}{(Z - Z_0)} - u & Z \text{ outside } \partial D. \end{cases}$$

Here the far field uniform velocity field -u is included and the above equation is for any Z away from ∂D. Here all terms with prime in the integrand are functionsof θ' defined along ∂D. By using the Plemelj formula, we can obtain $\overline{q}(Z)$ on the boundary by approaching $Z \in \partial D$ from inside and outside of the droplet:

$$\begin{aligned}
\overline{q}(\theta)|_{inner} &= \frac{1}{2\pi i} PV \int_0^{2\pi} \frac{\gamma' - \frac{\Omega i}{2}\overline{(Z'-Z_0)}Z'_\theta + \frac{i}{2\pi}\Gamma Z'_\theta/(Z'-Z_0)}{Z(\theta)-Z'} d\theta' \\
&- \frac{1}{2}[\frac{\gamma(\theta)}{Z_\theta(\theta)} - \frac{\Omega}{2} i\overline{(Z(\theta)-Z_0)} - \frac{\Gamma}{2\pi}\frac{i}{Z(\theta)-Z_0}] - \frac{\Omega}{2} i\overline{(Z(\theta)-Z_0)} - u \qquad (5.15) \\
\overline{q}(\theta)|_{outer} &= \frac{1}{2\pi i} PV \int_0^{2\pi} \frac{\gamma' - \frac{\Omega i}{2}\overline{(Z'-Z_0)}Z'_\theta + \frac{i}{2\pi}\Gamma Z'_\theta/(Z'-Z_0)}{Z(\theta)-Z'} d\theta' \\
&+ \frac{1}{2}[\frac{\gamma(\theta)}{Z_\theta(\theta)} - \frac{\Omega}{2} i\overline{(Z(\theta)-Z_0)} - \frac{\Gamma}{2\pi}\frac{i}{Z(\theta)-Z_0}] + \frac{\Gamma}{2\pi}\frac{i}{Z(\theta)-Z_0} - u. \qquad (5.16)
\end{aligned}$$

(5.16)-(5.15) shows that jump of the velocities across the boundary is purely tangential since

$$\begin{aligned}
[\overline{q}(\theta)] \cdot Z_\theta(\theta) &= tangential \quad velocity + i \cdot normal \quad velocity \\
&= \gamma(\theta),
\end{aligned}$$

which is a real number.

WLOG, we can let Z_0 be the origin. On ∂D, we take the velocity to be the average from inner and outer fluids. Thus

$$\overline{q}(\theta) = \frac{1}{2\pi i} PV \int_0^{2\pi} \frac{\gamma' - \frac{\Omega i}{2}\overline{Z'}Z'_\theta + \frac{i}{2\pi}\Gamma Z'_\theta/Z'}{Z(\theta)-Z'} d\theta' + \frac{i}{4\pi}\frac{\Gamma}{Z(\theta)} - \frac{\Omega i}{4}\overline{Z(\theta)} - u. \qquad (5.17)$$

Here $Z(\theta) = x(\theta) + iy(\theta), 0 \le \theta < 2\pi$, lies on the boundary of the droplet.

The boundary condition in (5.4) can be written as

$$Im[\frac{q}{Z_\theta}] \;=\; 0, \quad q \equiv U + iV. \tag{5.18}$$

Thus (5.12), (5.17) and (5.18) are the final equations without non-dimensionalization.

5.1.3 Setting up the Well-posed System

In order to reduce the number of independent parameters, we non-dimensionalize the associated quantities in (5.12), (5.17) and (5.18) by setting $t = T\tilde{t}$, $Z = L\tilde{Z}$, $q = \frac{L}{T}\tilde{q}$, $\gamma = \frac{L^2}{T}\tilde{\gamma}$, $\Omega = \frac{1}{T}\tilde{\Omega}$, $u = \frac{L}{T}\tilde{u}$, $B = \frac{L^2}{T^2}\tilde{B}$ and choosing the time scale $T = \frac{\Gamma^{1/3}}{g^{2/3}}$ and the length scale $L = \frac{\Gamma^{2/3}}{g^{1/3}}$.

The resulting non-dimensionalized form becomes (leaving ˜ out)

$$\overline{q}(\theta) = \frac{1}{2\pi i} PV \int_0^{2\pi} \frac{\gamma' - \frac{\Omega i}{2}\overline{Z'}Z'_\theta + \frac{i}{2\pi}Z'_\theta/Z'}{Z(\theta) - Z'} d\theta' + \frac{i}{4\pi}\frac{1}{Z(\theta)} - \frac{\Omega i}{4}\overline{Z(\theta)} - u \tag{5.19}$$

$$\gamma Re[\frac{q}{Z_\theta}] - A \cdot (\frac{\gamma^2}{4|Z_\theta|^2} + q\overline{q} + 2y) = B. \tag{5.20}$$

The non-dimensionalized equation for (5.18) is the same. Notice that the Boussinesq approximation of the non-dimensionalized system (5.18)-(5.20), which is the same except $A \cdot \frac{\gamma^2}{4|Z_\theta|^2}$ and $A \cdot q\overline{q}$ terms in (5.20) are dropped, still allows similar solutions. More specifically, if $(Z, \gamma, q, u, B, \Omega, A)$ is a solution, then $(CZ, \gamma, \frac{q}{C}, \frac{u}{C}, \frac{B}{C^2}, \frac{\Omega}{C^2}, \frac{A}{C^3})$ is also a solution for any real C. To remove this arbitrariness, we require the area of the droplet to be π.

$$\int_0^{2\pi} y dx \;=\; \pi. \tag{5.21}$$

Thus (5.18)-(5.21) form a well-posed problem.

(In the Boussinesq approximation, any solution of the dimensional equations (5.12), (5.17), (5.18) can be expressed through a scaling of the non-dimensionalized equations (5.18), (5.19), (5.20), by a proper choice of L, T and C. In the subsequent computational study, we show that there is a two parameter family of solutions corresponding to choice of A and Ω (within certain limits). Note that for the full equations, however, the scaling with respect to C is not valid, so that the solution depends on a third parameter. This dependence will not be explored in the present study.)

There exists a simple solution to this problem, which satisfies (5.18) - (5.21), i.e.,

$$\begin{aligned} A &= 0 \\ Z_0(\theta) &= \sin(\theta) + i\cos(\theta) \\ \gamma_0(\theta) &= \frac{\Omega}{2} - \frac{1}{2\pi} \\ B_0 &= -\frac{1}{8}(\Omega - \frac{1}{\pi})^2 \\ u_0 &= 0. \end{aligned}$$

5.2 Numerical Iterative Scheme

To solve the nonlinear system (5.18)-(5.21), we use the collocation method. We expand $Z(\theta)$ and $\gamma(\theta)$ in Fourier expansion around the known solution for $A = 0$; i.e.

$$\begin{aligned} Z(\theta) &= \sin(\theta)(1 + X_1) + i\cos(\theta) + i\sum_{j=1}^{N-1} Y_j \cos(\jmath \cdot \theta) \\ &= x + iy \qquad (5.22) \end{aligned}$$

$$\gamma(\theta) = \frac{\Omega}{2} - \frac{1}{2\pi} + \sum_{j=1}^{N-1} C_j \cos(\jmath \cdot \theta). \qquad (5.23)$$

Implicitly we assume that the droplet is symmetric about the imaginary axis $x = 0$ in (5.22), as was assumed in using the collocation method for steady flows in [16], [17], [18] and [26]. Plug (5.22) and (5.23) into (5.18)-(5.21). There are 2N+1 unknowns $\{Y_j, j = 1, ..., N-1; C_j, j = 1, ..., N-1; X_1, B, u\}$. Evaluate (5.19), (5.20) at N points, $\theta_{k-1/2} = (k - \frac{1}{2})\frac{\pi}{N}$ for $k = 1, ..., N$, plus (5.21) totally 2N+1 equations. The principal integral in (5.18) is done by summing over $\theta'_j = j \cdot \frac{\pi}{N}$, $j = 1, 2, ..., 2N$, for each $\theta_{k-1/2}$, so it is symmetric about the singularity. Newton's iterative scheme is used to solve this closed 2N+1 linear system for various values of A and Ω. Solutions are sought with N=128 for each A and Ω, and the iteration stops as the absolute value of the difference between two successive iterative solutions is less then 10^{-7}. The Newton's iteration scheme converges quadratically and it takes usually 3 to 4 iterations to reach the 10^{-7} error bound. For some sets of A and Ω, the solutions at N=64 (or N=96) and N=256 are sought to check the convergence, which we will show in section 5.3.

5.3 Test of Consistency

We check that our numerical results provide consistent solutions to the nonlinear system by the following two ways: First of all, we show the numerical solutions converge as the mesh size shrinks. We decide to study the case $\Omega = 0$ in more detail so that other researchers can later on have a comparison. Table 5.1-5.3 list the first 10 Fourier coefficients at three Atwood numbers A=-0.0075, -0.0150, and -0.02, which is the most extreme case that our

method can reach. In Table 5.1, the solutions obtained with finer mesh points make no significant difference. We define the error to be the L_2 norm of the difference between the computed Fourier coefficients with two different mesh points, $E = E_{N_1,N_2} = \max\{[\sum_i (Y_i^{N_1} - Y_i^{N_2})^2]^{1/2}, \sum_i (C_i^{N_1} - C_i^{N_2})^2]^{1/2}\}$, where the superscript N_1, N_2 means the solutions computed at the total number of mesh points N=N_1, or N=N_2, respectively. On the bottom of Table 5.1,it shows that they are much less then the iteration error bound 10^{-7} at A=-0.0075. In Table 5.2, we find that doubling the mesh points does give less error and the convergence is faster then quadrature convergence. In Table 5.3, we use the solution at N=96 instead of N=64, since the iteration does not converge at N=64 in this case, because there are not enough points to describe the two near angle corners. However, it still shows that the error tends to zero as N increases. For the cases where Ω is nonzero, we can also observe that the errors are smaller as the Atwood number is closer to zero with the same N, since the associated functions are smoother, and are larger when it is close to the most extreme solution. But the error always decreases as N increases, which shows convergence.

Secondly, we linearize the equations (5.19), (5.20) around A=0 by letting $A = \delta$, $\gamma = \gamma_0 + \gamma_1$, $Z = Z_0 + Z_1$, $q = q_0 + q_1$, $B = B_0 + B_1$, $u = u_0 + u_1$. The 0th-order equations are satisfied by the basic solution at $A = 0$, which can be checked easily:

$$\begin{aligned} \gamma_0 \cdot Re[\frac{q_0}{\frac{\partial Z_0}{\partial \theta}}] - B_0 &= 0 \\ Im[\frac{q_0}{\frac{\partial Z_0}{\partial \theta}}] &= 0 \end{aligned}$$

The 1st-order linearized equations are

$$t_0 \equiv \frac{1}{4\pi} - \frac{\Omega}{4}$$

$$t_0\gamma_1 + \gamma_0 Re[q_1\overline{\frac{\partial Z_0}{\partial\theta}} - q_0\frac{\overline{\frac{\partial Z_0}{\partial\theta}}}{\overline{\frac{\partial Z_0}{\partial\theta}}}\frac{\partial Z_1}{\partial\theta}] - \delta\cdot(\frac{\gamma_0^2}{4} + t_0^2 + 2\cos(\theta)) - B_1 = 0 \tag{5.24}$$

$$Im[q_1\overline{\frac{\partial Z_0}{\partial\theta}} - q_0\frac{\overline{\frac{\partial Z_0}{\partial\theta}}}{\overline{\frac{\partial Z_0}{\partial\theta}}}\frac{\partial Z_1}{\partial\theta}] = 0 \tag{5.25}$$

We obtain the errors by plugging into (5.24) and (5.25) the perturbation parts of our numerical solutions. The error, which is denoted by E_2, also converges quadratically as A is decreased and is shown in Table 5.4. Note that the linear equations are not yet solved due to the complexity of the form involved in the integral equation of q_1.

5.4 Results and Discussion

For a fixed Ω, we picture the stationary profile of the droplet at various A (the Atwood number) and the corresponding velocity field up to the last A, beyond which the iteration scheme fails to converge. We shall denote this A by A_{lim}. The velocity on the boundary is the average of the velocities inside and outside the droplet.

In our formulation, the far field uniform velocity is in the positive x direction and the circulation surrounding the droplet ($\Gamma = 1$ after non-dimensionalization) is in the clockwise direction. In addition, positive Ω inside the droplet will describe counterclockwise rotational flows and negative Ω will describe clockwise rotational flows (fig.5.2).

In fig.5.3, 5.5, 5.6, 5.9, 5.11, we show the plots of Ω=-0.5, -1.0, -1.5, 0.0, 0.025, 0.050, and 0.075 at different Atwood numbers. (The symbol "W" above the plots is the same as "Ω"

here.) Only the most left profile is at the correct x coordinate, while the other profiles are successively displaced by 0.5 units in the positive x direction. Also note that the plots for Atwood number near 0 are close to a unit circle although they look like an ellipse because of the different scales of the x and y axes.

At $\Omega = -0.5$, fig.5.3 and fig.5.4 together indicate that the vorticity supports the upper boundary, where the direction of the inner flow agrees with the outside flow, and did the opposite on the lower boundary, where the direction of the inner flow is against the outside flow. Examination of the velocity field shows that the two corners on the profile of A=-0.0975 are the stagnation points, where the velocities on the boundary (the average of the limiting velocities from inside and outside) vanish. Similar results are found for $\Omega = -1.0$ and $\Omega = -1.5$ in fig.5.5, and for $\Omega = 0.0$ in fig.5.6. Indeed, fig.5.7 and fig.5.8 indicate that there exists a stagnation point in the external flow as $|A|$ is small. It moves to the boundary as $|A|$ increases, splits into two stagnation points, then the two reaches the two corners at $A = A_{lim}$.

Such observation has a similarity to the result that Pullin and Grimshaw [16] found for nonlinear interfacial gravity waves in a two-layer Boussinesq fluid, in which the basic flow consists of a constant vorticity upper layer bounded by a rigid surface (denote by "$Dist$" the distance between the wall and the unperturbed flat interface) and an irrotational lower layer of infinite depth with continuous normal velocity at the density interface. They found that the most extreme wave, which has the highest amplitude at a given set of $(Dist, \Omega)$, was consistent with the appearance of one or more stagnation points on the wave profile.

However, their further study about the same problem of interfacial gravity waves showed that there are solutions beyond this one, since the uniform far-field velocity -u is a multi-valued function of one of the parameters (wave amplitude in their problem). Such solutions are nonphysical and unstable, but this might suggest the possibility of a profile beyond the appearance of the two corners, for example, fig.5.12, and need further research. Fig. 5.3 and fig. 5.5 also show that as $\Omega < 0$, the larger $|\Omega|$ is, the better the inner vorticity can support the upper boundary, so $|A_{lim}|$ increases as $|\Omega|$ increases.

At $\Omega = 0.025$, fig.5.9 and fig.5.10 show that the inner vorticity is against the outside flow on the upper boundary, and the same for $\Omega = 0.05$ and $\Omega = 0.075$ in fig.5.11. In such cases, $|A_{lim}|$ decreases as Ω increases.

The most extreme solution for $\Omega = 0.0$ is the one we have special interest in. The two singularities at the corners are the stagnation points, as is mentioned above, of which one is the separating point while the other is the reattaching point of the separating streamline, which meets the droplet at the front face at the left corner, then breaks itself to enclose the droplet, and the two reattach at the right corner. The semicircular shape of the solution is similar to the cap of the "mushroom" solution in the steady wave problem that Pullin and Grimshaw studied [17] [18], where larger vorticities agreeing with the outside flow allow the existence of steady waves with higher amplitude was also found.

5.5 Conclusion

We have set up the PDE system describing the stationary "flying droplet" subject to inner vorticity and outside circulation in a uniform flow. We have also computed symmetric solutions to this problem with different values of the parameters. The most visible observation is the appearance of a semicircular shape in the cases with $\Omega \leq 0$, $A \to A_{lim}$. We find the outgoing (ingoing) part of the stationary droplet is associated with the place where the inside and outside flows agree (disagree), and the two singularities on the boundary are the stagnation points. However, we need further analysis for the stability of such solutions, which has not been done in our current work. And whether there are solutions beyond the most extreme shapes reached by our method or whether there exist nonsymmetric solutions remains a challenging problem.

Table 5.1: $\Omega = 0$, $A = -0.0075$.

	N=64	N=128	N=256
Y_1	$-7.8067 \cdot 10^{-2}$	$-7.8067 \cdot 10^{-2}$	$-7.8067 \cdot 10^{-2}$
Y_2	$4.1546 \cdot 10^{-2}$	$4.1546 \cdot 10^{-2}$	$4.1546 \cdot 10^{-2}$
Y_3	$-1.3467 \cdot 10^{-2}$	$-1.3467 \cdot 10^{-2}$	$-1.3467 \cdot 10^{-2}$
Y_4	$4.6688 \cdot 10^{-3}$	$4.6688 \cdot 10^{-3}$	$4.6688 \cdot 10^{-3}$
Y_5	$-1.6291 \cdot 10^{-3}$	$-1.6291 \cdot 10^{-3}$	$-1.6291 \cdot 10^{-3}$
Y_6	$5.5005 \cdot 10^{-4}$	$5.5005 \cdot 10^{-4}$	$5.5006 \cdot 10^{-4}$
Y_7	$-1.7171 \cdot 10^{-4}$	$-1.7171 \cdot 10^{-4}$	$-1.7172 \cdot 10^{-4}$
Y_8	$4.5162 \cdot 10^{-5}$	$4.5162 \cdot 10^{-5}$	$4.5173 \cdot 10^{-5}$
Y_9	$-6.8149 \cdot 10^{-6}$	$-6.8146 \cdot 10^{-6}$	$-6.8243 \cdot 10^{-6}$
Y_{10}	$-2.4604 \cdot 10^{-6}$	$-2.4604 \cdot 10^{-6}$	$-2.4527 \cdot 10^{-6}$

	N=64	N=128	N=256
C_1	$-1.0113 \cdot 10^{-1}$	$-1.0113 \cdot 10^{-1}$	$-1.0113 \cdot 10^{-1}$
C_2	$-7.3682 \cdot 10^{-5}$	$-7.3681 \cdot 10^{-5}$	$-7.3692 \cdot 10^{-5}$
C_3	$-1.4172 \cdot 10^{-4}$	$-1.4172 \cdot 10^{-4}$	$-1.4171 \cdot 10^{-4}$
C_4	$9.8518 \cdot 10^{-5}$	$9.8518 \cdot 10^{-5}$	$9.8516 \cdot 10^{-5}$
C_5	$-4.4338 \cdot 10^{-5}$	$-4.4338 \cdot 10^{-5}$	$-4.4339 \cdot 10^{-5}$
C_6	$1.3713 \cdot 10^{-5}$	$1.3713 \cdot 10^{-5}$	$1.3717 \cdot 10^{-5}$
C_7	$-8.7583 \cdot 10^{-7}$	$-8.7583 \cdot 10^{-7}$	$-8.8080 \cdot 10^{-7}$
C_8	$2.9033 \cdot 10^{-6}$	$-2.9037 \cdot 10^{-6}$	$-2.8981 \cdot 10^{-6}$
C_9	$3.0686 \cdot 10^{-6}$	$3.0686 \cdot 10^{-6}$	$3.0632 \cdot 10^{-6}$
C_{10}	$-2.2186 \cdot 10^{-6}$	$-2.2181 \cdot 10^{-6}$	$-2.2135 \cdot 10^{-6}$

	$E_{64,128}$	$E_{128,256}$
A=-0.0075	$3.7247 \cdot 10^{-9}$	$5.1607 \cdot 10^{-8}$

Table 5.2: $\Omega = 0$, $A = -0.0150$.

	N=64	N=128	N=256
Y_1	-0.238573	-0.238577	-0.238576
Y_2	0.178393	0.178393	0.178393
Y_3	-0.048880	-0.048870	-0.048871
Y_4	0.000015	0.000017	0.000017
Y_5	0.011315	0.011303	0.011305
Y_6	-0.007410	-0.007411	-0.007411
Y_7	0.001009	0.001021	0.001019
Y_8	0.002396	0.002396	0.002396
Y_9	-0.002357	-0.002369	-0.002367
Y_{10}	0.000725	0.000725	0.000725

	N=64	N=128	N=256
C_1	-0.220206	-0.220207	-0.220207
C_2	-0.018526	-0.018530	-0.018529
C_3	0.009416	0.009415	0.009415
C_4	-0.003031	-0.003024	-0.003025
C_5	-0.000513	-0.000513	-0.000513
C_6	0.001592	0.001581	0.001583
C_7	-0.001127	-0.001127	-0.001127
C_8	0.000201	0.000214	0.000212
C_9	0.000409	0.000410	0.000410
C_{10}	-0.000484	-0.000501	-0.000498

	$E(1) = E_{64,128}$	$E(2) = E_{128,256}$	$\frac{E(1)}{E(2)}$
A=-0.0150	$1.4235 \cdot 10^{-4}$	$2.0112 \cdot 10^{-5}$	7.0777

Table 5.3: $\Omega = 0$, $A = -0.0200$.

	N=96	N=128	N=256
Y_1	-0.345313	-0.345600	-0.345555
Y_2	0.253923	0.254297	0.254270
Y_3	-0.023963	-0.023180	-0.023268
Y_4	-0.034751	-0.034838	-0.034843
Y_5	0.017215	0.016284	0.016382
Y_6	0.007839	0.007896	0.007903
Y_7	-0.011048	-0.010015	-0.010119
Y_8	-0.000268	-0.000380	-0.000381
Y_9	0.006782	0.005707	0.005811
Y_{10}	-0.002205	-0.002005	-0.002012

	N=96	N=128	N=256
C_1	-0.311016	-0.311197	-0.311172
C_2	-0.048804	-0.049085	-0.049054
C_3	0.014631	0.014754	0.014748
C_4	0.005604	0.006062	0.006018
C_5	-0.008024	-0.008174	-0.008171
C_6	0.001324	0.000664	0.000726
C_7	0.003949	0.004120	0.004122
C_8	-0.003071	-0.002204	-0.002286
C_9	-0.001414	-0.001608	-0.001616
C_{10}	0.003250	0.002179	0.002283

	$E_{96,128}$	$E_{128,256}$
A=-0.020	$1.2582 \cdot 10^{-2}$	$1.5756 \cdot 10^{-3}$

Table 5.4

$\Omega = -1.5$	E_2
A=-0.0025	$2.7736 \cdot 10^{-5}$
A=-0.005	$1.1145 \cdot 10^{-4}$
A=-0.001	$4.4993 \cdot 10^{-4}$
A=-0.002	$1.8338 \cdot 10^{-3}$

$\Omega = -1.0$	E_2
A=-0.0025	$4.1522 \cdot 10^{-5}$
A=-0.005	$1.6720 \cdot 10^{-4}$
A=-0.001	$6.7792 \cdot 10^{-4}$
A=-0.002	$2.7885 \cdot 10^{-3}$

$\Omega = -0.5$	E_2
A=-0.0025	$8.8302 \cdot 10^{-5}$
A=-0.005	$3.5814 \cdot 10^{-4}$
A=-0.001	$1.4737 \cdot 10^{-3}$
A=-0.002	$6.2618 \cdot 10^{-3}$

$\Omega = 0.0$	E_2
A=-0.0025	$5.2381 \cdot 10^{-4}$
A=-0.005	$2.0810 \cdot 10^{-3}$
A=-0.001	$2.2667 \cdot 10^{-2}$
A=-0.002	$8.2868 \cdot 10^{-2}$

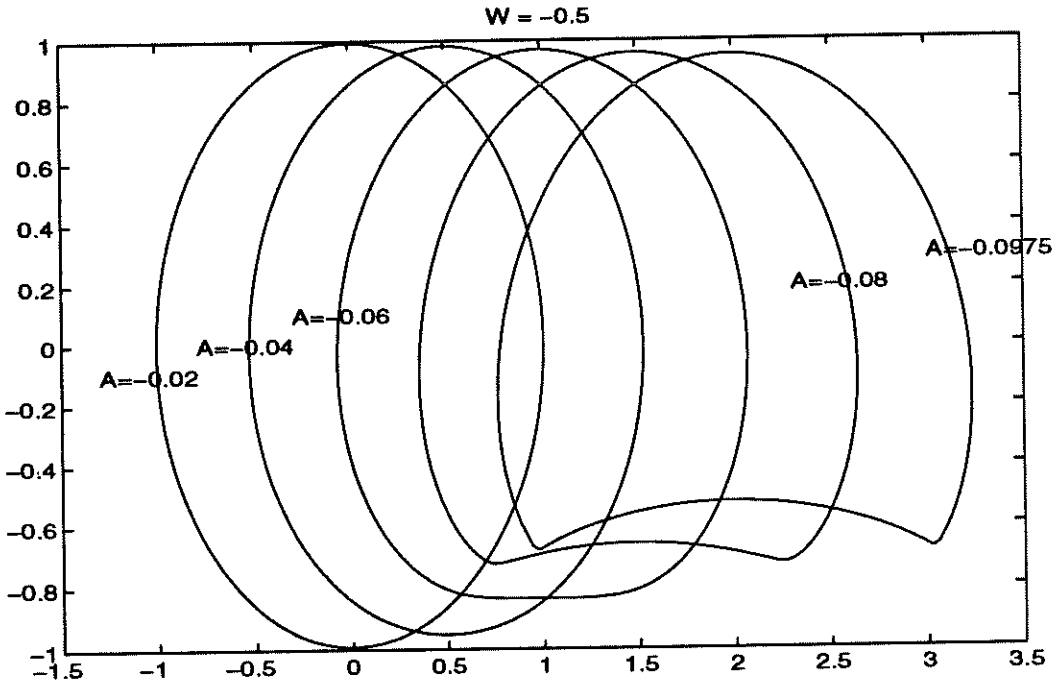

Figure 5.3: $\Omega = -0.5$

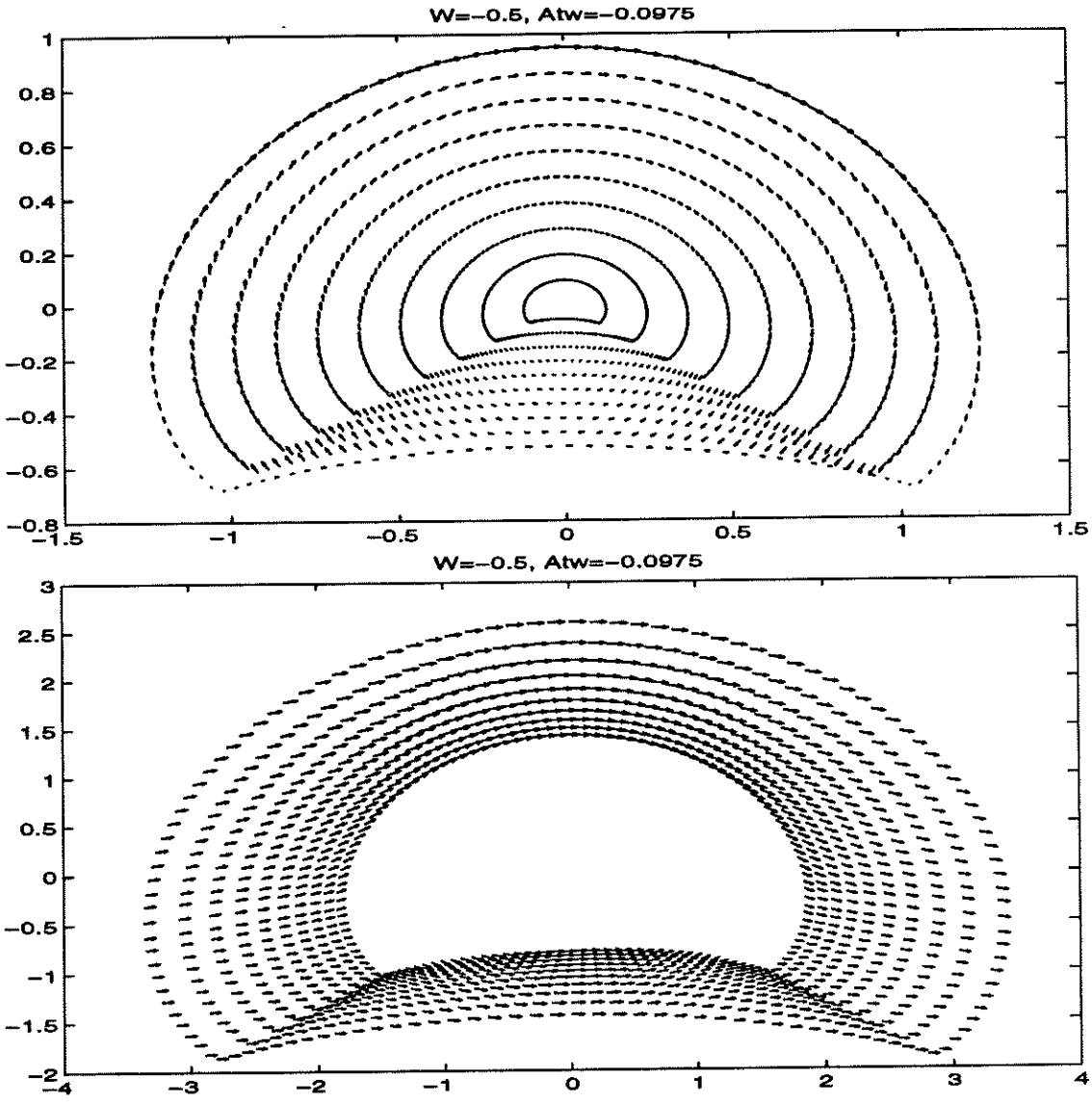

Figure 5.4: $\Omega = -0.5$. The upper plot is the velocity field inside the droplet , including the boundary. The lower plot is the velocity field outside the droplet.

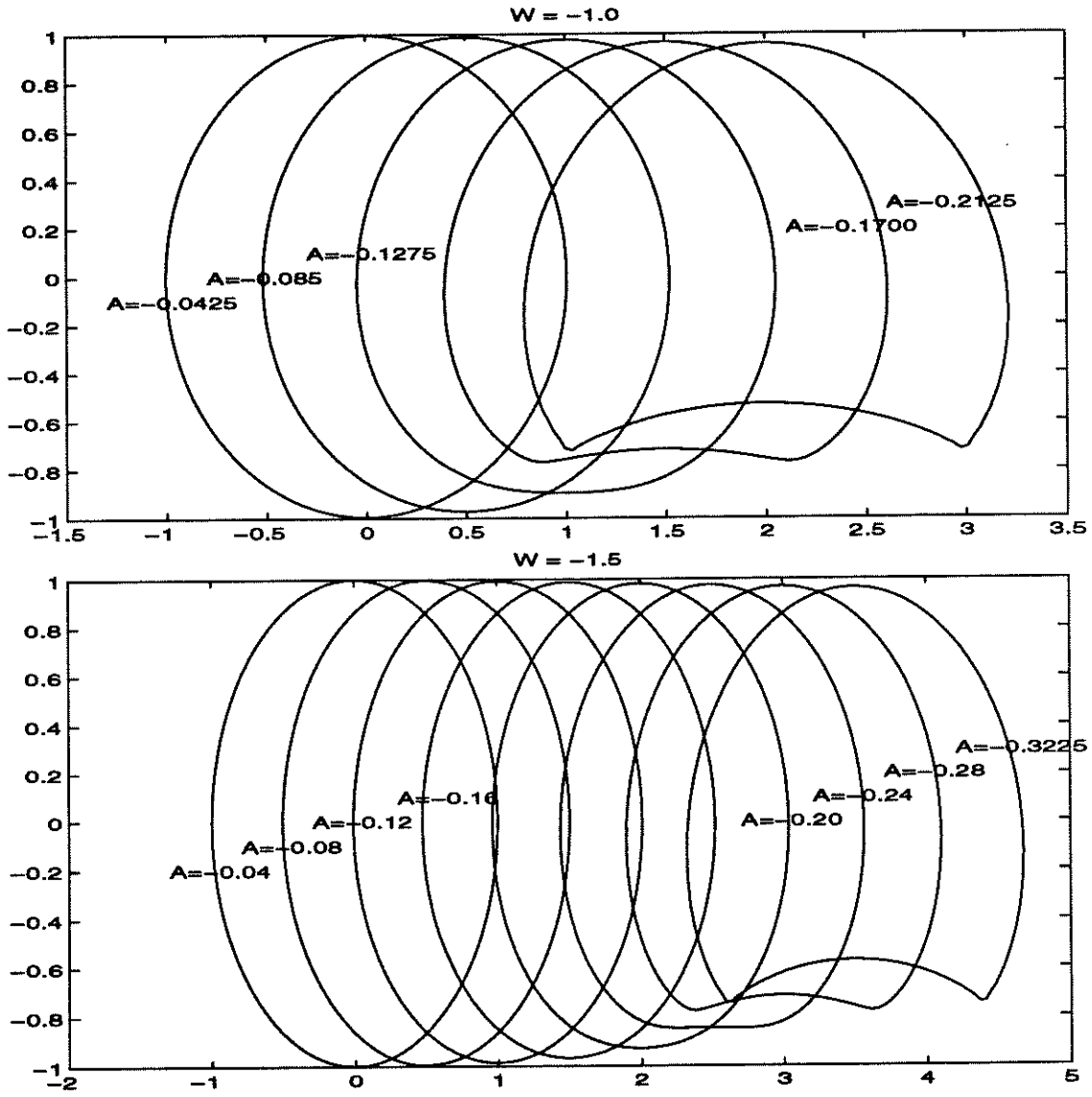

Figure 5.5: *Upper* : $\Omega = -1.0$, *lower* : $\Omega = -1.5$

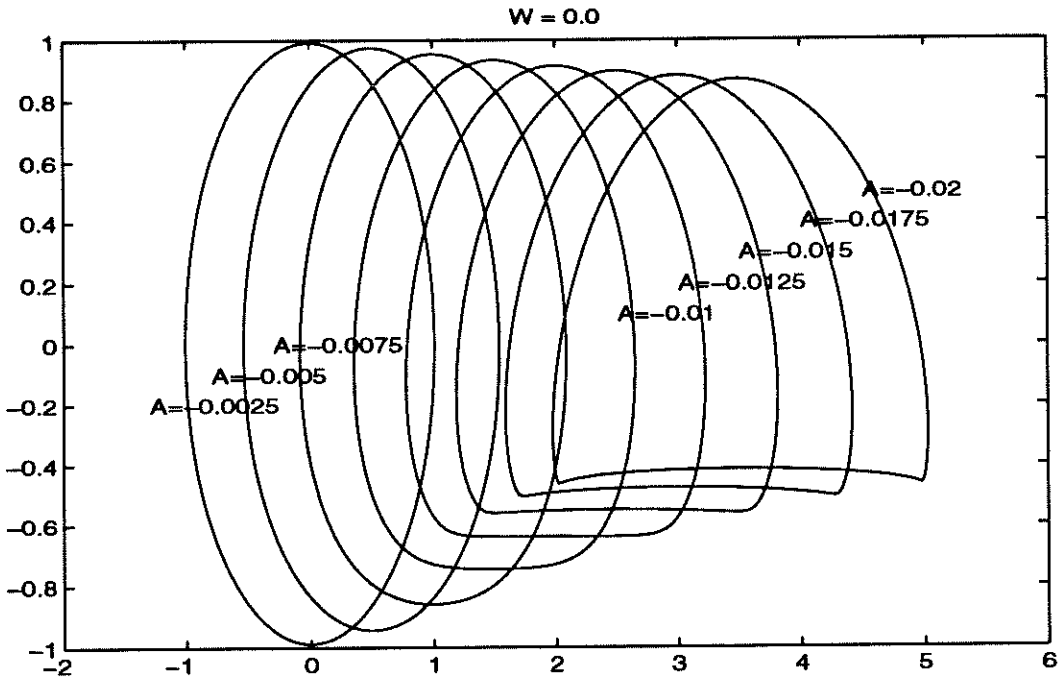

Figure 5.6: $\Omega = 0.0$

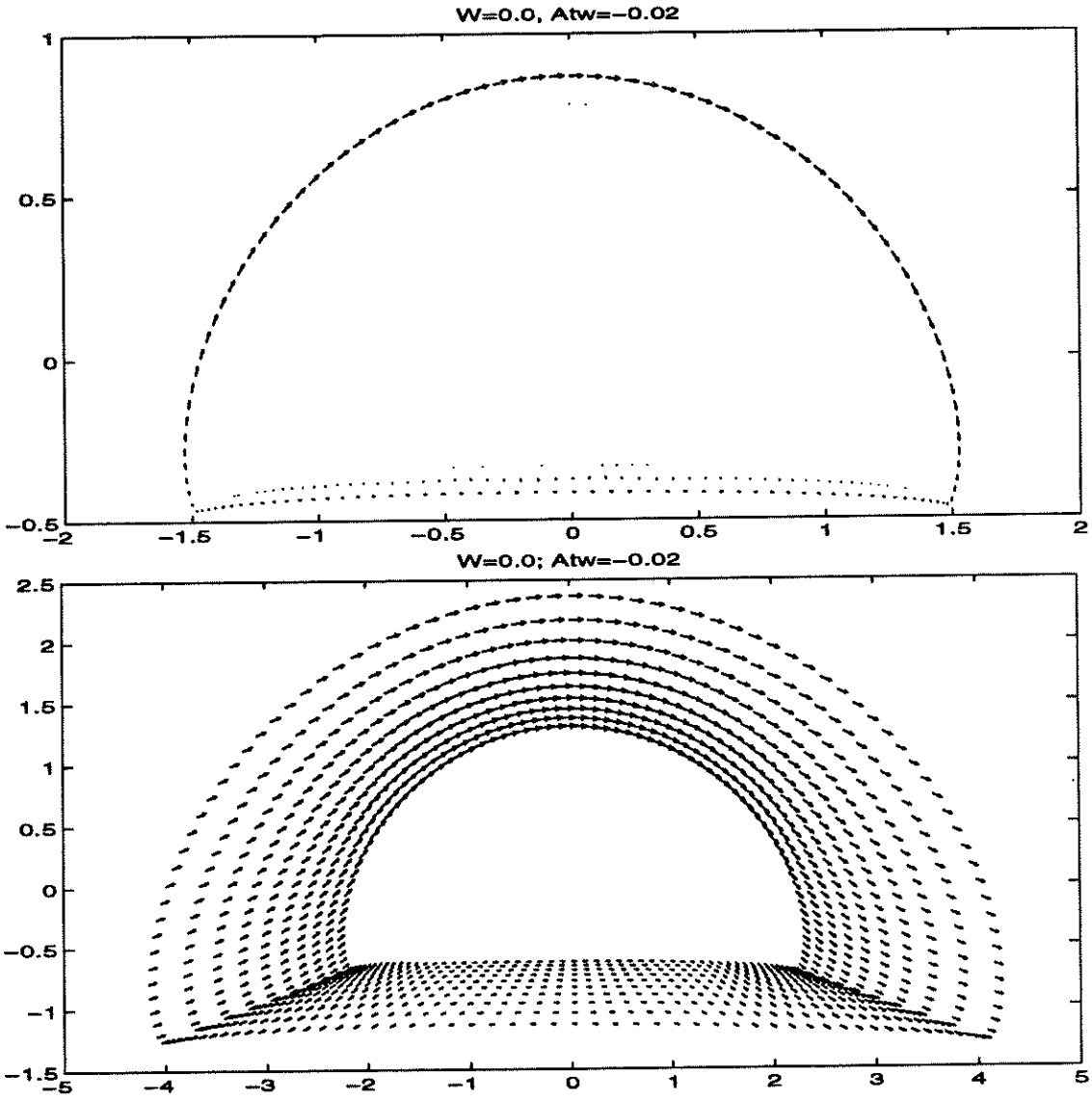

Figure 5.7: $\Omega = 0.0$. The upper plot is the velocity field inside the droplet, including the boundary. The lower plot is the velocity field outside the droplet.

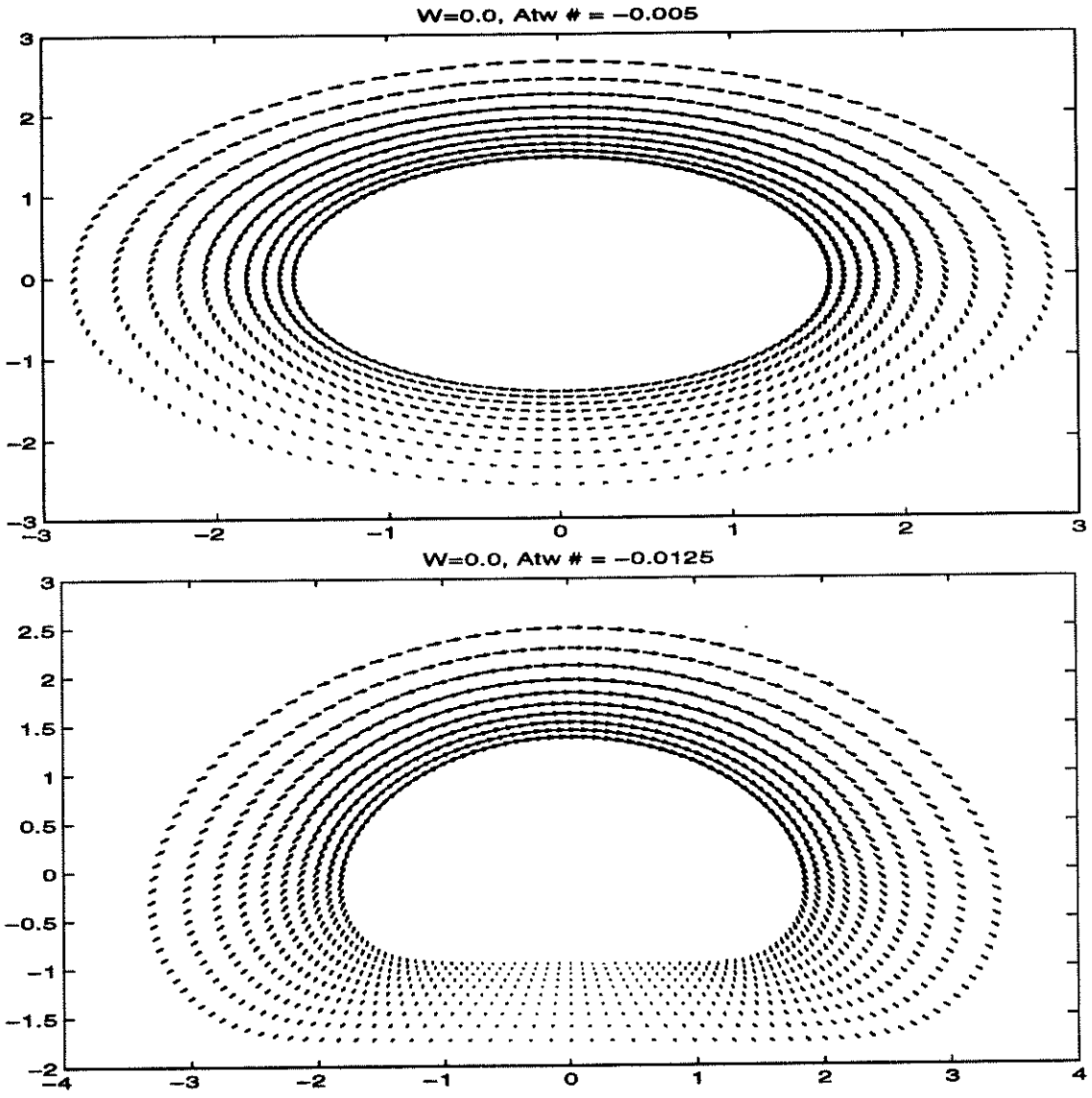

Figure 5.8: $\Omega = 0.0$. The velocity field outside the droplet at A = -0.005 and A = -0.0125.

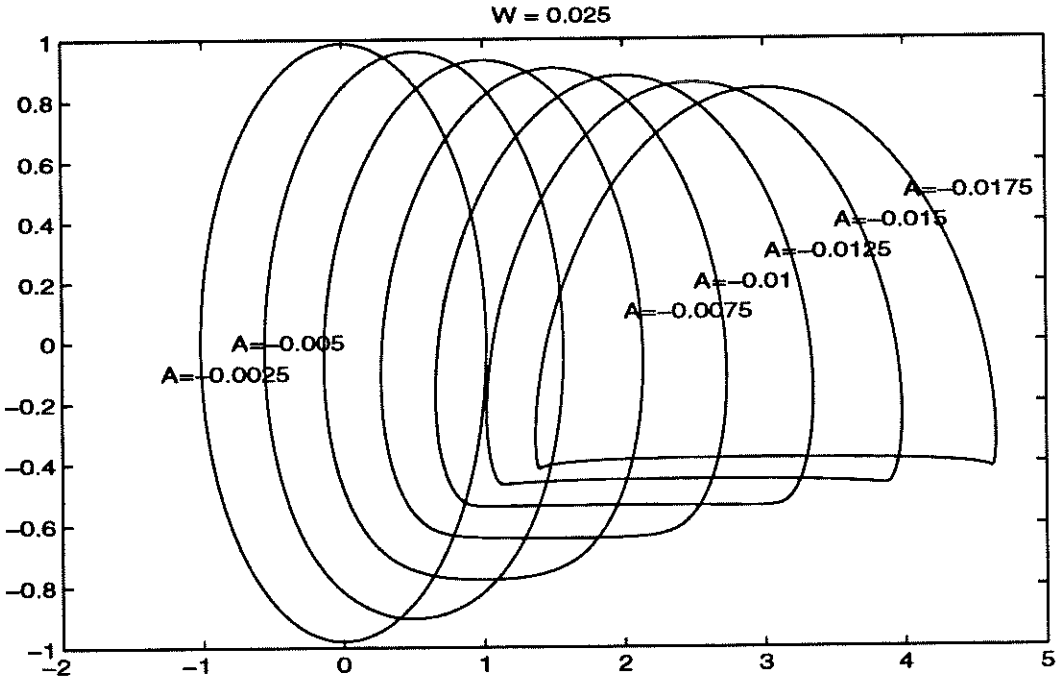

Figure 5.9: $\Omega = 0.025$

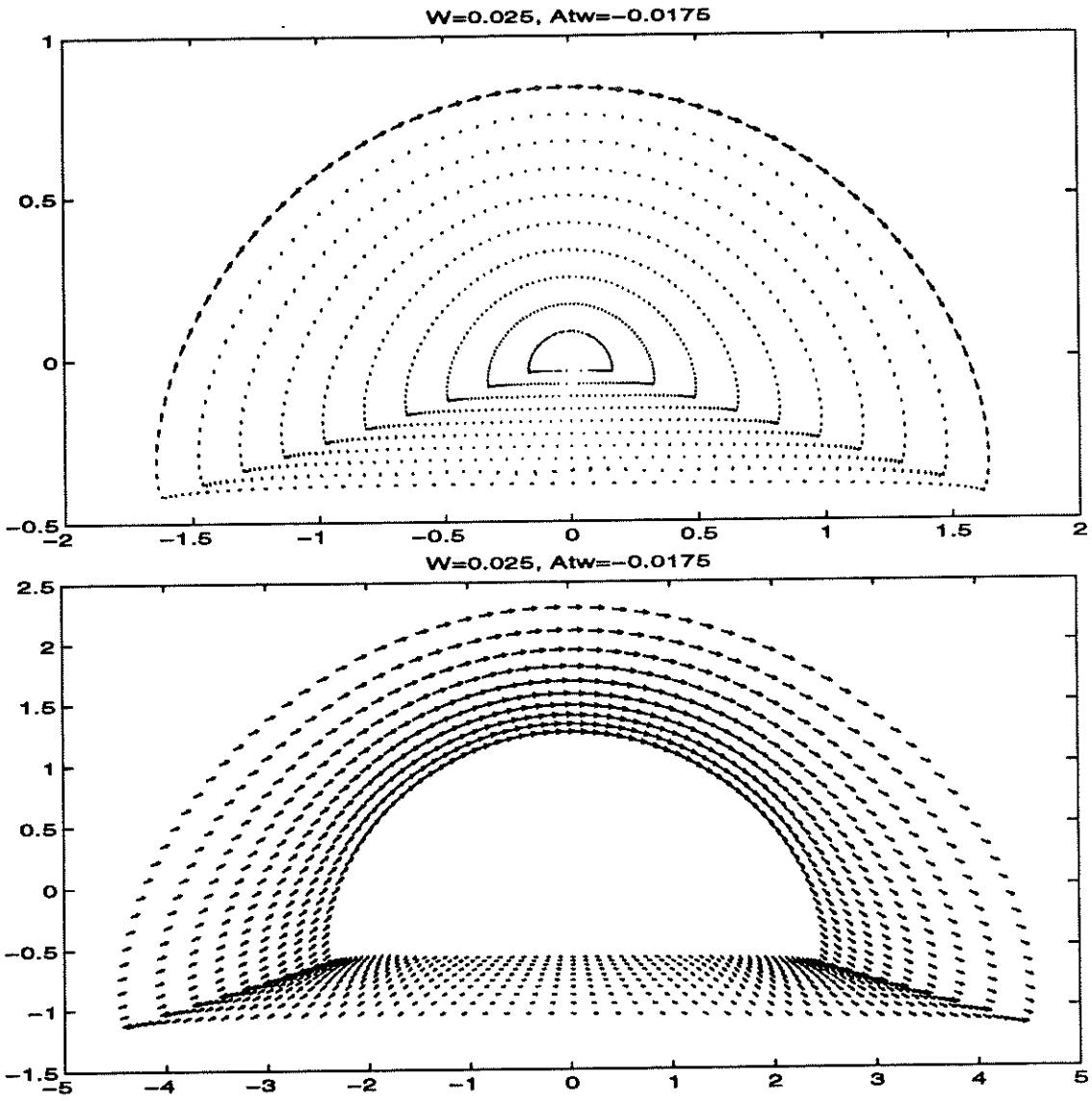

Figure 5.10: $\Omega = 0.025$. The upper plot is the velocity field inside the droplet, including the boundary. The lower plot is the velocity field outside the droplet.

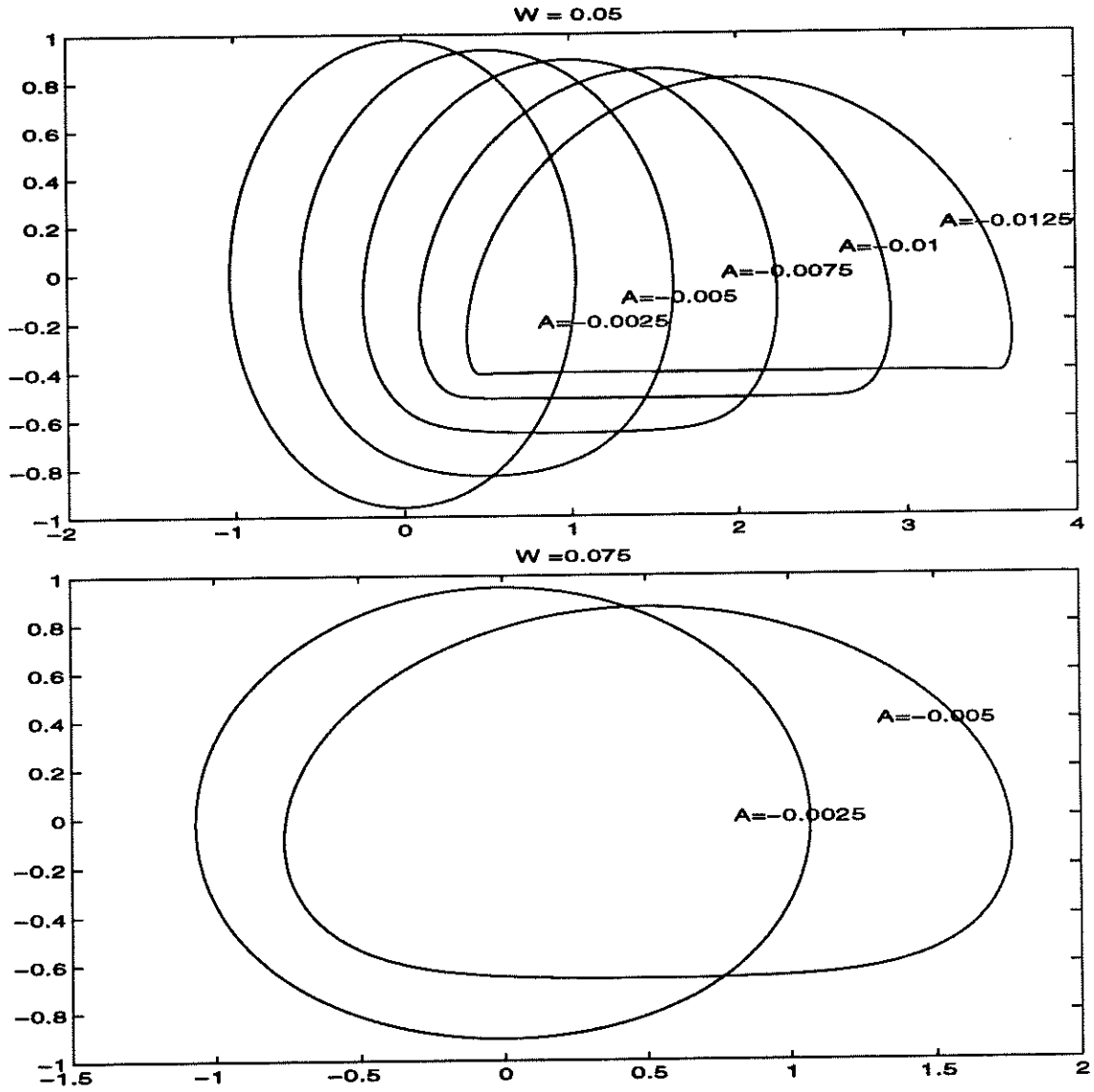

Figure 5.11: *Upper* : $\Omega = 0.05$, *lower* : $\Omega = 0.075$

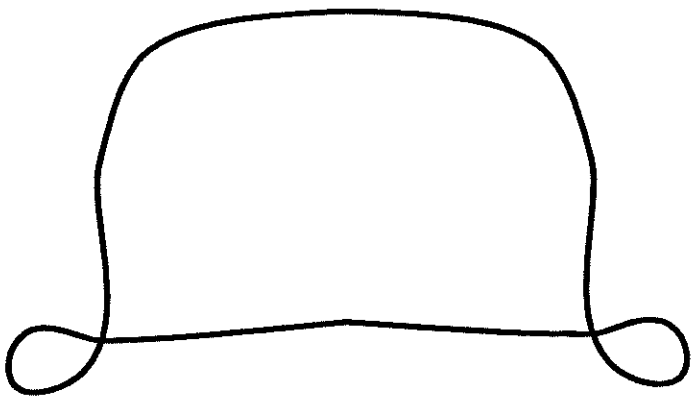

Figure 5.12:

CHAPTER 6

Appendix–Proof of Theorem 2.1

Here we prove the uniform boundedness of the desingularized integrand of I_{mn}. That is,

$$f(\alpha,\alpha',t) = \frac{\gamma_2(\alpha',t)}{Z_1(\alpha,t)-Z_2(\alpha',t)} - \frac{\gamma_2(\alpha,t)}{Z_1(\alpha,t)-Z_2(\alpha,t)+\partial_\alpha Z_2(\alpha,t)(\alpha-\alpha')}.$$

is uniformly bounded if the condition and the assumptions (A1), (A2),(A3) and (A4) in Theorem 2.1 are true.

The proof procedes as follows: Since $Z_1(\alpha,t)-Z_2(\alpha',t)\neq 0$ except at $\alpha'=\alpha=0$, $t=t^*$, there is no singularity in $\frac{\gamma_2(\alpha',t)}{Z_1(\alpha,t)-Z_2(\alpha',t)}$ when (α,t) is away from $(0,t^*)$. In this case, we show that both terms in f are bounded and hence f is bounded. On the other hand, when (α,t) is close to $(0,t^*)$, the denominators of both terms in f tend to zero as $\alpha'\to\alpha$. We locate the singularity of each term and find that they are nearly at the same point, so these two terms get cancelled on the real line.

6.1 For (α,t) away from $(0,t^*)$

Let d be a positive real number, then we have $|Z_1(\alpha,t)-Z_2(\alpha',t)|\geq d>0,\ \forall\alpha'$. And by (A1), there exists a constant M,

$$|\partial_\alpha Z_2(\alpha,t)|\leq M,\quad t\leq t^*. \tag{6.1}$$

Let $\delta = \frac{d}{2M}$.

(a)If $|\alpha - \alpha'| \geq \delta$, then

$$(6.2) \qquad |\underbrace{Z_1(\alpha,t) - Z_2(\alpha,t)}_{\text{pure imaginary by (A3)}} + \partial_\alpha Z_2(\alpha,t)(\alpha-\alpha')| \geq |Re[\partial_\alpha Z_2(\alpha,t)](\alpha-\alpha')|$$

$$\geq \mu\delta = \frac{\mu d}{2M} \quad by\ (A4)$$

(b)If $|\alpha - \alpha'| < \delta$, then

$$|Z_1(\alpha,t) - Z_2(\alpha,t) + \partial_\alpha Z_2(\alpha,t)(\alpha-\alpha')| \geq ||Z_1(\alpha,t) - Z_2(\alpha,t)| - |\partial_\alpha Z_2(\alpha,t)||\alpha-\alpha'||$$

$$(6.3) \qquad \geq d - M\delta = \frac{d}{2} \quad by\ (6.1),(b).$$

Define $\tilde{d} = \min[\frac{d\mu}{2M}, \frac{d}{2}]$, then

$$(6.4) \qquad |Z_1(\alpha,t) - Z_2(\alpha,t) + \partial_\alpha Z_2(\alpha,t)(\alpha-\alpha')| \geq \tilde{d}$$

(A1) implies that $|\gamma_2| \leq c$, where c is some constant. Hence from definition of f and (6.4),

$$|f(\alpha,\alpha',t)| \leq \frac{c}{d} + \frac{c}{\tilde{d}}$$

6.2 For (α,t) close to $(0,t^*)$

In this case,

$$|Z_1(\alpha,t) - Z_2(\alpha,t)| = |Z_1(\alpha,t) - Z_1(0,t^*) + Z_2(0,t^*) - Z_2(\alpha,t)|$$

$$(6.5) \qquad \leq |Z_1(\alpha,t) - Z_1(0,t^*)| + |Z_2(0,t^*) - Z_2(\alpha,t)| \ll 1$$

Define β_1 , β_2, which satisfy

$$Z_1(\alpha,t) - Z_2(\beta_1,t) = 0$$

$$Z_1(\alpha,t) - Z_2(\alpha,t) + \partial_\alpha Z_2(\alpha,t)(\alpha-\beta_2) = 0$$

Expand β_1 around α to obtain

$$\beta_1 = \frac{Z_1(\alpha,t) - Z_2(\alpha,t)}{\partial_\alpha Z_2(\alpha,t)} + \alpha - \frac{\partial^2_{\alpha\alpha} Z_2(\eta_1,t)}{2\partial_\alpha Z_2(\alpha,t)}(\beta_1 - \alpha)^2 \tag{6.6}$$

$$\beta_2 = \frac{Z_1(\alpha,t) - Z_2(\alpha,t)}{\partial_\alpha Z_2(\alpha,t)} + \alpha \tag{6.7}$$

Also,

$$\begin{aligned} Z_1(\alpha,t) - Z_2(\alpha',t) &= \underbrace{Z_1(\alpha,t) - Z_2(\beta_1,t)}_{=0} + Z_2(\beta_1,t) - Z_2(\alpha',t) \\ &= \partial_\alpha Z_2(\eta_2,t)(\beta_1 - \alpha') \end{aligned} \tag{6.8}$$

$$Z_1(\alpha,t) - Z_2(\alpha,t) + \partial_\alpha Z_2(\alpha,t)(\alpha - \alpha') = \partial_\alpha Z_2(\alpha,t)(\beta_2 - \alpha') \tag{6.9}$$

Here $\eta_1 \in (\alpha, \beta_1)$ and $\eta_2 \in (\beta_1, \alpha')$ are found by the mean value theorem. From (6.8), (6.9), $f(\alpha, \alpha', t)$ can be rewritten as

$$f(\alpha,\alpha',t) = \frac{\gamma_2(\alpha',t)}{\partial_\alpha Z_2(\eta_2,t)(\beta_1 - \alpha')} - \frac{\gamma_2(\alpha,t)}{\partial_\alpha Z_2(\alpha,t)(\beta_2 - \alpha')} \tag{6.10}$$

Define

$$g_1 = \frac{\gamma_2(\alpha',t)}{\partial_\alpha Z_2(\eta_2,t)} \quad , \quad g_2 = \frac{\gamma_2(\alpha,t)}{\partial_\alpha Z_2(\alpha,t)}. \tag{6.11}$$

By (6.10), (6.11), we need to bound

$$\begin{aligned} |f| = |\frac{g_1}{\beta_1 - \alpha'} - \frac{g_2}{\beta_2 - \alpha'}| &= |\frac{g_1 - g_2}{\beta_1 - \alpha'} + g_2 \frac{\beta_2 - \beta_1}{(\beta_1 - \alpha')(\beta_2 - \alpha')}| \\ &\leq |\frac{g_1 - g_2}{\beta_1 - \alpha'}| + |g_2||\frac{\beta_2 - \beta_1}{(\beta_1 - \alpha')(\beta_2 - \alpha')}|. \end{aligned} \tag{6.12}$$

By continuity,

$$|g_2| \leq |\frac{\gamma_2(0,t^*)}{\partial_\alpha Z_2(0,t^*)}| + 1$$

It suffices to show that

$$|\frac{g_1 - g_2}{\beta_1 - \alpha'}| \quad , \quad |\frac{\beta_2 - \beta_1}{(\beta_1 - \alpha')(\beta_2 - \alpha')}|$$

are uniformly bounded. We show these in **(6.2.1)** and **(6.2.2)** individually.

6.2.1 $|\frac{g_1 - g_2}{\beta_1 - \alpha'}|$

$$\begin{aligned}
g_1 - g_2 &= \frac{\gamma_2(\alpha', t)}{\partial_\alpha Z_2(\eta_2, t)} - \frac{\gamma_2(\alpha, t)}{\partial_\alpha Z_2(\alpha, t)} \\
&= \frac{\gamma_2(\alpha')\partial_\alpha Z_2(\alpha) - \gamma_2(\alpha)\partial_\alpha Z(\eta_2)}{\partial_\alpha Z_2(\eta_2)\partial_\alpha Z_2(\alpha)}, \quad \textit{leaving } t \textit{ out} \\
&= \frac{\gamma_2(\alpha)[\partial_\alpha Z_2(\alpha) - \partial_\alpha Z_2(\eta_2)] + \partial_\alpha \gamma_2(\eta_3)\partial_\alpha Z_2(\alpha)(\alpha' - \alpha)}{\partial_\alpha Z_2(\eta_2)\partial_\alpha Z_2(\alpha)}, \qquad \eta_3 \in (\alpha, \alpha') \\
&= \frac{\gamma_2(\alpha)\partial^2_{\alpha\alpha} Z_2(\eta_4)(\alpha - \eta_2) + \partial_\alpha \gamma_2(\eta_3)\partial_\alpha Z_2(\alpha)(\alpha' - \alpha)}{\partial_\alpha Z_2(\eta_2)\partial_\alpha Z_2(\alpha)}, \qquad \eta_4 \in (\alpha, \eta_2)
\end{aligned}$$

So,

$$|g_1 - g_2| \leq |\frac{\gamma_2(\alpha)\partial^2_{\alpha\alpha} Z_2(\eta_4)}{\partial_\alpha Z_2(\eta_2)\partial_\alpha Z_2(\alpha)}| \cdot |\alpha - \eta_2| + |\frac{\partial_\alpha \gamma_2(\eta_3)}{\partial_\alpha Z_2(\eta_2)}| \cdot |\alpha' - \alpha|$$

Consequently,

$$|\frac{g_1 - g_2}{\beta_1 - \alpha'}| \leq |\frac{\gamma_2(\alpha)\partial^2_{\alpha\alpha} Z_2(\eta_4)}{\partial_\alpha Z_2(\eta_2)\partial_\alpha Z_2(\alpha)}| \cdot |\frac{\alpha - \eta_2}{\beta_1 - \alpha'}| + |\frac{\partial_\alpha \gamma_2(\eta_3)}{\partial_\alpha Z_2(\eta_2)}| \cdot |\frac{\alpha' - \alpha}{\beta_1 - \alpha'}| \tag{6.13}$$

$\eta_2 \in (\alpha', \beta_1)$ from (6.8),

$$\eta_2 = \xi\beta_1 + (1 - \xi)\alpha', \quad \xi \in [0, 1]$$

$$|\frac{\alpha - \eta_2}{\beta_1 - \alpha'}| = |\frac{\alpha - \xi\beta_1 - \alpha' + \xi\alpha'}{\beta_1 - \alpha'}| = |\frac{\alpha - \alpha'}{\beta_1 - \alpha'} - \xi| \leq |\frac{\alpha - \alpha'}{\beta_1 - \alpha'}| + 1 \tag{6.14}$$

$|(\alpha,t)-(0,t^*)| \ll 1$, so $|\beta_1-\alpha| \ll 1$ by (6.6). Define

$$\kappa \equiv (\frac{Z_1-Z_2}{\partial_\alpha Z_2})(\alpha,t) \tag{6.15}$$

$$\beta_1 = \kappa+\alpha+\epsilon, \quad by\ (6.6), \tag{6.16}$$

$$\beta_2 = \kappa+\alpha, \quad by\ (6.7). \tag{6.17}$$

Here and in the following, ϵ denotes the term which is negligible compared to other terms in the equation. For example, if $|Z_1(\alpha,t)-Z_2(\alpha,t)|$ is of order ζ (from (6.5)), we get $\epsilon \sim \zeta^2$ by (6.6), hence is negligible in (6.16).

(1a)If $|\alpha-\alpha'| \geq 2|\kappa|$, then (6.16) implies

$$|\beta_1-\alpha'| = |\kappa+\epsilon+\alpha-\alpha'| \geq ||\alpha-\alpha'|-|\kappa|| + \epsilon \geq \frac{1}{2}|\alpha-\alpha'|+\epsilon$$

$$\Rightarrow \quad |\tfrac{\alpha-\alpha'}{\beta_1-\alpha'}| \leq \frac{|\alpha-\alpha'|}{\frac{1}{2}|\alpha-\alpha'|+\epsilon} \simeq 2 \tag{6.18}$$

(1b)If $|\alpha-\alpha'| < 2|\kappa|$, then

$$|\kappa+\epsilon+\alpha-\alpha'| = \sqrt{[Im(\kappa+\epsilon)]^2+[Re(\kappa+\epsilon)+\alpha-\alpha']^2}$$

$$\geq \sqrt{[Im(\kappa+\epsilon)]^2} \geq |Im(\kappa)|+\epsilon, \tag{6.19}$$

but by definition (6.15),

$$\kappa = (\frac{\overbrace{Z_1(\alpha,t)-Z_2(\alpha,t)}^{pure\ imaginary}}{\underbrace{\partial_\alpha Z_2(\alpha,t)}_{of\ order\ 1}}) = Im[\kappa]+\epsilon, \tag{6.20}$$

so (6.19), (6.20) and **(1b)** give

$$|\kappa+\epsilon+\alpha-\alpha'| \geq |Im[\kappa]|+\epsilon = |\kappa|+\epsilon > \frac{1}{2}|\alpha-\alpha'|+\epsilon \tag{6.21}$$

Therefore,

$$(6.22) \qquad |\frac{\alpha-\alpha'}{\beta_1-\alpha'}| \;=\; |\frac{\alpha-\alpha'}{\kappa+\epsilon+\alpha-\alpha'}| \le \frac{|\alpha-\alpha'|}{\frac{1}{2}|\alpha-\alpha'|+\epsilon} \simeq 2$$

By (1a), (1b), (6.14) and (6.22), (6.13) becomes

$$(6.23) \qquad |\frac{g_1-g_2}{\beta_1-\alpha'}| \;\le\; |\frac{\gamma_2(\alpha)\partial^2_{\alpha\alpha}Z_2(\eta_4)}{\partial_\alpha Z_2(\eta_2)\partial_\alpha Z_2(\alpha)}|(2+1)| + |\frac{\partial_\alpha\gamma_2(\eta_3)}{\partial_\alpha Z_2(\eta_2)}| \cdot 2$$

Evaluate $Im[\eta_2]$, $Im[\eta_3]$, $Im[\eta_4]$ as follows:

$$\eta_2 = \xi_2\beta_1 + (1-\xi_2)\alpha' \quad \xi_2 \in [0,1] \;\Rightarrow Im(\eta_2) = \xi_2 Im(\beta_1)$$

$$\eta_3 = \xi_3\alpha + (1-\xi_3)\alpha' \quad \xi_3 \in [0,1] \;\Rightarrow Im(\eta_3) = 0$$

$$\eta_4 = \xi_4\eta_2 + (1-\xi_4)\alpha \quad \xi_4 \in [0,1] \;\Rightarrow Im(\eta_4) = \xi_4 Im(\eta_2) = \xi_2\xi_4 Im(\beta_1)$$

Since by (A1), Z_j, γ_j are analytic in a strip $\{|Im(\alpha)| < \rho\}$ and

$$|\gamma_2|,\;\; |\partial_\alpha\gamma_2|,\;\; |\partial^2_{\alpha\alpha}Z_2| \;\le\; M^*$$

$$|\partial_\alpha Z_2| \;\ge\; \mu \quad \alpha \in R,\;\; t \in [t_0, t^*]$$

As $(\alpha,t) \to (0,t^*)$, $|Im(\beta_1)| \ll 1$ (6.6), so

$$|\partial^2_{\alpha\alpha}Z_2(\eta_4,t)|, |\partial_\alpha\gamma_2(\eta_3,t)| \;\le\; M^*+\epsilon$$

$$|\partial_\alpha Z_2(\eta_2,t)| \;\ge\; \mu+\epsilon$$

This shows that $|\frac{g_1-g_2}{\beta_1-\alpha'}|$ is uniformly bounded , by (6.23).

6.2.2 $\frac{|\beta_2-\beta_1|}{|\beta_1-\alpha'||\beta_2-\alpha'|}$

WLOG, we may assume that (α, t) is so close to $(0, t^*)$ that

$$|\kappa| < \frac{1}{4}\sqrt{\frac{2|\partial_\alpha Z_2(0,t^*)|}{|\partial^2_{\alpha\alpha} Z_2(0,t^*)|}}. \tag{6.24}$$

(2a) If $|\beta_1 - \alpha'| > \frac{1}{2}\sqrt{|\beta_2 - \beta_1|}$

$$\begin{aligned} |\beta_2 - \beta_1| &\leq |\frac{\partial^2_{\alpha\alpha} Z_2(0,t^*)}{2\partial_\alpha Z_2(0,t^*)}||\beta_1 - \alpha|^2 + \epsilon, && by(6.6),(6.7) \\ &= |\frac{\partial^2_{\alpha\alpha} Z_2(0,t^*)}{2\partial_\alpha Z_2(0,t^*)}||\kappa|^2 + \epsilon, && by(6.16) \\ &< \frac{1}{16} + \epsilon, && by(6.24) \end{aligned}$$

Hence

$$\sqrt{|\beta_2 - \beta_1|} < \frac{1}{4}, \qquad |\beta_2 - \beta_1| < \frac{1}{4}\sqrt{|\beta_2 - \beta_1|} \tag{6.25}$$

$$\begin{aligned} |\beta_2 - \alpha'| &= |\beta_2 - \beta_1 + \beta_1 - \alpha'| \\ &> ||\beta_1 - \alpha'| - |\beta_2 - \beta_1|| > \frac{1}{2}\sqrt{|\beta_2 - \beta_1|} - |\beta_2 - \beta_1| \end{aligned} \tag{6.26}$$

(6.26) is seen by **(2a)** and (6.25). Thus **(2a)**, (6.26) imply

$$\begin{aligned} \frac{|\beta_2 - \beta_1|}{|\beta_1 - \alpha'||\beta_2 - \alpha'|} &\leq \frac{|\beta_2 - \beta_1|}{\frac{1}{4}|\beta_2 - \beta_1| - \frac{1}{2}|\beta_2 - \beta_1|^{\frac{3}{2}}} \\ &= \frac{4}{1 - 2\sqrt{|\beta_2 - \beta_1|}} < \frac{4}{\frac{1}{2}} = 8 \qquad by\ (6.25) \end{aligned} \tag{6.27}$$

(2b)$|\beta_1 - \alpha'| \leq \frac{1}{2}\sqrt{|\beta_2 - \beta_1|}$

$$\begin{aligned} |\beta_1 - \alpha'| &= |\kappa + \alpha - \alpha'| + \epsilon \\ &= \sqrt{[Im(\kappa)]^2 + [Re(\kappa) + \alpha - \alpha']^2} + \epsilon \geq |Im(\kappa)| + \epsilon \simeq |\kappa| \end{aligned} \tag{6.28}$$

by (6.16, (6.21).**(2b)** implies that

$$|\beta_1 - \alpha'| \leq \frac{1}{2}\sqrt{|\beta_2 - \beta_1|} \leq \frac{1}{2}\sqrt{\frac{|\partial^2_{\alpha\alpha} Z_2(0,t^*)|}{2|\partial_\alpha Z_2(0,t^*)|}|\kappa|} + \epsilon \text{ by (6.6), (6.7), (6.16).}$$

$$\Rightarrow |\kappa| \geq \sqrt{|\beta_2 - \beta_1|} \cdot \sqrt{\frac{2|\partial_\alpha Z_2(0,t^*)|}{|\partial^2_{\alpha\alpha} Z_2(0,t^*)|}} \tag{6.29}$$

Thus (6.28), (6.29) combine as

$$|\beta_1 - \alpha'| \geq \sqrt{|\beta_2 - \beta_1|} \cdot \sqrt{\frac{2|\partial_\alpha Z_2(0,t^*)|}{|\partial^2_{\alpha\alpha} Z_2(0,t^*)|}}. \tag{6.30}$$

We also have

$$\begin{aligned} |\beta_2 - \alpha'| &= |\beta_2 - \alpha + \alpha - \alpha'| = |\kappa + \alpha - \alpha'| \\ &\geq |Im(\kappa)| \simeq |\kappa| \geq \sqrt{|\beta_2 - \beta_1|} \cdot \sqrt{\frac{2|\partial_\alpha Z_2(0,t^*)|}{|\partial^2_{\alpha\alpha} Z_2(0,t^*)|}}. \end{aligned} \tag{6.31}$$

The last inequality is by (6.29). (6.30), (6.31) give that

$$\frac{|\beta_2 - \beta_1|}{|\beta_1 - \alpha'||\beta_2 - \alpha'|} \leq \frac{|\beta_2 - \beta_1|}{(\sqrt{|\beta_2 - \beta_1|} \cdot \sqrt{\frac{2|\partial_\alpha Z_2(0,t^*)|}{|\partial^2_{\alpha\alpha} Z_2(0,t^*)|}})^2} = \frac{|\partial^2_{\alpha\alpha} Z_2(0,t^*)|}{2|\partial_\alpha Z_2(0,t^*)|} \tag{6.32}$$

(6.27) and (6.32) imply that

$$\frac{|\beta_2 - \beta_1|}{|\beta_1 - \alpha'||\beta_2 - \alpha'|} \leq \max[8, \frac{|\partial^2_{\alpha\alpha} Z_2(0,t^*)|}{2|\partial_\alpha Z_2(0,t^*)|}]. \tag{6.33}$$

Bibliography

[1] C. Anderson. A vortex method for flows with slight density variations. *J.Comp.Phys., vol.61, pp.417*, 1985.

[2] G.R. Baker, D.I. Meiron, and S.A. Orzag. Analytic structure of vortex sheet dynamics 1, kelvin-helmholtz instability. *J.Fluid Mech., vol.114, pp.283*, 1982.

[3] G.R. Baker, D.I. Meiron, and S.A. Orzag. Generalized methods for free surface flow problems. *J.Fluid Mech., vol.123, pp.477*, 1982.

[4] G.R. Baker and D.W. Moore. The rise and distortion of a two-dimensional gas bubble in an inviscid liquid. *J.Phys. Fluids, vol.A 1 (9), pp.1451*, 1989.

[5] G.R. Baker and M. Shelley. On the connection between thin vortex layers and vortex sheets. *J.Fluid Mech., vol.215, pp.161*, 1990.

[6] G.R. Baker and M.J. Shelley. Boundary integral techniques for multi-connected domains. *J.Comp.Physics. vol.64, No.1*, 1986.

[7] G.K. Batchelor. *An Introduction to Fluid Dynamics.* Cambridge University Press, pp. 325, 348, 1967.

[8] J.T. Beale, T. Hou, and J. Lowengrub. Growth rates for the linear motion of fluid interfaces away from equilibrium. *C.P.A.M., vol.46, pp.1269*, 1993.

[9] J.T. Beale, T. Hou, and J. Lowengrub. Convergence of a boundary integral method for water waves. *to be present in SIAM*, 1994.

[10] J.R. Blake, B.B. Taib, and G. Doherty. Transient cavities near boundaries. part 1. rigid boundary. *J.Fluid Mech., vol.170, pp. 479*, 1986.

[11] J.R. Blake, B.B. Taib, and G. Doherty. Transient cavities near boundaries. part 2. free surface. *J.Fluid Mech., vol.181, pp. 197*, 1987.

[12] S.I. Chernyshenko. Royal aircraft establishment library translations report no. 2133. 1983.

[13] E.D. Cokelet and M.S. Longuet-Higgins. The deformation of steep surface waves on water 1, a numerical method of computation. *Proc. Roy. Soc. London A., vol.350, pp.1*, 1976.

[14] J.B. Conway. *Functions of One Complex Variable, 2nd Ed.* Springer-Verlag, 1978.

[15] J.F. Davidson and J.K. Walters. The initial motion of a gas bubble formed in an inviscid liquid. part 1, the two-dimensional bubble. *J.Fluid Mech., vol.12, pp.408*, 1962.

[16] R.H.J. Grimshaw and D.J. Pullin. Interfacial progressive gravity waves in a two-layer shear flow. *Physics Fluids 26 (7), pp.1731*, 1983.

[17] R.H.J. Grimshaw and D.J. Pullin. Extreme interfacial waves. *Physics Fluids 29 (9), pp.2802*, 1986.

[18] R.H.J. Grimshaw and D.J. Pullin. Finite-amplitude solitary waves at the interface between two homogeneous fluids. *Physics Fluids 31 (12), pp.3550*, 1988.

[19] R. Krasny. Desingularization of periodic vortex sheet rollup. *J.Comp.Phys., vol.65, pp.65*, 1986.

[20] R. Krasny. A study of singularity formation in a vortex sheet by the point vortex approximation. *J.Fluid Mech., vol.167, pp.65*, 1986.

[21] H. Lamb. *Hydrodynamics.* Dover, New York, 1945.

[22] T.S. Lundgren and N.N. Mansour. Vortex ring bubbles. *J.Fluid Mech., vol.224, pp.177*, 1991.

[23] A. Markushevich. *Theory of Functions of a Complex Variable.* Chelsea, New York, 1985.

[24] D.W. Moore. The spontaneous appearance of a singularity in the shape of an evolving vortex sheet. *Proc. R. Soc. Lond. vol.A365, pp.105*, 1979.

[25] D.W. Moore. On the point vortex method. *SIAM J. Sci. Stat. Comput., vol.2, pp.65*, 1981.

[26] D.W. Moore, P.G. Saffman, and S. Tanveer. The calculation of some batchelor flows: the sadovskii vortex and rotational corner flow. *Phys. Fluids 31 (5), pp.978*, 1988.

[27] V.S. Sadovskii. *Appl. Math. Mech. 35, pp.773*, 1971.

[28] M.J. Shelley. A study of singularity formation in vortex sheet motion by a spectrally accurate method. *J.Fluid Mech., vol.244, pp.493*, 1992.

[29] van de Vooran. A numerical investigation of the rolling up of vortex sheets. *Pro.R.Soc.Lond. A373, pp.67*, 1980.